



Contents lists available at ScienceDirect

## Progress in Polymer Science

journal homepage: [www.elsevier.com/locate/ppolysci](http://www.elsevier.com/locate/ppolysci)

## Recent advances in synthesis, characterization and rheological properties of polyurethanes and POSS/polyurethane nanocomposites dispersions and films

Samy A. Madbouly, Joshua U. Otaigbe\*

School of Polymers and High Performance Materials, 118 College Drive #10076, The University of Southern Mississippi, Hattiesburg, MS 39406, USA

### ARTICLE INFO

#### Article history:

Received 23 April 2009

Received in revised form 16 August 2009

Accepted 24 August 2009

Available online 2 September 2009

#### Keywords:

Aqueous polyurethane dispersions

Rheology

Hybrid polyurethane/POSS nanocomposites

Gelation kinetics

Polymer nanocomposites

Thin films and coatings

### ABSTRACT

Aqueous polyurethane dispersions (PUDs) have recently emerged as important alternatives to their solvent-based counterparts for various applications due to increasing health and environmental awareness. There are a number of important variables in the preparation of aqueous PUDs such as carboxylic acid content, solid content, degree of pre-/post-neutralization of the carboxylic acids and chain extension that all impact the dispersion particle sizes and distributions, viscosity, molecular weights, and glass transition temperatures of the PUDs and thin films made from them. This article reviews some new insights into the synthesis, characterization, structure evolution and kinetics, and rheological properties of representative examples of polyurethanes and POSS/polyurethane nanocomposites dispersions and films with prescribed rheological properties, macromolecular structure dynamics and function with the aim of understanding the complex relationships amongst the polymer structure, rheological properties, and performance of the PUDs and nanocomposite films under conditions that they are likely to encounter during use. It will be demonstrated that incorporation of small amounts of POSS into PU films can significantly enhance the thermal stability and mechanical properties, and present a new class of materials for special industrial applications. The unanswered questions are discussed to guide future research directions, and facilitate progress in this area so that the materials can be rationally engineered during synthesis and processing to yield new materials with enhanced properties for a number of applications. Overall, the present review article will provide a quantitative experimental basis for any future theory development of the relatively new waterborne PUDs and hybrid PU/POSS nanocomposites, and their structural dynamics, phase behavior, molecular relaxation, and rheological properties, increasing our level of understanding of the behavior of this important class of polymeric materials and other similar water soluble polymers.

Published by Elsevier Ltd.

### Contents

1. Introduction .....	1284
2. Synthesis of PUDs .....	1287
2.1. Prepolymer emulsification process .....	1287
2.2. Acetone process .....	1288

\* Corresponding author. Tel.: +1 601 266 5596; fax: +1 601 266 5504.  
E-mail address: [Joshua.Otaigbe@usm.edu](mailto:Joshua.Otaigbe@usm.edu) (J.U. Otaigbe).

3.	Characterization of PUDs .....	1288
3.1.	Particle size and dispersion stability .....	1288
3.2.	Overview of recent literature on aqueous PUDs .....	1289
4.	Rheological properties and gelation kinetics of PUDs .....	1293
4.1.	Impact of solid content .....	1294
4.2.	Effect of degree of neutralization .....	1298
4.3.	Effect of chain extension .....	1299
4.4.	Effect of temperature .....	1300
4.5.	Determination of $T_{gel}$ .....	1301
4.6.	Phase separation and gel structure of PUDs .....	1302
4.7.	Real-time measurements .....	1303
4.8.	Determination of $t_{gel}$ .....	1304
4.9.	Critical phenomena at the gel point .....	1305
4.10.	Gelation kinetics .....	1306
4.11.	Isothermal gelation kinetics .....	1307
4.12.	Model-fitting method .....	1307
4.13.	Isoconversional method .....	1309
4.14.	Non-isothermal gelation kinetics .....	1309
5.	PU/POSS nanocomposites .....	1309
5.1.	Typical synthesis of PU/POSS hybrids (10 wt% POSS) .....	1310
5.2.	Characterization of PU/POSS nanocomposites films .....	1313
5.2.1.	Wide angle X-ray analysis .....	1313
5.2.2.	Tensile and DMA tests .....	1313
5.3.	Rheological behavior of pure PU and PU/POSS nanocomposites films .....	1315
5.3.1.	Pure PU film ( <b>PUO</b> ) .....	1315
5.3.2.	PU/POSS nanocomposites .....	1317
5.3.3.	Effect of POSS concentration on zero shear viscosity and thermal stability .....	1321
6.	PU/POSS nanocomposites obtained from non-dispersion methods .....	1323
7.	Conclusions and outlook .....	1327
	Acknowledgements .....	1328
	References .....	1328

## 1. Introduction

The evaporation of volatile organic compounds (VOCs) during the formulations of coatings, ink, and paints cause a wide variety of air quality problems. Consequently, governmental organizations such as the Environmental Protection Agency (EPA) in the United States and Local Air Quality Regulators have stepped up their efforts to limit the amounts of VOCs released to the atmosphere. These regulations and consumer demands are forcing industries to develop environmentally friendly products that will minimize adverse consequences to the environment [1–3]. Amongst several options to develop new technology, water is the best choice to use as a medium in formulating coatings systems. To reduce or eliminate organic solvents from the formulations, solvents should be partially or completely replaced with environmentally benign solvents (e.g., water), in the coating formulations to achieve little or no VOC content [4–12]. Due to the strong demands for low-pollution chemical industry, a recent renaissance has occurred in the area of aqueous polyurethanes, which has the potential to significantly reduce current environmental pollution from industries that are accustomed to using organic solvents that are costly and harmful to the environment. In the past 60 years, a number of studies aimed at improving the production technology and quality of waterborne polyurethanes have been reported in journal publications and patents. For example, the work of Dieterich and his colleagues in

Bayer AG is noteworthy because it pioneered the field and inspired much of the work in this area [13,14]. Today, waterborne polyurethanes have begun to penetrate new application areas previously reserved almost exclusively for their solvent borne analogs, especially as coatings for various fibers, adhesives for alternative substrates, primers for metals, caulking materials, emulsion polymerization media for different monomers, paint additives, defoamers, associate thickeners, pigment pastes, and textile dyes [15–27].

Polyurethane dispersions (PUDs) belong to a special class of colloidal dispersions that are blends of different chemical species where the interfacial area plays a dominant or at least an important role, so that their properties depend strongly on the interfacial forces or physicochemical interactions. In general, a colloidal dispersion is stable when the droplets (discontinuous phase) persist uniformly in the liquid medium (continuous phase). The dispersion becomes unstable when the droplets diffuse together to form a single bigger droplet that leads to a reduction in the total surface area (coalescence), or to form an aggregate of particles without producing a new particle (flocculation). The role of polymer in stabilization or flocculation of colloidal dispersions has been studied extensively [28–31].

Since the current polyurethanes are synthesized in aqueous environments, both colloidal and chemical aspects of the dispersion will affect the final film properties. Slight variations in the temperature, stirring rate, addition of

components, order of addition, pH, shear history, and other processing parameters can alter both the colloidal and polymer physical properties. These waterborne products are expected to exhibit superior performance relative to that of conventional solvent borne systems. Because of their versatility and environmental friendliness, aqueous PUDs are now one of the most rapidly developing and active branches of polyurethane (PU) chemistry and technology.

Polyurethanes (PU) are segmented polymers comprising of alternating sequences of soft segments and hard segments that constitute a unique microphase-separated structure. Ions can be readily introduced into either hard or soft segments of polyurethanes to yield a wide range of polyurethane ionomers with prescribed properties [32,33]. There has been extensive work done in the field of synthesis and characterization of various kinds of polyurethanes and polyurethane ionomers [34–36]. Ionomer type PU dispersion is made by the dispersion of amphiphilic prepolymers prepared by the addition of diisocyanates, polyols, and dimethylolpropionic acid (DMPA) and subsequent chain extension [37–39]. As in the case of conventional segmented polyurethanes, polyurethane ionomers contain low-polarity flexible segments and urethane groups that are polar and capable of interaction via hydrogen bonds. Ionic groups in a polyurethane tend to interact with each other and aggregate but are attached to the ‘alien’ hydrophobic neighborhood. As will be demonstrated later, by varying the structure, molecular weight of the segments, and the ratio of the soft to the hard segments, a broad range of physical properties can be obtained. The materials can be hard and brittle, soft and tacky, or anywhere in between.

Various types of diisocyanates can be used to synthesize PU as depicted in Table 1. The diisocyanates can be either aromatic or aliphatic with different chemical reactivities. The aromatic diisocyanates are more reactive than aliphatic ones, which can only be utilized if their reactivities match the specific polymer reaction and special properties desired in the final product. For example, polyurethane coatings made from aliphatic isocyanates are light stable [40–43], while coatings made from an aromatic isocyanate will undergo photodegradation [44,45].

The soft segments used in polyurethane elastomers are dihydroxy terminated long chain macroglycols with low molecular weight ( $M_w = 500\text{--}5000\text{ g/mol}$ ) such as polyethers, polyesters, polydienes and polyolefins (Table 2). Polyester-based urethanes are very sensitive to the hydrolytic cleavage of the ester linkage compared to polyether-based urethanes. Kim et al. developed a new type of polyester polyol, with alkyl side groups, such as poly(2,4-diethyl-1,5-pentamethylene adipate) glycol (PDPAd) to improve the hydrolytic stability of waterborne PUD [46]. Polyethylene oxide (PEO) based urethanes exhibit poor water resistance due to the hydrophilic nature of the ethylene oxide. The low cost and reasonable hydrolytic stability of polypropylene oxide (PPO) make it a good candidate for a wide range of applications [47].

Polyurethanes properties and applications are primarily dependent on the low molecular weight chain extenders. Poor physical properties of polyurethane with no microphase separation between the hard and soft

segments are normally produced by a direct reaction of diisocyanate and polyol without the chain extension step. Therefore, excellent mechanical properties of polyurethane can be obtained by introduction of a chain extender to increase the hard segment length and to permit microphase separation and consequently increase the modulus and glass transition temperature ( $T_g$ ) of the polymer. Polyurethane chain extenders can be categorized into two classes: aromatic diol and diamine, and the corresponding aliphatic diol and diamine. In general, polyurethanes that are chain-extended with an aliphatic diol or diamine produce a softer material than do their aromatic chain-extended counterparts [48]. Common chain extenders for polyurethane synthesis are shown in Table 3.

Basically, PUs are hydrophobic (immiscible with water). However, it is possible to emulsify, disperse or even dissolve the PUs in water if necessary structural modifications are done. PUs can be dispersed in water with the aid of a protective colloid, external emulsifier or by structural modification [14,49]. The first two methods suffer from a few disadvantages, as they require strong shear force to disperse the polymer, which results in coarse particles and poor dispersion stability. A special method of dispersing PU in aqueous media is by structural modification, i.e., modifying hydrophobic PU backbone with built-in hydrophilic groups [49]. This emulsifier is usually a diol with ionic groups (carboxylate, sulfonate, or quaternary ammonium salt) or non-ionic groups [poly(ethylene oxide)]. For example,  $\alpha,\alpha$ -dimethylolpropionic acid (DMPA), is bound to the polymer as an internal emulsifier. Then a base group, typically triethylamine (TEA), is used to neutralize these acid groups. This technique of built-in hydrophilic groups is termed internal emulsifiers or self-emulsifiers. It provides four advantages to PU molecules; (i) the hydrophilically modified PU can be dispersed under mild conditions; (ii) dispersions with finer particle size are obtained and hence the stability of the dispersion is subsequently increased; (iii) the emulsion has good dispersion stability; (iv) the films formed from the dispersion have improved solvent and water resistance.

Several processes have been developed for the synthesis of PUDs. In industry, PUDs can be prepared by several methods, such as the so-called acetone process, prepolymer emulsification process, melt dispersion, and cetimine–cetazine processes. The first two methods are the most widely used in industry. The acetone process is used to prepare PUDs for adhesives applications, while the prepolymer emulsification process is used to prepare PUDs for coatings industry. The preparation of PUDs by the prepolymer emulsification mixing process has received some attention in the literature [50–60]. Typically a prepolymer is synthesized by the reaction of suitable diols (see Table 2) with a molar excess of diisocyanates (see Table 1) in the process just mentioned. Internal emulsifier or surfactant is added to the mixture to allow the dispersion of the polymer in water; where the internal emulsifier will form part of the polymer main chain. Organic solvent (typically N-methylpyrrolidone (NMP)) with approximately 15 wt% is used to dissolve the internal surfactant and reduce the viscosity of the medium. Finally, the prepolymer is dispersed

**Table 1**  
Different types of diisocyanates used to synthesize PUDs.

Chemical structure	Name of diisocyanates
	1,5-Naphthalene diisocyanate (NDI)
	2,4-, 2,6-Toluene-diisocyanate (TDI)
	3,3'-Tolidene-4,4'-diisocyanate
	3,3'-Dimethyl-diphenylmethane-4,4'-diisocyanate
	4,4'-Methylenediphenyl diisocyanate (MDI)
	Para-phenylene diisocyanate
	Cyclohexyl diisocyanate
$\text{OCN-CH}_2\text{-}\overset{\text{CH}_3}{\underset{\text{CH}_3}{\text{C}}}\text{-CH}_2\text{-}\overset{\text{CH}_3}{\text{CH}}\text{-CH}_2\text{-CH}_2\text{-NCO}$	2,2,4-Trimethyl-1,6-hexamethylene diisocyanate
	4,4'-Dicyclohexylmethane diisocyanate
	Isophorone diisocyanate
$\text{OCN-CH}_2\text{-CH}_2\text{-CH}_2\text{-CH}_2\text{-CH}_2\text{-CH}_2\text{-NCO}$	1,6-Hexamethylene diisocyanate

in water followed by chain extension with a water-soluble diamine to build up the molecular weight of the polymer.

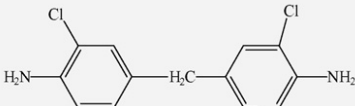
The so-called 'acetone process' is an alternative route to preparing PUDs [61–68]. The acetone process is the most widely used synthesis method for producing PUDs after the prepolymer process [61–68]. The chain extension and dispersion steps are the main differences between acetone process and prepolymer process. The synthesis of the prepolymer is the same in each process. In the acetone

process, the solvent is acetone (instead of NMP) which is used at relatively high concentrations. The prepolymer is chain extended with diol/diamine, the dispersing groups neutralized and dispersion effected by the slow addition of water to the polymer solution. Finally, the acetone is removed by distillation yielding a product containing no VOCs. Despite this advantage there are very few references [69–74] related to this process in the open literature.

**Table 2**  
Different types of polyols that can be used to synthesize PUDs.

Chemical structure	Polyol names
$\text{HO}-(\text{-CH}_2\text{CH}_2\text{O-})_n\text{-H}$	Polyethylene oxide
$\text{HO}-\left(\text{-CH}_2\underset{\text{CH}_3}{\text{CHO}}\text{-}\right)_n\text{-H}$	Polypropylene oxide
$\text{HO}-(\text{-CH}_2\text{CH}_2\text{CH}_2\text{CH}_2\text{O-})_n\text{-H}$	Polytetramethylene oxide
$\text{HO}-\left(\text{-C}\underset{\text{CH}_3}{\text{CH}_2}\text{-}\right)_n\text{-OH}$	Polyisobutylene
$\text{HO}-(\text{-H}_2\text{C}=\text{HC}=\text{CHCH}_2\text{-})_n\text{-OH}$	1,4-Polybutadiene diol
$\text{HO}-\left(\text{CH}_2\right)_2\left(\text{O}-\overset{\text{O}}{\parallel}{\text{C}}-\left(\text{CH}_2\right)_2-\overset{\text{O}}{\parallel}{\text{C}}-\text{O}-\left(\text{CH}_2\right)_2\right)_n\text{-OH}$	Polyethylene adipate
$\text{HO}-\left(\text{CH}_2\right)_4\left(\text{O}-\overset{\text{O}}{\parallel}{\text{C}}-\left(\text{CH}_2\right)_4-\overset{\text{O}}{\parallel}{\text{C}}-\text{O}-\left(\text{CH}_2\right)_4\right)_n\text{-OH}$	Polytetramethylene adipate
$\text{HO}-\left(\text{CH}_2\right)_5\left(\text{O}-\overset{\text{O}}{\parallel}{\text{C}}-\left(\text{CH}_2\right)_5\right)_n\text{-OH}$	Polycaprolactone
$\text{H}-\left(\text{O}-\text{CH}_2-\left(\text{CH}_2\right)_2-\text{CH}_2-\text{O}-\overset{\text{O}}{\parallel}{\text{C}}-\text{C}_6\text{H}_4-\overset{\text{O}}{\parallel}{\text{C}}-\right)_{n_1}\left(\text{O}-\text{CH}_2-\left(\text{CH}_2\right)_2-\text{O}-\overset{\text{O}}{\parallel}{\text{C}}-\text{CH}_2-\left(\text{CH}_2\right)_2-\text{CH}_2-\text{O}-\overset{\text{O}}{\parallel}{\text{C}}-\right)_{n_2}\text{-OH}$	Poly(hexylene adipate-isophthalate) diol

**Table 3**  
Different types of chain extenders used to synthesize PUDs.

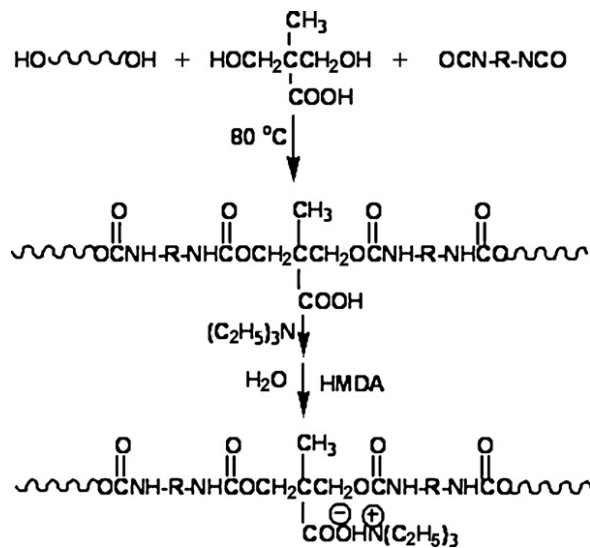
Chemical structure	Chain extender name
$\text{OH}-\text{CH}_2\text{CH}_2\text{CH}_2\text{CH}_2-\text{OH}$	1,4-Butandiol
$\text{OH}-\text{CH}_2\text{CH}_2\text{CH}_2\text{CH}_2\text{CH}_2\text{CH}_2-\text{OH}$	1,6-Hexandiol
$\text{OH}-\text{CH}_2\text{CH}_2-\text{OH}$	Ethylene glycol
$\text{NH}_2-\text{CH}_2\text{CH}_2-\text{NH}_2$	Ethylene diamine
	4,4'-Methylene bis(2-chloroaniline)
$\text{NH}_2-\text{CH}_2\text{CH}_2\text{CH}_2\text{CH}_2\text{CH}_2\text{CH}_2-\text{NH}_2$	1,6-Hexamethylene diamine

## 2. Synthesis of PUDs

### 2.1. Prepolymer emulsification process

In a typical prepolymer emulsification process, the polymerization is carried out in a constant temperature oil

bath [58,59]. Poly(hexylene adipate-isophthalate) diol and dimethylolpropionic acid (DMPA) are charged into the dried flask at 70 °C. While stirring, NMP (12 wt% based on total feed) is added and stirring is continued until homogenized mixture is obtained [58]. Isophorone diisocyanate (IPDI) and dibutyl tin dilaurate (DBTDL, catalyst) are added



Scheme 1.

drop wise and stirring is continued for 30 min at 70 °C. The mixture is then heated to 80 °C for about 3 h to afford NCO terminated prepolymers. The change of the NCO content during the reaction is determined using a standard dibutylamine back titration method [58]. Upon reaching the theoretical NCO value, the reactions are cooled to 60 °C, and the neutralizing solution [i.e., triethyl amine, TEA, (DMPA equiv.) dissolved in NMP (2 wt%)] is added and followed by stirring for 30 min while maintaining the temperature at 60 °C.

The neutralized prepolymer is added to the mixture of water and surfactant (4 wt% based on total solid) under agitation at 750 rpm to produce the dispersion. After 20 min, 20 wt% solution of hexamethylene diamine (HMDA) in water is added over a period of 30 min, and chain extension carried out for the next 1 h. At the end, a defoamer (Foamstar-I) is added, and stirring continued for 5 min at a speed of 250 rpm. For experiments requiring control of the polymer molecular weight, diethyl amine is included in the chain extension step. In the preparation of all polymers the ratio of isocyanate groups/amine groups (from chain extension/termination) was 1.1/1. The elementary steps for the synthesis of PUD through NMP-process are shown in Scheme 1.

## 2.2. Acetone process

In this process, 73.3 g of the polyester diol (0.071 hydroxyl equiv.) and 3.1 g of DMPA (0.046 hydroxyl equiv., 0.023 acid equiv.) are charged to the reactor [75]. While mixing, 85 g acetone is added and stirring is continued until a homogeneous mixture is obtained. IPDI (21.2 g, 0.19 isocyanate equiv.) and 3 drops of DBTDL are added dropwise with continued stirring at 60 °C. Upon reaching the theoretical NCO value, the prepolymer is chain-extended with butane diol, BD (2.4 g, 0.053 hydroxyl equiv.) and the reaction is allowed to continue for 2 h to complete the polymerization. The final polymer is neutralized by the addition of 2.3 g triethyl amine (0.023 equiv.) and stirred for 30 min

while maintaining the temperature at 55 °C. Formation of the dispersion is accomplished by slowly adding water to the neutralized acetone solution of the polyurethane polymers at 45–50 °C over 30 min with agitation speed of 600 rpm. After stirring for 30 min the reaction mixture is transferred to a rotary evaporator and the acetone removed at 35 °C and a partial vacuum of 70 mm Hg to afford organic solvent free dispersion. The reaction in Scheme 2 shows the elementary steps for the synthesis of PUD via acetone process.

## 3. Characterization of PUDs

### 3.1. Particle size and dispersion stability

The effect of DMPA content on particle size and viscosity  $\eta$  of the PUDs prepared via prepolymer emulsification and acetone processes is shown in Fig. 1a and b, respectively [58,59]. For all samples the other parameters were kept constant for this portion of the study with 32 wt% solids, with neutralization and chain extension to 90%. For both series of PUDs (i.e., prepolymer and acetone process), the particle size decreased dramatically with an increase in DMPA content and then decreased slowly or remained constant at higher DMPA concentrations,  $\eta$  showed a corresponding increase with DMPA content, and remained almost constant after 5 wt%. With increasing DMPA content and a stoichiometric amount of  $N(C_2H_5)_3$ , the number of  $-COO^-HN^+(C_2H_5)_3$  ionic groups in PU dispersion increased. Each particle in the dispersion is absorbed by a thin layer of water due to the presence of hydrophilic  $-COO^-HN^+(C_2H_5)_3$  groups on the surface of the

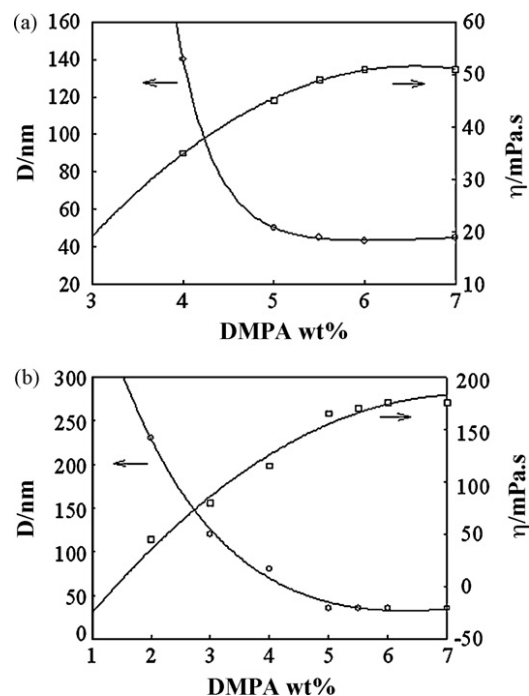
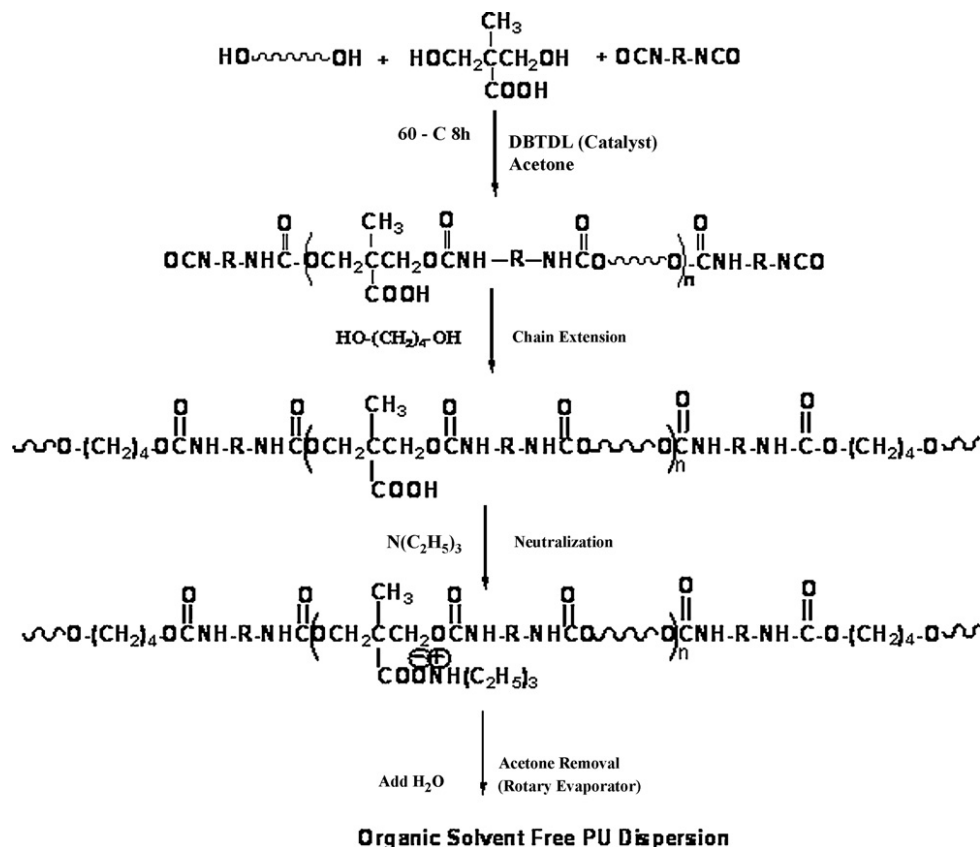


Fig. 1. Effect of DMPA content on the diameters of the particle size and viscosity of PUDs prepared via: (a) prepolymer emulsification process and (b) acetone process (modified from [58,59]).



Scheme 2.

particle. With a decrease in the size of polymer dispersion particles, the relative size of the water layer to total particle size is increased. Concurrent with the particle size decrease there is an increase in the number of particles. Hence, the effective volume of the dispersed phase increases, resulting in an increase in viscosity. The pH of the PU dispersions decreased slightly from 8.3 to 7.7 with an increase in DMPA content from 4 to 7 wt%. To prepare stable dispersions, 4 and 2 wt% of DMPA were required in prepolymer emulsification and acetone processes, respectively. The reason why the prepolymer process required a high concentration of DMPA could be attributed to either a decrease in surface activity of the carboxylate group on the surface of PU particles caused by NMP or a decrease in the stability of the particles resulting from the low molecular weight prepolymers [58,59].

### 3.2. Overview of recent literature on aqueous PUDs

Aqueous PUDs with different solid contents of up to 50% have been synthesized by Li et al. [62]. The synthesis of the prepolymer based on isophorone diisocyanate (IPDI) and poly-1,4-butylene adipate glycol (PBA) with different molecular weight ( $M_n = 1000, 2000, \text{ and } 3000$ ) was carried out via the acetone process. The effects of the DMPA content, NCO/OH molar ratio, and molecular weight ( $M_n$ ) of the diol (soft segment) on the properties of PUDs were studied. Dynamic light scattering results revealed

that, with increasing concentration of DMPA, small particles with narrow distribution could be obtained. The molar ratio of NCO/OH plays an important role in controlling the particle size. For example, the particle size decreased slightly when  $\text{NCO/OH} \leq 1.5$ , while it reached a maximum value at  $\text{NCO/OH} = 1.7$ . The particle size decreased dramatically with NCO/OH molar ratio higher than 1.7. The TEM micrographs of the PUDs (Fig. 2) revealed that only the dispersions prepared with diol of  $M_n = 1000$  and  $2000$  g/mol have spherical particle size dispersed in water. Increasing the molecular weight created irregular elongated particle shape as clearly evident in Fig. 2.

Aruna and Kumar [76] prepared aqueous PUDs from isocyanate-terminated ionic polyurethane prepolymers by chain extension with dihydrazides. Excellent adhesive properties have been reported for these waterborne dispersions that can be used to bond leather and canvas [76]. The base polymers were synthesized as a function of: (1) concentration of DMPA with chain extender constant and (2) different chain extenders with constant concentration of DMPA. The DMPA content was found to have strong influence on the particle size and viscosity of the dispersion (e.g., the particle size decreased and the viscosity increased with increasing DMPA content). A shear strength and peel strength analysis of specimens revealed that the waterborne dispersions were excellent adhesives for bonding leather surfaces. Thus, a very efficient, eco-friendly waterborne dispersion of polyurethane that could

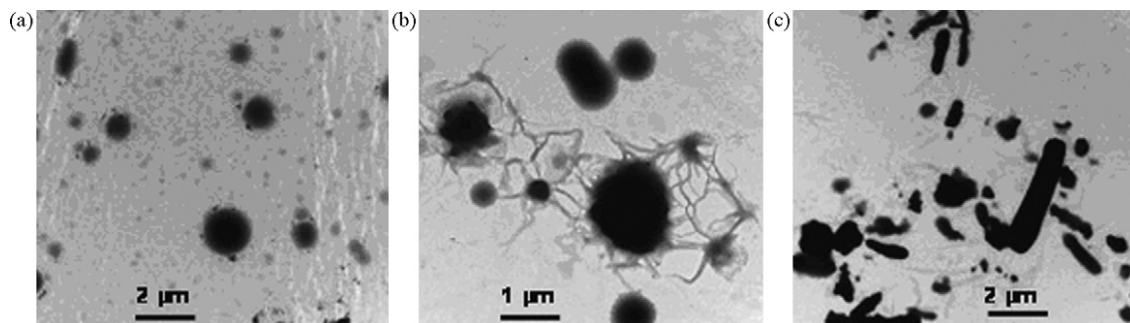


**Fig. 2.** TEM micrographs for PUDs prepared from different  $M_n$  of polyol with keeping the concentration of DMPA content: (a) 1000 g/mol; (b) 2000 g/mol; (c) 3000 g/mol (modified from [62]).

find applications in bonding leather in the footwear industry was successfully prepared.

Aqueous PUDs were prepared from toluene diisocyanate, polytetramethylene glycol, and 1,4-butanediol, with different weight percent of DMPA as anionic center [77]. IR spectroscopy was used to follow the polymerization reaction. The effect of DMPA content on the particle size distribution was studied. Average particle size of the prepared emulsion polyurethanes decreased with increasing DMPA content. In addition, the contact angle decreased by increasing the ionic content. The decreased contact angle was ascribed to the increase in the hydrophilicity of the polyurethanes because of the incorporation of more hydrophilic moiety in the polymer backbone.

A series of waterborne polyurethanes containing different amounts of DMPA were synthesized by Rahman and Kim using a prepolymer mixing process [78]. Relationships between the DMPA content and physical, mechanical, and thermal properties, as well as, adhesive behavior under different use conditions were investigated. Stable aqueous dispersions were obtained when the DMPA content was more than 10 mol%. At higher DMPA content, the particle size of the dispersion was lower but the viscosity of the dispersion was higher.

Wei and Xin synthesized in acetone a series of anionic polyurethane with different molecular structures [79]. Different hexamethylene diisocyanate (HDI) and toluene diisocyanate (TDI) were employed in the synthesis. When the DMPA content was 0.3 mmol/g, the colloidal stability of the polyurethane dispersions (with nanoscale particle size) was good. No additional acetone was necessary during the process of emulsification. The structures of the polyurethane were characterized by FTIR-ATR spectrometry and GPC. It was found that the mass ratio of HDI to TDI could be quantitatively analyzed by means of FTIR-ATR. The molecular weight and distribution did not show a regular trend with the changing of HDI/TDI ratio. The influence of diisocyanate on the particle size and the coating properties was also studied. It was found that HDI played a dominant role in obtaining nanoscale particles. These polyurethane dispersions gave an average particle size less than 100 nm when mass ratio of HDI/TDI was above 0.25. The polyurethane dispersions with nanoscale particles had a transparent appearance that gave a bluish cast film. The authors indicated that the hydrophilic efficiency would be

improved and the coating hardness decreased if more HDI was employed [79].

PUDs have been designed and synthesized based on different types of soft segments, namely, poly(2,4-diethyl-1,5-pentamethylene adipate) glycol (PDPAD) and poly(2,4-diethyl-1,5-pentamethylene-1,4-cyclohexane dicarboxylate) glycol (PDPCD) [80]. These dispersions were subsequently modified with fluoro oligomer (BA-N fluoroalc.). The hydrolytic stability was found to be significantly improved by the PDPCD segments while the contact angle with water drop increased with increasing the amount of Zonyl for PDPAD-based PU. In addition contact angle was marginally increased with PDPCD-based PU. Furthermore, the PDPCD provided PUD with enhanced mechanical properties compared with the PDPAD.

Environmentally friendly vegetable-oil-based waterborne polyurethane dispersions with very promising properties have been successfully synthesized without difficulty from a series of methoxylated soybean oil polyols (MSOLs) with different hydroxyl functionalities ranging from 2.4 to as high as 4.0 [81]. Fig. 3 shows the TEM image of the particle size for the soybean-oil-based waterborne polyurethane (SPU) dispersions. In general, control of the average particle size is important with respect to the specific application of the PU dispersions. For example, dispersions of relatively larger particles are preferred in surface coatings for rapid drying, and smaller particle sizes are desirable when deep penetration of the dispersion into a substrate is essential. The SPU-135 (the number 135 denotes the total OH number in the MSOL) dispersion was found to be clear with an average particle size of approximately 12 nm diameter. The particle size of the SPU dispersion increased with increasing OH functionality of the MSOL; average particle sizes of approximately 60 and 130 nm diameter were observed for the SPU-149 and SPU-200 dispersions, for which the OH functionalities of the MSOLs were about 2.8 and 4.0, respectively. In the study just mentioned [81], the particle size of the SPU dispersions from MSOLs with different hydroxyl functionalities can be controlled in two ways. First, higher cross-linking can be obtained for the dispersions by increasing the OH functionality of the polyols which results in an increase in particle size. However, when the OH number of the MSOL increased, the amount of diisocyanate and DMPA in the system also increased to maintain a constant molar ratio



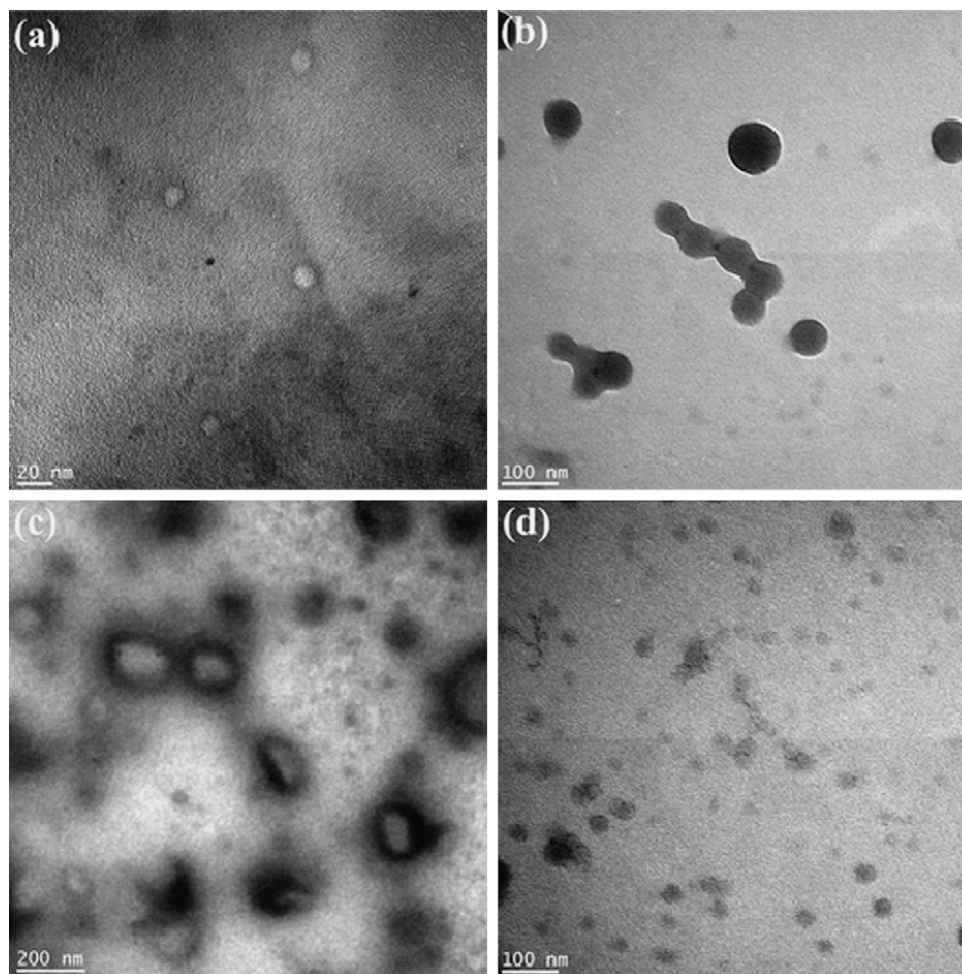


Fig. 3. TEM images of the dispersions of: (a) SPU-135, (b) SPU-149, (c) SPU-200, and (d) SPU-149II (adapted from [81]).

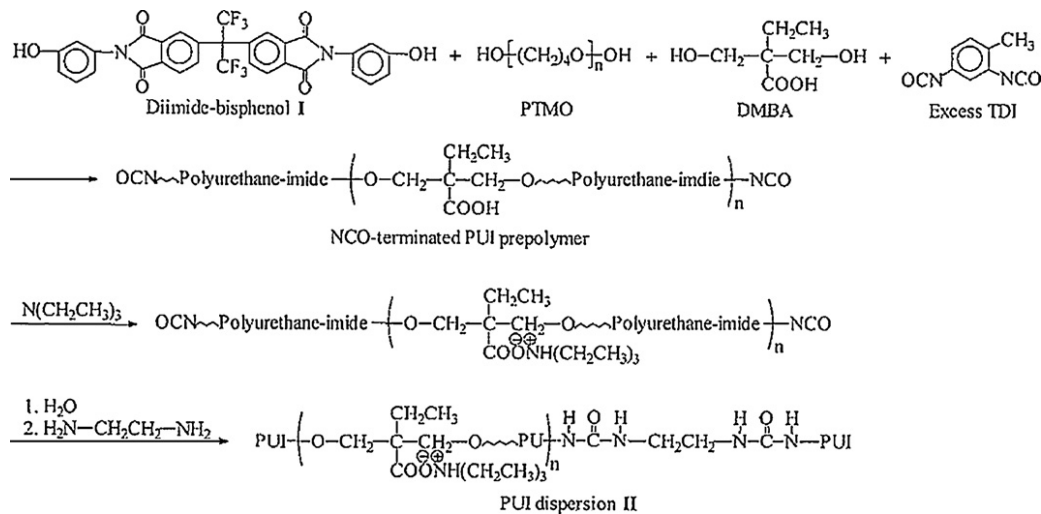
between the NCO and OH groups. The increased content of hydrophilic DMPA should have the opposite effect. Therefore, the increase in the particle size for the resulting SPU dispersions with different OH functionalities in this study [81] is mainly due to the occurrence of higher cross-linking in the SPU dispersions. When compared with SPU-149, SPU-149II exhibits a relatively smaller particle size of about 30 nm diameter, indicating that the DMPA content seems to be a major governing factor in determining the particle size of the SPU dispersions from the same polyol. The relatively wide range of particle size from 12 nm diameter for SPU-135 to 130 nm diameter for SPU-200 suggests that the dispersions prepared by this technology should be quite promising for applications from adhesives to elastomeric or hard coatings.

A series of aqueous anionic PUDs with ionic groups in the soft segments were synthesized by Bao et al. from a polyether glycol, maleic anhydride modified castor oil, isophorone diisocyanate, and  $\alpha,\alpha$ -dimethylolpropionic acid using the prepolymer mixing process [82]. The samples obtained were neutralized by the addition of triethylamine. The reaction mixture was dispersed in water and the polymer chains were extended with ethylene diamine. The effect of NCO/OH molar ratio on the structure

and properties of these polyurethanes were characterized. The particle size distribution became broader and the average particle diameter increased with increasing the NCO/OH molar ratio. This experimental fact was attributed to the decrease in chain flexibility and increase in viscosity of the dispersed particles. IR studies on the system just mentioned showed that the hydrogen bonding increased with increasing NCO/OH molar ratio.

Aqueous PUDs derived from isophorone diisocyanate, various polycarbonatediols of different molecular weights, and dimethylolbutyric acid were prepared by Lee et al. [83]. They found that the molar ratio of reactants affected the properties of the PUDs significantly. The observed trends in properties were related to the effects of their ionic groups and polycarbonatediol soft-segment contents. The molecular weight of the polycarbonatediols also significantly affected the particle size of the aqueous PUDs and the resulting properties of the films made from them. As the molecular weight of the polycarbonatediols decreased, the particle size of the PUDs decreased, as expected.

Poly(urethane-imide) (PUI) was prepared from environmentally friendly PUDs to improve the poor processability of PI and to decrease solvent emission [84]. The PUIs



Scheme 3.

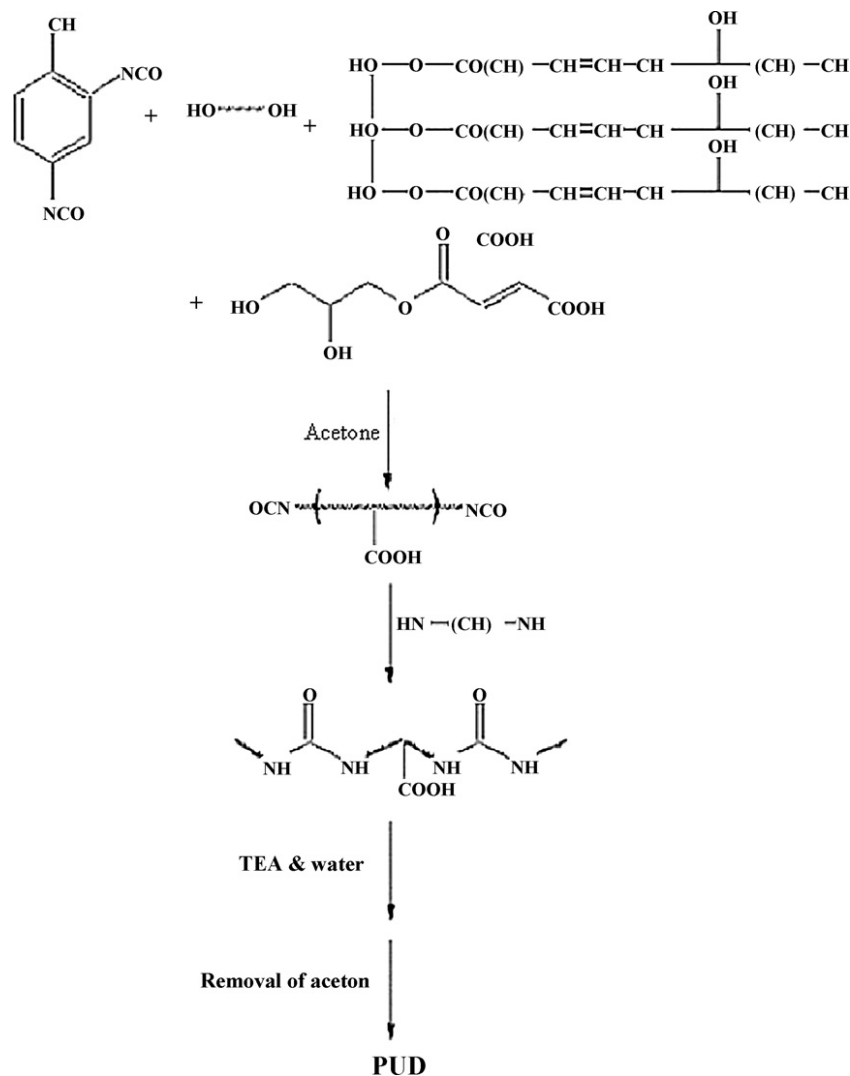
were synthesized using a prepolymer process. A series of PUI dispersions with 25 wt% solid content, viscosities of 7.5–11.5 cps, and particle sizes of 63–207 nm was prepared. The authors studied the possibility of introducing the imide function into the PU backbone by reacting varying concentrations of imide that contains bisphenol with the diisocyanate monomer. In the experiments just mentioned, the authors [84] synthesized the anionic PUI dispersion using toluene diisocyanate (TDI) and 2,2-bis[*N*-(3-hydroxyphenyl)phthalimidyl] hexafluoropropane (I) as the hard segment, 2,2-bis(hydroxymethyl)butyric acid (DMBA) as the ionic center, and poly(tetramethylene oxide) (PTMO) as the soft segment. Reaction in Scheme 3 shows the elementary steps of synthesis of the PUI dispersions. The PUIs exhibited improved thermal stability but with no char yield as the temperature increased. The inclusion of a little imide increased the decomposition temperature of PUI while maintaining the elasticity of the polymer, indicating a successful translation of PUI into the water-based form.

A maleic anhydride modified castor oil (MCO) was used to prepare aqueous PUDs with ionic groups in the soft segments using the prepolymer mixing process [85]. The aliphatic polyether PU prepolymer was prepared with MCO and polyether glycol as the polymeric glycol component. The prepolymer was dispersed under vigorous agitation by adding water and by chain extension with ethylene diamine. The effects of the mass ratio of MCO and polyether glycol on the properties of the resultant waterborne PUDs were studied. Structures and properties of the dispersions were examined by FT-IR, particle size analyzer and SEM. The PUDs exhibited higher phase mixing with increasing mass ratios of MCO and polyether glycol.

Gao et al. [86] synthesized a series of PUDs from castor oil, polypropylene glycol, toluene diisocyanate, and (2*E*)-4-(2,3-dihydroxypropoxy)-4-oxobut-2-enoic acid (glycol semi-ester) (GSE). Scheme 4 shows the typical elementary steps for synthesis of these PUDs. The synthesis reaction could be divided into two steps. The first step is

related to the formation of NCO-terminated prepolymer, and the second one is the chain extension and dispersion in water. The rheological properties, particle size, and morphology of the PUDs just mentioned were examined with a stress-controlled rheometer, light scattering ultrafine particle analyzer, and transmission electron microscopy. The results obtained revealed that the particle size of PUDs mainly depends on the concentrations of castor oil, GSE, and polymer. With increasing GSE concentration and decreasing castor oil and polymer concentration, the particle size decreases as evident in Fig. 4a. This observation can be ascribed to the decrease of the particle size of the polymer dispersion caused by the decrease of the relative size of water layer to total particle size. Similar behavior has been observed by decreasing the concentration of castor oil and solid content as shown in Fig. 4b and c, respectively (i.e., the particle size of PUDs decreases with decreasing concentration of castor oil and solid content). Furthermore, increasing concentrations of castor oil, GSE, and polymer increased the viscosity of PUDs because of the increase of effective volume of the dispersed phase.

An automated synthesis system has been recently employed to produce PUDs [87]. The results of automated chemspeed methods were comparable with that of traditional laboratory methods. A series of PUD synthesis experiments were performed using various process parameters to optimize the procedure used in the automated reactor system. Process variables such as agitator design, rate of neutralization, and rate of water dispersion were varied to obtain the desired product end-use property. The controlled addition of neutralizer, water, and chain extender is an added advantage with this automated technique and gave consistent results. The rate of water addition was found to be the most important parameter that controls the final PUDs properties. This investigation [87] provided some useful indications on how to optimize the properties of aqueous PUDs, and it gave promising product development process in terms of particle size of the dispersions and physical properties of the final product.



Scheme 4.

#### 4. Rheological properties and gelation kinetics of PUDs

Many dispersions including latex systems are known to exhibit complex rheological behavior. Rheological properties of waterborne PUDs systems are of both practical importance and theoretical interest. In addition the stability, digestibility, film forming properties, viscoelastic properties of PUDs are expected to be strongly dependent on their colloidal state, structure and composition. It is therefore essential to understand the rheological behavior of these important dispersions so that they can be prepared and used in a controlled and reproducible manner.

Many of the patents and journal articles on PUDs appear to focus almost exclusively on the application of these interesting systems. There are relatively few reported systematic studies on PUDs to generate basic data aimed at providing fundamental insights into the relationships amongst the polymer structure, rheological properties, and coating performance under conditions that the PUDs are

likely to encounter during use. By systematically varying the solid content and particle size of the present PUDs one can control the particle–particle interactions, phase behavior, morphology, rheology and mechanical properties. The intrinsic differences between the special PUDs of this study and conventional polymer colloids, suspensions, and emulsions require that analyses of the PUDs be based on their actual behavior so as to generate accurate and useful data that will guide the synthesis and processing of this important class of materials. It is hoped that this review article will provide a quantitative and qualitative experimental basis for any future theory development of the relatively new waterborne PUDs and the prediction of their rheological properties, increasing our level of understanding of the behavior of these systems.

In this review article we describe details of the rheological properties of a well-characterized model PUD systems as functions of solid content, degree of pre- and post-neutralization, chain extension and temperature [59]. The rheological data obtained are

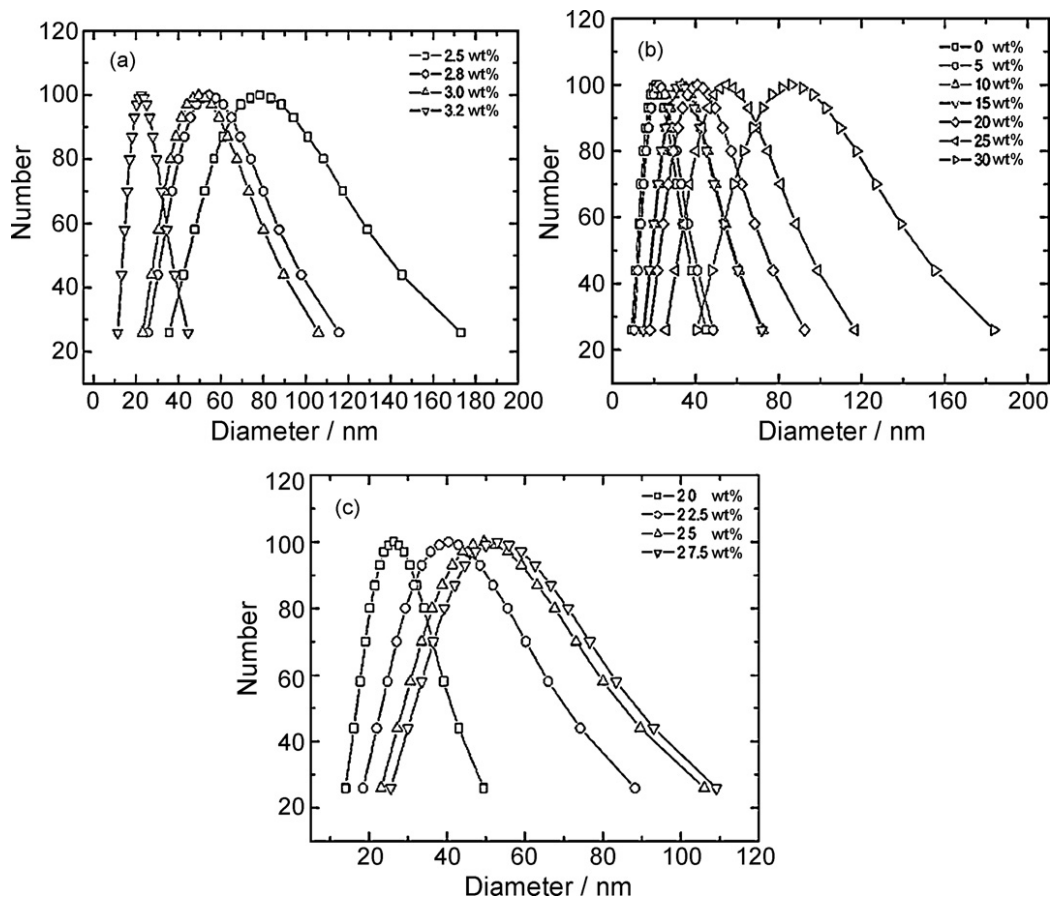


Fig. 4. Particle size distribution of PUDs as a function of: (a) carboxylic acid wt%; (b) castor oil wt%; (c) polymer wt% (modified from [86]).

interpreted using different theoretical principles such as Cross model, Krieger–Dougherty equation and time–temperature–superposition (WLF); where appropriate the viscoelastic behavior of the PUDs will be compared to that of critical gelling systems and Brownian suspensions reported in the literature [60]. It is expected that the rheological behavior of the PUDs can be controlled by changing the experimental parameters used here, providing a fundamental basis for optimizing their applications and performance in response-driven polymer film formation.

#### 4.1. Impact of solid content

A transition of liquid to solid structure as a result of gelation with increasing concentration has been reported for hard sphere dispersions [88]. This transition is manifested as a non-decaying component of the dynamic structure factor and implies a structural arrest of the crowded suspension. Similar phenomenon has been recently reported for weakly attractive soft colloids [88]. The gelation process in the soft colloids just mentioned was found to be intrinsically related to the fluid to solid transition, that is manifested as a kinetic arrest, and is driven by the crowding or clusters of particles. This behavior is a characteristic of a wide range of soft materials that lose their ability to flow at

high volume fractions [88]. Consequently, it is important to understand and control this transition process and in more general terms the different kinds of interactions between the particles during the liquid–solid transition in colloidal dispersions.

Here, we discuss the rheological behavior of PUDs synthesized via prepolymer emulsification process [59]. All of the PUDs samples used in the current studies described here were prepared at 5.5 wt% DMPA, 100% neutralization and chain extended to 90%. The double logarithmic scale of the complex viscosities of PUD as a function of shear frequency at 30 °C for different PU concentrations is shown in Fig. 5. Clearly, this figure shows that the viscosities of the dispersions are strongly influenced by the solid concentration of PU. A frequency independent complex viscosity behavior is observed over the frequency range studied for dispersions having solid concentrations with PU  $\leq$  42 wt%. The viscosity increased dramatically (about 4 orders of magnitude) when the concentration of PU was increased from 24 to 46 wt%. In addition the viscosity decreased with increasing shear frequency. The frequency ( $\omega$ ) dependence of  $|\eta^*|$  is independent of  $\omega$  if  $\omega$  is sufficiently smaller than the reciprocal of the characteristic times  $\lambda$  of all relaxation modes, and the decrease of  $|\eta^*|$  with  $\omega$  simply indicates that some modes have  $1/\lambda$  smaller than  $\omega$  as will be shown later.

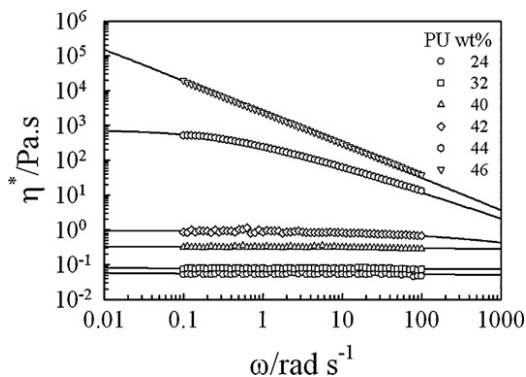


**Fig. 5.** Variation of  $\eta^*$  as a function of shear frequency for PUDs with different PU contents at 30 °C. The lines are computed from Eq. (1) using nonlinear regression technique (adapted from [59]).

The frequency dependence of the dynamic viscosity of PUD can be expressed through the Cross model [89] by the following equation:

$$\eta^* = \frac{\eta_0}{1 + (\omega/\omega_c)^\beta} \quad (1)$$

where  $\eta_0$  is the zero-shear viscosity,  $\omega_c$  is the critical shear frequency value at which the viscosity decreases to half its initial value and  $\beta$  is a material constant that depends on the nature of the dispersion. Eq. (1) is used to calculate  $\eta_0$  as a fitting parameter to the experimental results using non-linear regression analysis. An excellent description of the data was obtained as shown in Fig. 5. Table 4 represents the fitting parameters that were obtained from the regression. Here the lines in Fig. 5 are computed from Eq. (1) using the parameters listed in Table 4, while the points are experimental data [59].

Fig. 6a illustrates the volume fraction ( $\phi$ ) dependence of the dimensionless viscosity of the dispersions,  $\eta_r$  (reduced by the solvent viscosity). The critical volume fraction ( $\phi_c$ ) at which the viscosity of the dispersions increased strongly was determined using Krieger–Dougherty equation [90]:

$$\eta_r = \left(1 - \frac{\phi}{\phi_c}\right)^{-k\phi_c} \quad (2)$$

$$\text{with } \eta_r = \frac{\eta_D}{\eta_S} \quad (3)$$

where  $k$  is a shape parameter,  $\eta_D$  is the viscosity of dispersions and  $\eta_S$  is the solvent viscosity. The experimental data can be described using the above Eqs. (2) and (3), where the symbols are experimental data while the line is the calculated line using  $k$  and  $\phi_c$  as fitting parameters.

**Table 4**

Characteristic rheological parameters for the PUDs with different concentrations using Eq. (1).

PU (wt%)	$\eta_0$ (Pa s)	$\omega_c$ (rad s <sup>-1</sup> )	$\beta$
46	$9.9 \times 10^5$	0.01	0.87
44	738	0.4	0.74
42	0.94	677	0.44
40	0.316	836	0.8
32	0.14	$4.6 \times 10^5$	0.31
24	0.098	$5.8 \times 10^5$	0.287

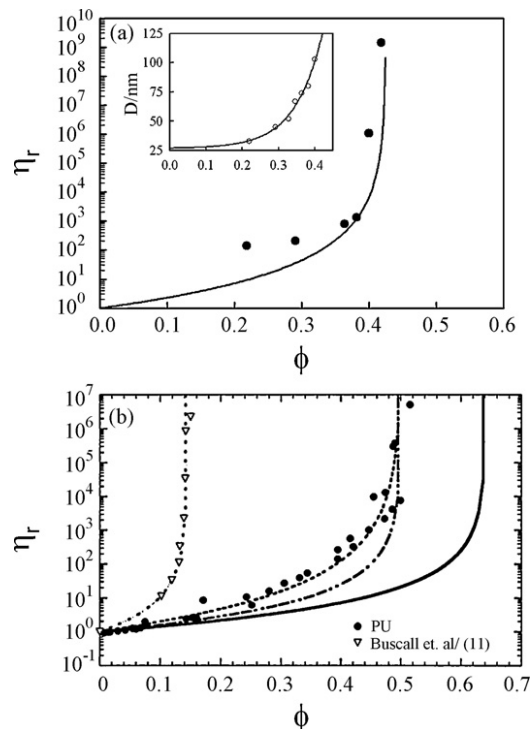


**Fig. 6.** (a) Volume fraction ( $\phi$ ) dependence of reduced viscosity,  $\eta_r$  at 30 °C for the PUDs. The line passing through the experimental data is the fitting line of Eq. (2) using nonlinear regression technique. The inset plot shows the PU particle diameter as a function of volume fraction (adapted from [59]). (b) Relative zero shear viscosity as a function of volume fraction. Also plotted are data on charged spheres from Buscall et al. [63b]. The solid line shows the prediction for model hard sphere suspensions. The line through the data of Buscall et al. is drawn from Eq. (2) with  $\phi_c = 0.144$ . Also shown is Eq. (1) with  $\phi_c = 0.50$  (dash-dotted line) intermediate concentrations. A better fit is obtained if the exponent in Eq. (1) ( $k\phi_c$ ) is set at 3 (dotted line) (adapted from [63]).

It must be stated here that the data shown in Fig. 6a are the values of the zero shear viscosity of the dispersions (i.e.,  $\eta_D = \eta_0$  only for this figure). The value of  $\phi_c$  obtained from this regression analysis was found to be 0.43. The Krieger–Dougherty equation works well for hard spheres dispersions with volume fraction less than 0.55. It is well known that the value of  $\phi_c$  strongly depends on the system under consideration. For example small, mono-dispersed samples show lower value of  $\phi_c$  than that of large ones and  $\phi_c$  increases with polydispersity [91]. The rheological behavior depicted in Fig. 6a is governed by the interplay between the particle–particle interaction (repulsive force between the similar charges surrounding the particles) and hydrodynamic interaction. The interaction potential depends on the charge density on the particle surface. It is essential to mention here that all the samples of different volume fractions were prepared at constant concentration of internal surfactant (5.5 wt% DMPA) [58], i.e., all the particles have similar charge density regardless of the change in the volume fraction. Therefore, the repulsive force between particles should be constant for all concentrations. Another important factor that should be considered is the large increase of the particle size with concentration as clearly depicted in the inset plot of Fig. 6a. The increase in particle

size at a fixed ionic content as a function of solids during the dispersion step is surprising. This may be a result of either (i) the NMP partitioning differently at higher solids (it is fixed at 12% of total system) or (ii) a high NMP content in the continuous phase may decrease dispersant efficiency [58].

The increase in viscosity with concentration is directly related to the increase in particle size [59]. At low concentration the effect of particle size is insignificant because the particles are far apart and do not significantly interact with each other. On the other hand, at high concentration the particles become very crowded and the viscosity increases due to the significant increase in the hydrodynamic interactions between the particles. On the basis of the above discussion, it appears that the interaction potential due to the repulsive force between the similar charged particles is significant at low concentration. However, at high concentration the particle size increases and both the inter-particle distance and interaction potential decrease, making the hydrodynamic interaction the only factor responsible for the observed increase in the viscosity of the PUDs. The poor fitting of the experimental data with Eq. (2) is mainly due to two reasons: the first one is that Eq. (2) is normally used for hard sphere suspensions containing particles that are not deformable under shear flow. The second reason is the observed increase in the particle size of the PU dispersion with increasing volume fraction (see the inset plot of Fig. 6a).

In the case of the acetone process, the dispersion particles are formed early in the phase inversion step as the addition of water causes the polyurethane polymer to phase separate from the acetone water mixture [75]. At this point the ionic concentration of each particle and number of particles are fixed; continued addition of water only dilute the particles. Recently Wicks and Nanda [75] found a slight reduction of PU particle size of PUDs prepared via acetone process with increased solids content. This experimental fact was attributed to the increase of the ionic concentration of the particles.

A simple model for rheological behavior of concentrated colloidal dispersions of hard spheres has been developed by Brady [92]. This model specifies that the viscosity diverges at random close packing because the number of contacting particles becomes infinite and the short-time self-diffusivity vanishes as the touching particles are stuck by the hydrodynamic lubrication forces [92]. In addition, optical measurement of the contributions of colloidal forces to rheology of concentrated suspensions has been reported by Bender and Wagner [93]. The normalized stress-optical coefficients calculated from dichroism and viscosity measurements of near hard-sphere colloidal suspensions were found to be relatively constant with respect to the volume [93]. Eq. (2) has been used to fit the data of different dispersions as shown in Fig. 6b [63]. This equation under predicts the viscosity at intermediate concentrations and over predicts the viscosity at high concentrations. The smaller value of  $d\eta_0/d\phi$  at high concentration is attributable to the PU particles ability to deform. The enhancement of viscosity at intermediate concentrations is suggestive of long-range interactions. Similar behavior has been observed for low cross-linked den-

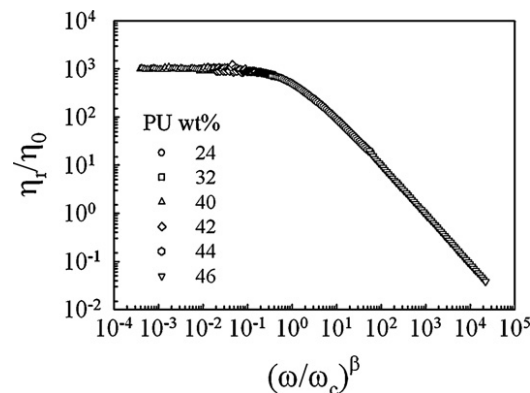


Fig. 7. Master curve of normalized viscosity,  $\eta_r/\eta_0$  at 30 °C for PUDs with different PU concentrations discussed in the text (adapted from [59]).

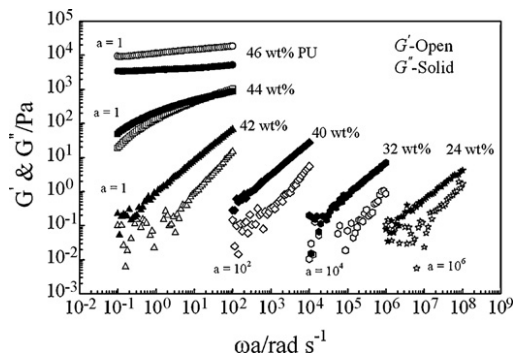
sity polymethylmethacrylate microgels. In this system, the viscosity enhancement was attributed to increased interparticle interactions from low polymer segment density tails at the particle surface. This effect was more pronounced for the lower cross-link density microgels.

The master curve of the dynamic viscosity of PUD at different concentration can be obtained by normalizing the relative viscosity  $\eta_r$  by zero shear viscosity and the shear frequency by the critical shear frequency  $\omega_c$  for each concentration [94]. This can be simply described by the following relation:

$$\frac{\eta_r}{\eta_0} = f\left(\frac{\omega}{\omega_c}\right)^\beta \quad (4)$$

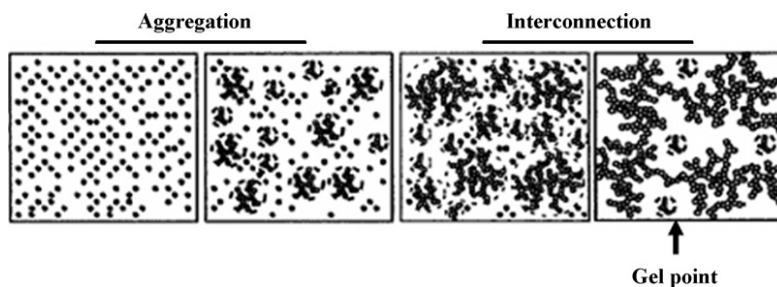
where  $f(\omega/\omega_c)^\beta$  is assumed to be a universal function, independent of molecular weight, concentration and temperature. From Eq. (4) it is apparent that the parameters  $\eta_0$ ,  $\omega_c$  and  $\beta$  are crucial in calculating the master curve. These parameters were accurately evaluated for different concentrations of PU at 30 °C (Table 4) by fitting the classical frequency dependence of dynamic viscosity to the Cross model [89], as shown earlier in Fig. 5. A satisfactory master curve for PUD was obtained at 30 °C as shown in Fig. 7. The master curve shows frequency independent behavior at small shear frequency range followed by strong frequency dependent behavior at high frequencies. This is an important result that should be useful in predicting the behavior of the PUDs especially under deformation and flow conditions that are experimentally inaccessible.

Fig. 8 demonstrates the effect of PU concentration on the dynamic shear moduli,  $G'$  and  $G''$  at 30 °C. The x-axis was shifted to higher frequency range by a factor  $a$  ranging from 1 to  $10^6$  as shown in the figure to obtain a valid comparison. One can see that the values of both  $G'$  and  $G''$  are increased with increasing PU wt% in the dispersions (i.e., the higher the concentration of PU the higher the values of  $G'$  and  $G''$ ). The fact that, the magnitudes of  $G'$  and  $G''$  are increased strongly with composition (especially at 44 and 46 wt% PU) suggests that PUD can form a critical gel (fractal structure) with high PU content. It is apparent that the magnitudes of  $G'$  are much lower than that of  $G''$  for all concentrations in the range of PU wt%  $\leq 42$  and both of them are shear frequency dependent. For 44 wt% PU the values of  $G'$



**Fig. 8.** Dynamic shear moduli,  $G'$  (open symbols) and  $G''$  (solid symbols) as a function of shear frequency for the PUDs with different PU contents at 30 °C. The x-axis is extended by a factor  $a = 1-10,000$  to obtain a valid comparison (adapted from [59]).

becomes a little higher than  $G''$  only at the higher frequency range indicating that 44% PU is located in the gel boundary. At 46 wt% PU the values of  $G'$  and  $G''$  are no longer frequency dependent and  $G'$  is almost one order of magnitude higher than  $G''$ . This is a typical behavior for the formation of a fractal structure or gel that is attributed to the strong interaction between the particles, leading to optimal packing. The experimental fact that the magnitudes of  $G'$  and  $G''$  are frequency independent is ascribed to the formation of an equilibrium modulus,  $G_{eq}$ , a typical criterion for the formation of an elastic gel. It is remarkable that the gelation behavior of PUD with 46 wt% PU is in good agreement with the kinetic modeling of aggregation and gel formation in quiescent dispersions of polymer colloids postulated by Lattuada et al. [95]. Based on this model, the gel is formed by fractal aggregations that have grown to such an extent that they occupy the total volume of the dispersion. In order to form the network the aggregates have to interconnect with each other. This interconnection step is quite different from the preceding aggregation step in that the aggregates do not diffuse randomly but directly experience their nearest neighbors. Therefore, they have to move cooperatively in order to rearrange their spatial configuration substantially, becoming increasingly unlikely near the gel point [95]. Fig. 9 shows schematically that the formation of gel, the aggregation and interconnection steps are not identical as already discussed [95]. On the basis of the preceding discussion it is apparent that the viscoelastic behavior of the PUDs explored in this review article can be divided into two different regimes. At wt% PU  $\geq 44$  (regime 1), the disper-



**Fig. 9.** Schematic diagram of aggregation and gel formation (adapted from [95]).

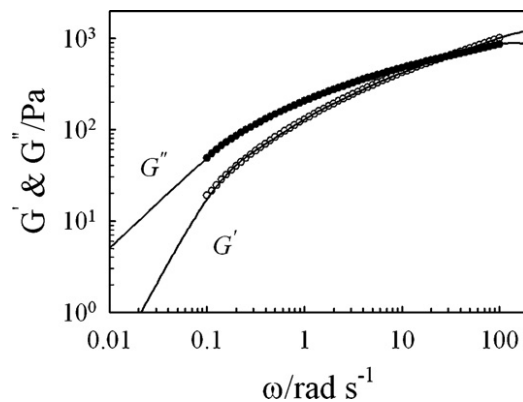


**Fig. 10.** Dynamic shear moduli  $G'$  and  $G''$  as a function of shear frequency for the PUD with 44 wt% PU at 30 °C. The solid lines are calculated from the Maxwell model of multiple modes (Eqs. (5) and (6)) (adapted from [59]).

sions behave as critically gelling systems [96,97]; however, on the other hand, in the second regime at wt% PU  $\leq 42$ , the dispersions behave as typical Brownian suspensions [92,93,98].

The above dynamic data can be modeled using the generalized Maxwell model/Maxwell–Wiechert model, according to the following equations [99]:

$$G'(\omega) = \sum_0^{\infty} \frac{G_i \omega_i^2 \lambda_i^2}{1 + \omega_i^2 \lambda_i^2} \quad (5)$$

$$G''(\omega) = \sum_0^{\infty} \frac{G_i \omega_i \lambda_i}{1 + \omega_i^2 \lambda_i^2} \quad (6)$$

where  $\lambda_i$  is the characteristic relaxation time,  $G_i$  is the elastic constant,  $\omega$  is the angular frequency and  $i$  indicates the number of modes required to fit the dynamic moduli. The experimental data shown in Fig. 8 can be fitted well with a number of Maxwell elements connected in series as described by the above Eqs. (5) and (6). Fig. 10 shows an example of the dynamic shear moduli for 44 wt% PU as a function of angular frequency. The lines drawn through the experimental data are the fitting lines using the Maxwell model. Excellent description of the data was obtained with five Maxwell elements in series.

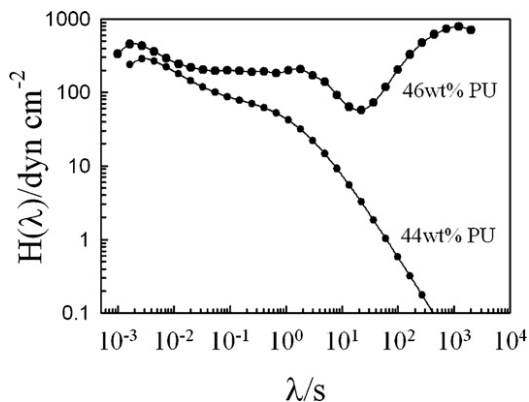


**Fig. 11.** Relaxation spectra of 44 and 46 wt% PUDs at 30 °C (adapted from [59]).

The distribution of relaxation times for PUDs can be examined based on the inverse Laplace transformation:

$$G'(\omega) = \int_{-\infty}^{\infty} H(\lambda) \left[ \frac{\omega^2 \lambda^2}{1 + \omega^2 \lambda^2} \right] d(\ln \lambda) \quad (7)$$

$$G''(\omega) = \int_{-\infty}^{\infty} H(\lambda) \left[ \frac{\omega \lambda}{1 + \omega^2 \lambda^2} \right] d(\ln \lambda) \quad (8)$$

where  $H(\lambda)$  is the relaxation spectrum and  $\lambda$  is the relaxation time. Fig. 11 shows the relaxation spectra for 46 and 44 wt% PU samples. Three relaxation peaks can be clearly seen for the 46 wt% PU, however, only two relaxation peaks were observed for the 44 wt% PU sample. The relaxation peak appearing at very long relaxation time for the sample of 46 wt% PU is related to the dynamics of the highly solid structure of the fractal gel ( $G'$  is much higher than  $G''$  as shown in Fig. 8) that is typically characterized by a very long relaxation time. This relaxation peak does not appear in any other composition of lower PU concentration. Other two relaxation peaks appear around 0.002 and 2 s for the two samples showing a slight composition effect. Clearly these results show that the variation of volume fraction of PU leads to a significant change in the relaxation spectrum particularly near the critical composition where the dispersion changes from a liquid-like consistency to a solid-like structure (fractal gel).

#### 4.2. Effect of degree of neutralization

All the samples used here to study the neutralization effects were prepared at 32 wt% solids, with 5.5 wt% DMPA and chain extension up to 90%. The degree of pre-neutralization was found to have no significant effect on the rheological behavior of PUD. The PUD (32 wt% PU) has a nearly constant viscosity (i.e., frequency independent) behavior regardless of the degree of pre-neutralization. To study the effect of the degree of post-neutralization, additional triethyl amine (TEA) was added to the PU dispersions made with different levels of pre-neutralization. The viscosity of PUD changed dramatically by the degree of post-neutralization. Fig. 12 shows the shear frequency

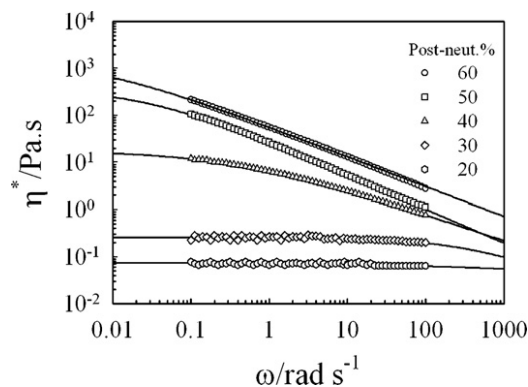


**Fig. 12.** Variation of  $|\eta^*|$  as a function of shear frequency for PUDs with different degrees of post-neutralization at 30 °C. The lines are computed from Eq. (1) using non-linear regression technique (adapted from [59]).

dependence of the complex viscosity of PUD with different degrees of post-neutralization at 30 °C. The viscosity increases dramatically (three orders of magnitude) by increasing the degree of post-neutralization from 30% to 60%. The solid lines are computed from Cross model (Eq. (1)). The fitting parameters obtained from this regression are listed in Table 5. This dramatic increase in the viscosity of PUD is attributed to the trapping of the  $-\text{COOH}$  groups inside the core of the particle. During the post-neutralization process the  $-\text{COOH}$  groups will be converted to the hydrophilic  $-\text{COO}^-\text{HN}^+(\text{C}_2\text{H}_5)_3$  groups that can attract some water molecules inside the particle, leading to an increase in the particle size while keeping the number of the particles constant. Consequently, the free volume decreases and the viscosity increases. The decrease in the free volume and the increase in the particle size is schematically illustrated in Fig. 13. Additional details on the chemical reaction mechanisms of the PUD neutralizations are given elsewhere [58].

The effect of degree of post-neutralization on the distribution of relaxation times is shown in Fig. 14. Obviously, the relaxation spectrum changes significantly with the variation of the degree of post-neutralization. At high degree of post-neutralization such as 60% and 50%, two relaxation processes are detected, however, only one relaxation process is observed at low degrees of post-neutralization, such as 40% (Fig. 14). The relaxation peak appearing at low relaxation time (0.0025 s) does not change with the different degrees of post-neutralization. But the peak appearing at long relaxation time is shifted to long relaxation time with increasing degree of post-neutralization and disappears with decreasing degree of post-neutralization, as shown for 40 wt% post-neutralization (Fig. 14). Therefore, this relax-

**Table 5**  
Characteristic rheological parameters for the PUD with different degrees of post-neutralization using Eq. (1).

Post-neutralization (%)	$\eta_0$ (Pa s)	$\omega_c$ (rad s <sup>-1</sup> )	$\beta$
60	$1.6 \times 10^3$	0.0053	0.63
50	$3.6 \times 10^2$	0.026	0.71
40	15.6	0.37	0.55
30	0.26	350	0.68
20	0.076	$3.6 \times 10^3$	0.27



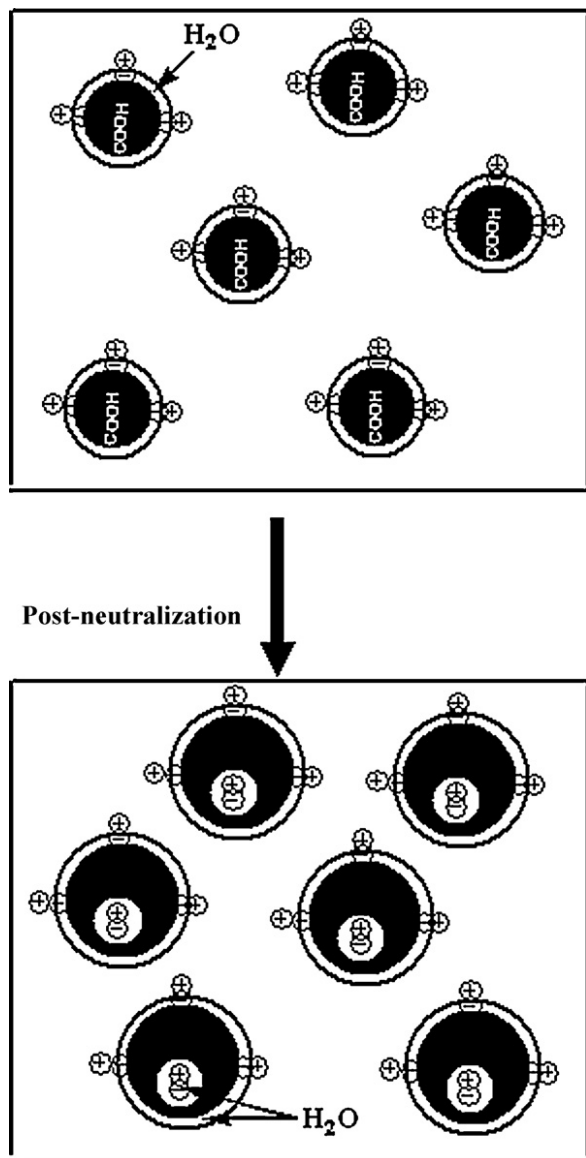


Fig. 13. Schematic diagram showing the effect of post-neutralization on the PU particle size (adapted from [59]).

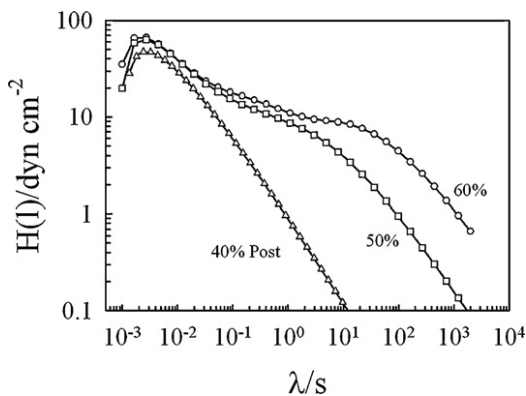


Fig. 14. Relaxation spectra of PUDs at 30 °C for different degrees of post-neutralization (adapted from [59]).

**Table 6**  
Effect of degree of chain extension on molecular weights of PU dispersion.

Chain extension (%)	$M_n$ (g/mol) (calculated)	$M_n$ (g/mol) (GPC)	$M_w$ (g/mol) (GPC)
0	2,200	2,900	8,200
50	4,500	4,000	13,000
70	7,900	5,000	16,000
90	29,000	14,000	32,000

ation peak is directly related to the long relaxation mode of the high viscosity of the PU dispersion. With decreasing degree of post-neutralization, the viscosity decreases strongly and consequently the long relaxation peak disappears. Similar behavior has been observed for the PUDs prepared via acetone process [100].

### 4.3. Effect of chain extension

The effect of degree of chain extension on molecular weight is presented in Table 6. The weight average molecular weights  $M_w$  and number average molecular weights  $M_n$  were determined using gel permeation chromatography (GPC) with respect to PMMA standards [58]. The PU films were found to be soluble in hot THF. The  $M_n$  values increased with increasing degree of the chain extension (Table 6). The  $M_n$  values measured by GPC are lowered compared to the theoretical  $M_n$  values (Table 6). This is most likely due to different hydrodynamic volume of PU compared to PMMA standard, or perhaps the insolubility of high molecular weight fractions. The degree of chain extension was found to have a negligible influence on both particle size and viscosity of the PUD. Although the molecular weight of PU increases by about 4 times with increasing chain extension from zero to 90%, the viscosity of the dispersions does not change significantly. This observation is attributed to the fact that all the dispersions have almost the same particle size and particle size distribution regardless of the differences in the chain extension. This similarity in both particle size and its distribution leads to similar interaction between the particles in each dispersion and consequently similar viscosity. The experimental procedure used for chain extension is responsible for the observed little change in the viscosity of PUDs. As already described, the dispersions were prepared prior to chain extension, making it possible to maintain the particle sizes and their distribution, and consequently insignificant change in the viscosity of PUDs. In the case of the so-called acetone process Nanda and Wicks [75] found that the particle size decreased from 107 to 95 nm with a corresponding increase in viscosity from 75 to 82 mPa s as the chain extension was reduced from 90% to 0%. This was opposite of what was expected and most likely represents the fact that at higher polymer viscosity the stress increases at the interface during phase inversion. Having the dispersed phase (i.e., polymer phase) viscosity significantly higher than that of the continuous phase (acetone plus water) results in low phase deformation with an increase in molecular weight; and hence larger particles [75].

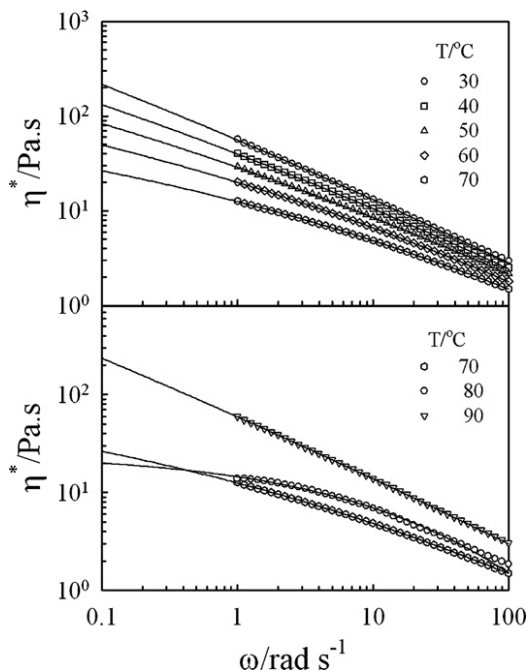


**Fig. 15.** Frequency dependence of dynamic viscosity for PUD of 60% post-neutralization at different temperatures. Solid lines are fits of Eq. (1) to the experimental data (adapted from [59]).

#### 4.4. Effect of temperature

To investigate the effect of temperature on the rheological behavior of the PUD, one highly viscous example (i.e., 60% post-neutralization) has been used for this part of study. The double logarithmic scale of the complex viscosities of this sample at different temperatures is represented in Fig. 15. The frequency dependence of the viscosity of this PUD composition can be expressed through the Cross model (Eq. (1)), as shown by the fitting lines through the experimental points. Excellent descriptions of the data are obtained using this model. The increase in temperature from 70 to 90 °C led to a dramatic increase in the viscosity as Fig. 15 shows. This increase in the viscosity is consistent with the sample behaving as solid-like structure. This behavior is not observed for all the PUD samples, for example the sample of 0% post-neutralization (i.e., 100% pre-neutralization) does not show any increase in viscosity with increasing temperature [58]. These experimental results point to the fact that the increase in the viscosity is related to a typical gelation process induced thermally. This process is thought to be a function only of the particle size; the bigger the particle the higher the possibility for gel formation. In the case of 60% post-neutralization the particle size is 300 nm, but it is only 45 nm for 0% post-neutralization [58]. Therefore, the thermal energy increases the interaction between the big particles, leading to gel formation. This energy is not sufficient to induce gelation in the case of small particle size (i.e., 0% post-neutralization). Based on this experimental result it is clear that the increase in viscosity with increasing temperature is not related to the evaporation of water. In addition, the formation of gel has been confirmed by heat-

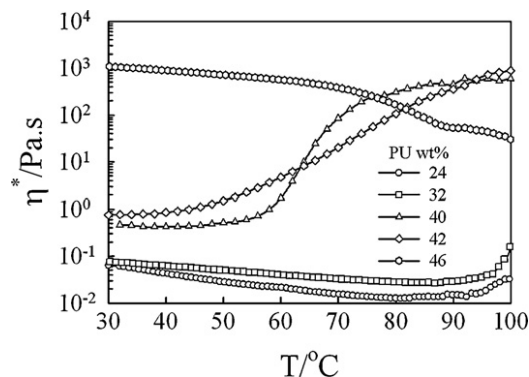


**Fig. 16.** Temperature dependence of complex share viscosity,  $\eta^*$ , for PUDs with different compositions at 2 °C/min heating-rate and 10 rad s<sup>-1</sup> angular frequency (adapted from [60]).

ing the dispersions in tightly closed glass bottles at around 70 °C in a water bath for 2 h. The sample of 60% post-neutralization changed to a solid gel but the sample of 0% post-neutralization does not show any obvious increase in the viscosity and it remained in the liquid state throughout the heating period.

Fig. 16 demonstrates the temperature dependence of the dynamic viscosity  $\eta^*$  for PUDs of different PU wt% at 2 °C/min heating rate and 10 rad s<sup>-1</sup> angular frequency. As expected, all the samples of different compositions are influenced by increasing the temperature [60]. The viscosity increases strongly at about 95 °C for the samples of 24 and 32 wt% PU. This increase in viscosity is mainly due to the evaporation of water. A dramatic increase (three orders of magnitude) in the viscosity is observed for the sample of 40 wt% PU at around 65 °C. This is attributed to the formation of a fractal gel at this temperature. For the sample of 42 wt% PU, the viscosity increases slightly with temperature in the range of  $T \leq 50$  °C after that the viscosity increases strongly in a linear behavior at higher temperature range. This behavior indicates that the gelation process for the 42 wt% PU sample takes place at lower temperature than that of 40 wt% PU [60].

To understand the gelation process in the PU dispersions, we present results of a systematic investigation of the effects of thermal induced gelation on the viscoelastic material functions of 40 wt% PU dispersion with 90% pre-neutralization as a function of frequency. Fig. 17 demonstrates the temperature dependence of dynamic storage modulus,  $G'$  at 2 °C/min heating-rate and different shear frequencies for the 40 wt% sample. The value of  $G'$  is almost constant with increasing temperature at a temperature range lower than the gel temperature (i.e.,  $T < 60$  °C). A sudden increase in  $G'$  (several orders of magnitude, dependent on the value of the shear frequency) at  $T_{onset}$  about 60 °C was observed at all values of frequencies due to the onset of the formation of fractal gel. The magnitude of the elevation in  $G'$  increases greatly with increasing temperature due to the evolution of the gelation process and the significant increase in branching (i.e., formation of fractal gel). In addition,  $G'$  is no longer frequency dependent at a higher temperature range due to the formation of an equilibrium storage modulus,  $G'_{eq}$  which is a typical

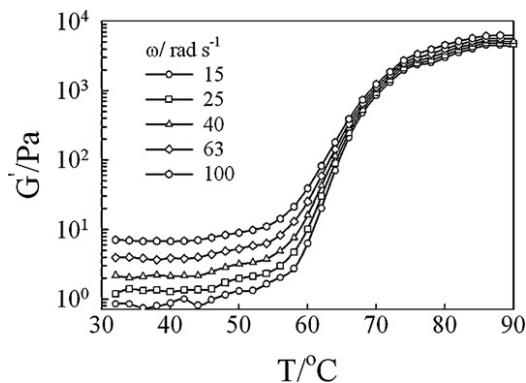


**Fig. 17.** Temperature dependence of dynamic storage modulus,  $G'$  for PUD with 40 wt% PU at 2 °C/min heating-rate and different angular frequencies (adapted from [60]).

criterion for the formation of an elastic fractal gel. Similar behavior was observed for temperature dependence of  $G''$  and  $\eta^*$  [60].

#### 4.5. Determination of $T_{gel}$

The gelation temperature,  $T_{gel}$ , can be evaluated for the present PUD system by two different methods [60]. The first method is from the temperature dependence of the loss tangent,  $\tan \delta$  at different constant shear frequencies as demonstrated in Fig. 18 for PUDs with 40 wt% PU. Estimates of  $T_{gel}$  can be obtained from the point at which  $\tan \delta$  is frequency independent and all curves at different constant shear frequencies coincide. Based on this method,  $T_{gel}$  for 40 wt% PU is 68 °C [60]. The second method evaluates  $T_{gel}$  from the simultaneous temperature dependence of the dynamic shear moduli,  $G'$  and  $G''$  as shown in Fig. 19. At temperatures below  $T_{onset}$ , both  $G'$  and  $G''$  are frequency dependent and  $G''$  is about one order of magnitude higher than  $G'$  near  $T_{onset}$ , both  $G'$  and  $G''$  increase with temperature and coincide at  $T_{gel}$ . At higher temperature than  $T_{gel}$ , the gelation process proceeds and  $G'$  increases more rapidly than  $G''$  ( $G'$  becomes higher than  $G''$ ) which is a criterion for the formation of a fractal gel. The determination of  $T_{gel}$  from the crossover of  $G'$  and  $G''$  is frequency

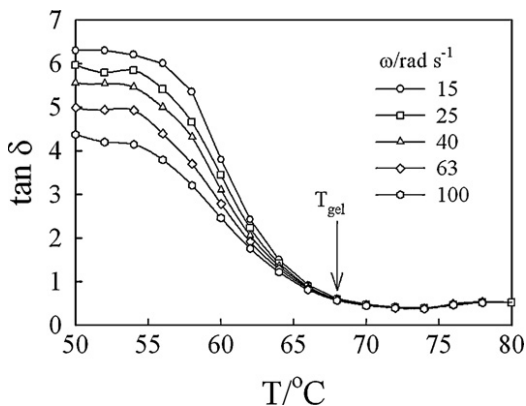


**Fig. 18.** Temperature dependence of loss tangent,  $\tan \delta$ , for PUD with 40 wt% PU at 2 °C/min heating-rate and different angular frequencies (adapted from [60]).

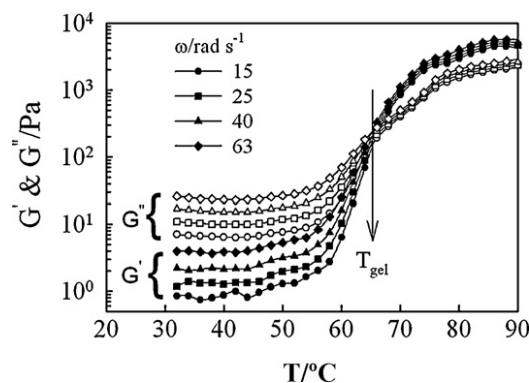


**Fig. 19.** Temperature ramps of  $G'$  and  $G''$  for PUD with 40 wt% PU at 2 °C/min heating-rate and different angular frequencies (adapted from [60]).

independent for this system and equal to 68 °C for 40 wt% PU sample, in good agreement with the values obtained from  $\tan \delta$  versus  $T$ . However, it is known for other systems reported in the literature that the crossover of  $G'$  and  $G''$  is not a general criterion for determination of  $T_{gel}$  due to its strong frequency dependence. For example,  $T_{gel}$  of thermally cross-linked poly(vinyl methyl ether) determined at 100 rad/s was found to be about 20 °C higher than that obtained at 1 rad/s as previously reported [101]. A similar behavior was reported by Zhao et al. [102] who found that the temperature at which the  $G'$  and  $G''$  intersect was shear stress and frequency dependent for sol–gel transition of a hybrid gel. Winter et al. [97,103] reported that when the gelation point cannot be evaluated from the crossover of  $G'$  and  $G''$  it could be related to the critical conversion point of cross-linking reaction. According to the above discussion, it is apparent that, in general, at the  $T_{gel}$  the branching becomes remarkable and the fractal polymer network starts to form. At  $T > T_{gel}$  the branching proceeds and a fractal gel that is characterized by  $G' > G''$  is formed. In addition, both  $G'$  and  $G''$  reach equilibrium values (i.e., they become frequency independent). Based on the above it appears that, the rheological material parameters ( $G'$ ,  $G''$ ,  $\eta^*$  and  $\tan \delta$ ) of PUDs are very sensitive to the thermal induced gelation process and the formation of a fractal gel network.

Similar sensitivity to thermal induced gelation would be expected for the temperature dependence of zero-shear viscosity,  $\eta_0$ . The value of  $\eta_0$  as a function of temperature can be obtained from fitting the shear frequency dependence of the complex dynamic viscosity to Cross model (Eq. (1)). The temperature dependence of  $\eta_0$  is shown in Fig. 20. Clearly,  $\eta_0$  follows the same trend as that observed in the dynamic ramp of  $G'$  (Fig. 17), where there is a sudden change in sign of the slope and an increase in  $\eta_0$  versus  $T$  (v-shaped) at  $T_{gel}$ . Note that the arrow in Fig. 20 indicates the value of the  $T_{gel}$  estimated from the intersection of the two different slopes of  $\eta_0$  at different temperatures. This method showed a  $T_{gel} = 68$  °C in good agreement with the value determined from  $\tan \delta$  versus  $T$  for PUD with 40 wt% PU sample (Fig. 18).

Fig. 21 shows the master curves of the dynamic shear moduli,  $G'$  and  $G''$  for 40 wt% PU at  $T_0 = 40$  °C reference

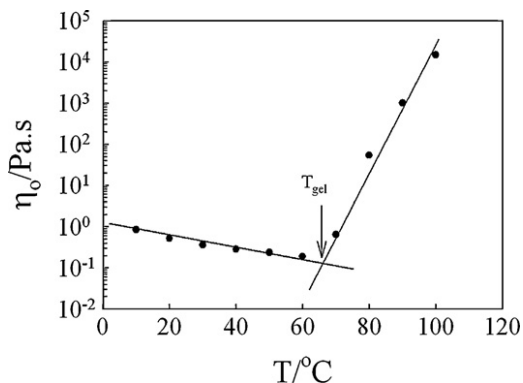


Fig. 20. Zero-shear viscosity as a function of temperature for PUD with 40 wt% PU. The arrow shows the value of  $T_{gel}$  (adapted from [60]).

temperature. Obviously the master curve cannot be constructed for the whole range of temperature. The WLF principle is only valid for temperatures lower than the  $T_{gel}$ ; the principle failed for  $T \geq 70^\circ\text{C}$ . This can be seen very clearly in the low frequency region as a deviation from the terminal slope in the  $G'$  and  $G''$  curves. At  $T \geq 80^\circ\text{C}$ ,  $G'$  and  $G''$  cannot be plotted on the same master curve, i.e., they strongly increase (2–3 orders of magnitude) and  $G'$  exceeds  $G''$ .

#### 4.6. Phase separation and gel structure of PUDs

Five samples of different concentrations (i.e., 34, 36, 38, 40 and 42 wt% PU) were annealed in tightly closed glass bottles for 2 h at  $70^\circ\text{C}$  in a water bath [60]. All the samples

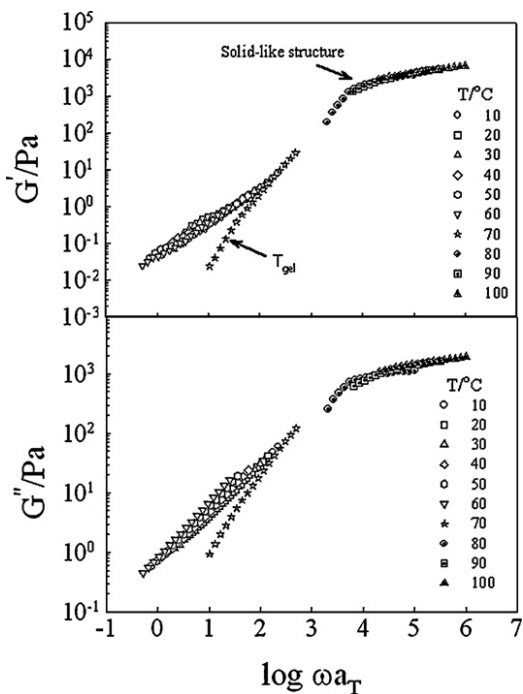
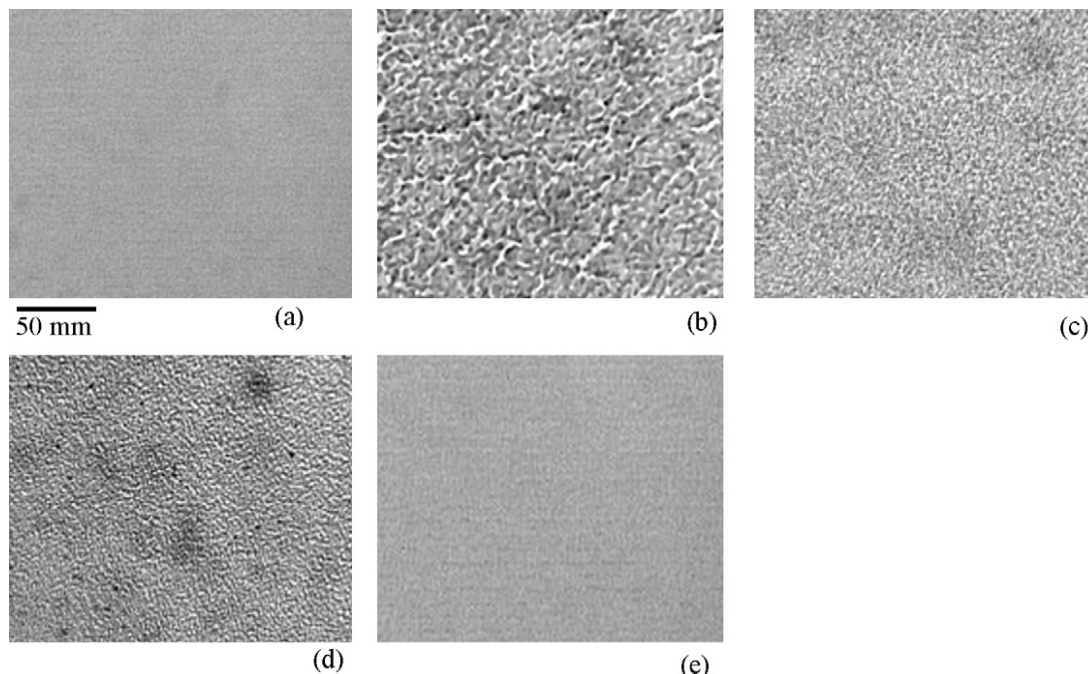


Fig. 21. Master curves of storage and loss moduli for PUD with 40 wt% PU at  $40^\circ\text{C}$  (adapted from [60]).

changed to fractal gel except the 34 wt% PU which remained in the liquid state during the entire period of annealing time. The morphology of the different samples was examined using an optical microscope. Different morphology can be obtained as a function of concentration as shown in Fig. 22. A typical co-continuous structure with a unique periodicity and phase connectivity has been observed for only 36, 38 and 40 wt% PU. On the other hand, no morphology was detected for 34 and 42 wt%. Note that it is well known that a co-continuous structure is a unique structure for the mixtures that have undergone a phase separation via spinodal decomposition. Therefore, the observation of co-continuous morphology (Fig. 22) indicates that these three samples were in the two-phase regime for a period of time long enough to allow the samples to phase separate via spinodal decomposition [60]. Differences in the observed morphologies and phase separation depicted in Fig. 22 are attributed to the different location of the samples in the phase diagram shown below as well as the extent of the quenching depth of each sample.

To support this hypothesis a phase diagram is illustrated schematically in Fig. 23. This phase diagram shows a liquid–liquid phase separation (LCST-type phase diagram) and a liquid–solid transition (gelation), both of them are located in the same temperature range which reflects the complex behavior of the temperature effect of this dispersions. On the basis of this phase diagram it appears that, a co-occurrence of liquid–liquid transition (phase separation) and liquid–solid transition (gelation) of aqueous PUDs can be induced thermally. The straight line with open circular symbols shows the location of the five samples in the phase diagram at  $70^\circ\text{C}$ . The sample of 34 wt% PU is outside the liquid–liquid and liquid–solid transitions phase diagrams, therefore neither gelation nor phase separation morphology was detected for this composition at  $70^\circ\text{C}$ . For the 42 wt% PU, it is outside the LCST-phase diagram but inside the liquid–solid transition regime, therefore, only gelation process can be observed without any phase separation morphology as shown in Fig. 22e. The other three samples (i.e., 36, 38 and 40 wt%) are located inside both the LCST and the liquid–solid phase diagram, therefore the two transitions simultaneously occur at the same time. The reason for the observed different morphologies may be ascribed to the value of the quenching depth,  $\Delta T$  in the LCST-phase diagram; coarse morphology implies a large value of  $\Delta T$ . This phase diagram shows that the value of  $\Delta T$  decreases with increasing concentration for these three samples, therefore, the different morphologies of PUDs in Fig. 22 is not surprising at all. It is very difficult to construct a *real* phase diagram for the complex PUD system of this study because of the simultaneous occurrence of the two transitions in the same temperature range. Based on the observed morphologies (Fig. 22), one can conjecture that the dramatic increase in the viscoelastic material functions of 40 wt% is not only caused by the gelation process but also by the contribution of the concentration fluctuations produced during the liquid–liquid phase separation. The simultaneous occurrence of liquid–liquid phase separation and gelation in this composition (40 wt% PU) makes the thermal behavior very complex and intriguing. However, only the gelation process was observed for the



**Fig. 22.** Optical photomicrographs for five different PUDs after annealing in tightly closed glass bottles at 70 °C for 2 h in a water bath: (a) 34 wt%; (b) 36 wt%; (c) 38 wt%; (d) 40 wt%; and (e) 42 wt% PU (adapted from [60]).

42 wt%, implying that the temperature dependence of viscoelastic material functions of 42 wt% PU is typical of a classical gelation process. It is also important to note that the contribution of the PU concentration fluctuations to the viscoelastic material functions during the phase separation process is very little compared to the contribution of the very long relaxation times of the elastic gel [59]. Therefore, the gelation process is clearly responsible for the observed dramatic change in the viscoelastic behavior of the dispersions.

It is noteworthy that, a coexistence of phase separation and gelation process within a single composition ratio has been reported for a variety of water-soluble biopoly-

mer aqueous solutions such as agarose, gelatin, fibrinogen and cellulose derivatives [104–108]. In these biopolymer solutions, the phase separation curve crosses the gelation curve in the concentration *versus* temperature phase diagram as in the present PUD case. Thermal-induced coupling of phase separation and gelation in an aqueous solution of hydroxypropylmethyl cellulose (HPMC) has been reported by Kita et al. [108] who used fluorescence measurements on concentrated HPMC solution to confirm that the hydrophobic interaction is the driving force of gelation coupled by the phase separation.

#### 4.7. Real-time measurements

Dynamic rheology is a powerful tool to monitor cross-linking and microstructural changes in a material because it allows properties to be probed in at-rest conditions without disruption of the microstructure. In addition, it is an effective method for studying the curing process of thermosetting polymers and for the examination of the viscoelastic properties and transition temperatures of the cured products. The viscoelastic behavior of polymer gels near the sol–gel transition has been studied experimentally [109–114] and theoretically [115–119]. The main emphasis of these studies was to find the relationship between linear viscoelastic properties and the structure of gels at the gel point. The experimental determination and prediction of gelation is important for the processing of cross-linking polymers, whereas the criticality of the phenomenon and the universality of the properties on the gelation threshold make gelation interesting from a fundamental point of view [120,121].

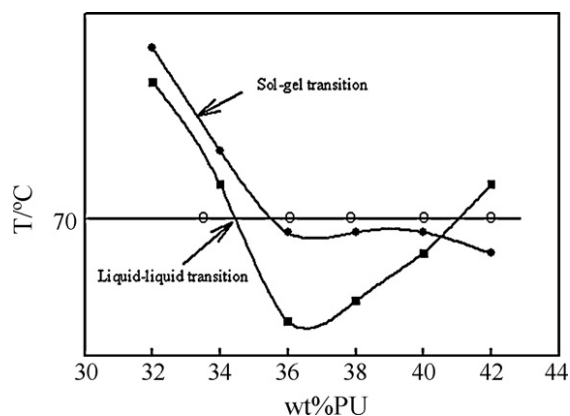


**Fig. 23.** Phase diagrams showing a liquid–liquid phase separation and liquid–solid transition for PUDs. The straight line and the open circular symbols show the locations at 70 °C of the different five morphologies depicted in Fig. 22 (adapted from [60]).

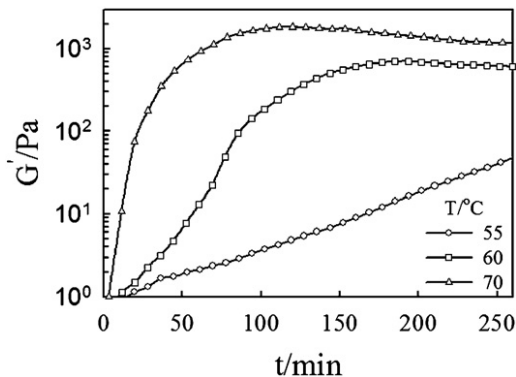


**Fig. 24.** Time dependence of dynamic storage modulus,  $G'$ , of PUD (40 wt% PU) at constant shear frequency ( $\omega = 1 \text{ rad s}^{-1}$ ) for different constant temperatures (adapted from [130]).

The formation of polymer gels can be monitored from the time evolution of viscoelastic material functions at the gel point, where the entire network process can be divided into two parts separated by the gel point. The gel-point is one of the most important parameter of gelation that is characterized by the appearance in the reactive system of a macromolecule with infinitely large molecular weight. The sol–gel transition point can be determined by a sudden change of a range of physical properties [102]. In theory, the criterion of gel formation is the existence of one long chain running through the whole system. In practice, a sudden loss of flow is the most common and conventional test to determine the sol–gel transition point, since at the gelation point, the viscoelastic properties change abruptly from an initially liquid-like state to a solid-like state [122–128]. Several models for gelation have been proposed and the most well-known is percolation theory [129,130]. The percolation theory was generalized to predict how the viscoelastic properties, such as dynamic shear moduli and viscosity are expected to scale with time or frequency [131].

Isothermal time dependence of elastic stored modulus,  $G'$  at different temperatures and constant shear frequency ( $\omega = 1 \text{ rad s}^{-1}$ ) is shown in Fig. 24 [130]. A dramatic increase in  $G'$  at all temperatures was clearly observed as a result of formation of an elastic fractal gel. At long times the value of  $G'$  levels off and becomes time independent. The magnitudes of the elevation in  $G'$  and the time at which  $G'$  levels off,  $t_{lo}$ , were found to be strongly temperature dependent, i.e., the magnitude of the elevation in  $G'$  increases and  $t_{lo}$  decreases with increasing temperature. The fact that, the magnitude of the elevation in  $G'$  increases greatly with increasing time and temperature is attributed to the gelation process and the significant increase in branching (formation of fractal gel). The  $G'$  reaches a plateau value at long times particularly at 60 and 70 °C. The plateau value is related to an equilibrium modulus,  $G_{eq}$  (a typical criterion for the formation of an elastic, fractal gel). At 55 °C the gelation process is significantly slower than that at 60 and 70 °C, implying that a longer curing time than the one observed at higher temperatures is needed to reach the plateau region. Similar behavior has been observed for the other viscoelastic material functions, such as  $G''$  and  $\eta^*$  [130].

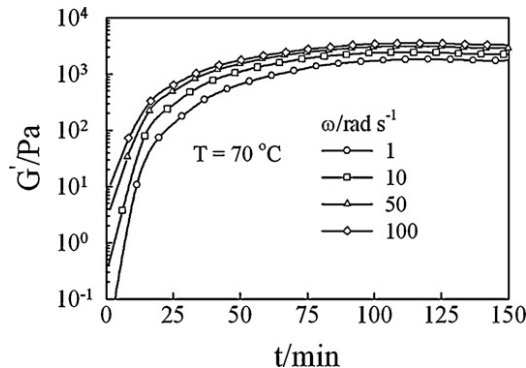


**Fig. 25.** Variation of  $G'$  as a function of time at 70 °C for different constant shear frequencies (adapted from [130]).

Fig. 25 shows the time dependence of  $G'$  at 70 °C for different constant shear frequencies. Obviously, the variation of  $G'$  with time and frequency can be divided into two different regimes. At  $t \leq 50 \text{ min}$  (regime I),  $G'$  increases rapidly with time and the magnitude of the elevation in  $G'$  is shear frequency-dependent. (The magnitude of the elevation at low frequency is higher than that at high frequency.) This regime (regime I) includes the gel point at which the branching of polymer becomes remarkable and the fractal gel starts to form. At  $t > 50 \text{ min}$  (regime II),  $G'$  is no longer time dependent and only slightly frequency dependent as a result of the formation of an equilibrium modulus,  $G_{eq}$ , which is a typical criterion for the formation of an elastic, fractal gel. Similar behavior can be obtained for the variation of  $G''$  and  $\eta^*$  with gelation time at different shear frequencies [130].

#### 4.8. Determination of $t_{gel}$

One can determine  $t_{gel}$  from rheological data based on the Winter–Chambon criterion [96,132]. According to this criterion, the gel point is identified as the instant in time when the moduli scale in an identical fashion with time, i.e., storage and loss moduli show the following power law behavior:

$$G' \sim G'' \sim \omega^n \quad (9)$$

The exponent  $n$  is called the relaxation exponent and can be linked to microstructural parameters. According to this relation, if the power law holds in a sufficiently wide range of shear frequency, the loss tangent,  $\tan \delta = G''/G'$ , can be written as

$$\tan \delta = \tan \left( \frac{n\pi}{2} \right) \quad (10)$$

This equation implies that  $\tan \delta$  is independent of  $\omega$  at the gel point. The validity of this theory has been extended to a variety of chemically and physically cross-linking systems. Fig. 26 shows time dependence of  $\tan \delta$  at 70 °C and different constant shear frequencies. One can see that  $\tan \delta$  is frequency independent at  $t_{gel} = 17 \text{ min}$ , indicating that the system has reached the gel point and the cluster of the networks is macroscopically percolated. At a time longer than the gel point,  $\tan \delta$  decreases gradually with time due to the fact that the magnitude of elevation in  $G'$  is higher

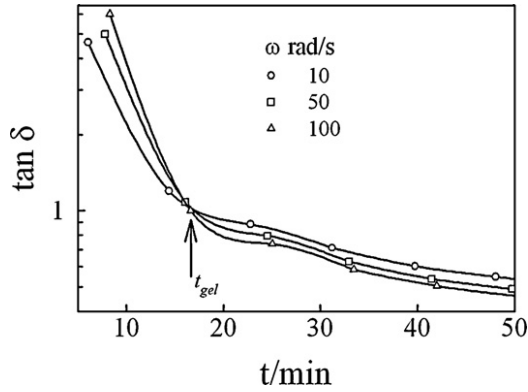


Fig. 26. Loss tangent,  $\tan \delta$ , as a function of time at 70 °C for different constant shear frequencies. The gel point,  $T_{gel}$ , is obtained from the intersection point (adapted from [130]).

than that in  $G''$  as a result of the formation of an elastic fractal gel [130]. On the basis of this experimental fact, it is apparent that the Winter–Chambon theory is applicable to this system over a wide range of frequency (as shown in Fig. 26), suggesting that there is a self-similar structure (or critical gel) at the gel point. Beyond the gel point, elastic effects dominate, since the fractal gel is capable of storing energy. This is why  $G'$  increases at a more rapid rate than  $G''$  at long times.

4.9. Critical phenomena at the gel point

Fig. 27 shows the frequency dependence of  $G'$  at different time intervals at 70 °C. One can see that at  $t=3$  min, the value of  $G'$  increases with increasing frequency with a slope of about 2, indicating a classical liquid behavior. The value of  $G'$  increases with both frequency and gelation time. At a very long time,  $G'$  is no longer frequency dependent and reaches an equilibrium value  $G_{eq}$  due to the formation of an elastic fractal gel [130]. Similar behavior was obtained for the frequency dependence of  $G''$  for different gelation times, i.e.,  $G''$  increases rapidly with time and frequency and attains an equilibrium value (time and frequency independent) (Fig. 28).

The frequency dependence of  $\eta^*$  for different gelation times is depicted in Fig. 29. Obviously,  $\eta^*$  is almost fre-

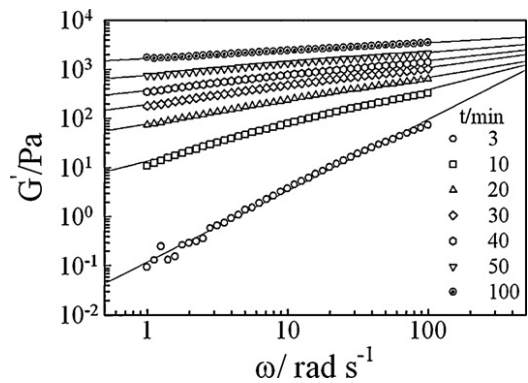


Fig. 27.  $G'$  as a function of shear frequency for different constant gelation times at 70 °C (adapted from [130]).

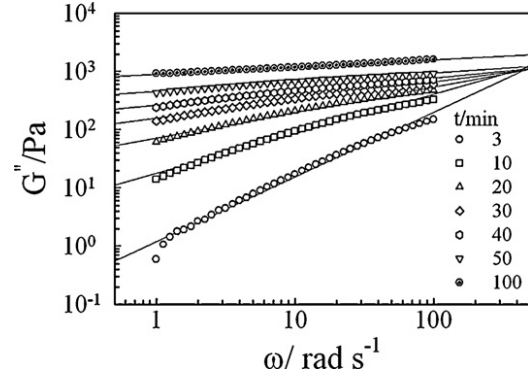


Fig. 28. Dependence of  $G''$  on shear frequency for different constant gelation times at 70 °C (adapted from [130]).

quency independent at  $t=3$  min; after that the value of  $\eta^*$  increases abruptly with increasing gelation time, and the entire curve becomes strongly frequency dependence [130].

It is apparent that Figs. 27 and 28 demonstrate the variations of  $G'$  and  $G''$  as a function of shear frequency based on the power law of Eq. (9), respectively. This behavior is applicable over the entire range of frequency. The values of the exponents  $n'$  and  $n''$  for  $G'$  and  $G''$ , respectively, are gelation time dependent. Fig. 30 shows the time dependence of  $\eta'$  and  $\eta''$  at 70 °C for 40 wt% PU. The values of the two exponents decrease exponentially with time, becoming identical at the gel point (i.e., at  $t_{gel}=17$  min,  $n'$  and  $n''=0.58$ ). The values of the exponents are very close to that obtained for different systems reported in the literature and are found to be in good agreement with that theoretically predicted from percolation theory ( $n \sim 2/3$ ) [129]. At very long times the values of the two exponents decrease and become as low as 0.2, indicating the formation of an elastic or rigid fractal gel.

The zero shear viscosity,  $\eta_0$ , and the equilibrium shear modulus,  $G_{eq}$ , are also expressed in power law scaling functions near the gel point:

$$\eta_0 \sim \varepsilon^{-k} \quad (p < p_c) \tag{11}$$

$$G_{eq} \sim \varepsilon^z \quad (p > p_c) \tag{12}$$

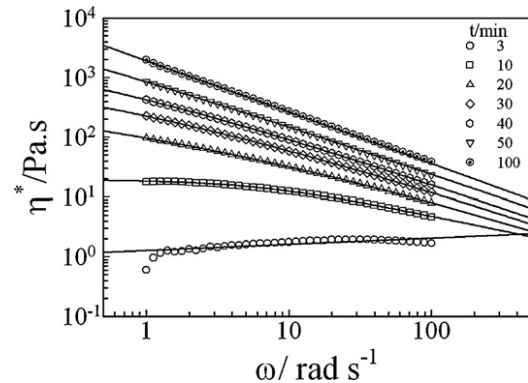
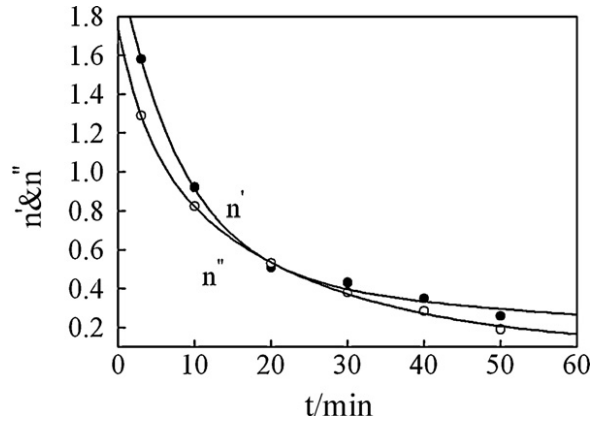


Fig. 29. Variation of  $\eta^*$  as a function of shear frequency for different constant gelation times at 70 °C. The solid lines are calculated from Cross model (Eq. (1)) (adapted from [130]).



**Fig. 30.** Time dependence of exponents  $n'$  and  $n''$  obtained from  $G'$  and  $G''$  data at 70 °C, respectively, according to Eq. (9) (adapted from [130]).

where  $p$  and  $p_c$  are the reaction extents at time  $t$  and  $T_{gel}$ , respectively. The relative distance from the gel point,  $\varepsilon$ , can be defined as

$$\varepsilon = \frac{|p - p_c|}{p_c} \quad (13)$$

The values of  $\eta_0$  at different times can be determined from fitting the classical frequency dependence of  $\eta^*$  for different gelation times (Fig. 29) to the Cross model (Eq. (1)).

The values of  $G_{eq}$  can be obtained from the frequency-independent values of  $G'$  from Fig. 27. Fig. 31 shows the  $\varepsilon$  dependence of  $G_{eq}$  and  $\eta_0$  in a double logarithmic scale; the slopes of the two linear curves directly determine the values of  $z$  and  $k$ , respectively. The exponent  $n$  can be predicted from the critical exponent values of  $k$  and  $z$  as reported by Martin et al. [115].

$$n = \frac{z}{(k + z)} \quad (14)$$

The values of  $z$  and  $k$  obtained from the slopes of the two curves of Fig. 31 are 0.85 and 0.95, respectively, which yields a value of  $n=0.47$  which is slightly lower than the theoretical value predicted by percolation theory ( $n \sim 2/3$ ).

On the basis of the discussion in the previous sections, it is apparent that the viscoelastic properties of PUDs are

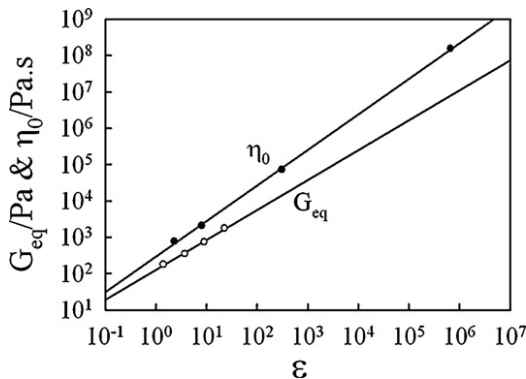


**Fig. 31.** Dependence of zero-shear viscosity,  $\eta_0$ , and equilibrium shear modulus,  $G_{eq}$ , on the relative distance from the gel point,  $\varepsilon$  in a double logarithmic scale at 70 °C (adapted from [130]).

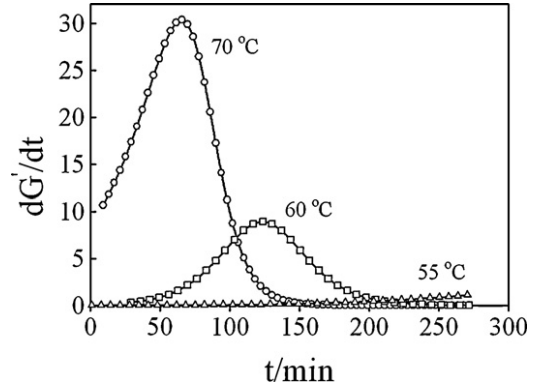


**Fig. 32.** Time dependence of  $dG'/dt$  at different constant temperatures and 1 rad s<sup>-1</sup> for PUD (40 wt% PU) (adapted from [133]).

very sensitive to the structure changes accompanying the formation of an elastic fractal polymer gel. In addition, the critical phenomenon near the gel point can be well described by the scaling power laws based on percolation theory and Winter–Chambon approaches.

#### 4.10. Gelation kinetics

The rate of change of  $G'$  with time at a given temperature,  $(dG'/dt)_T$ , is directly related to the extent of the gelation reaction [133]. Fig. 32 shows the time dependence of  $(dG'/dt)_T$  for different constant temperatures. Clearly,  $dG'/dt$  initially increases to a maximum value and then decreases again. The inflection point (or maximum point) shifts to longer time with decreasing temperature. The initial increase in  $dG'/dt$  is related to the very quick rate of gelation corresponding to the initial time period of the measurement, as seen in the rapid increase of  $G'$  with time once the gel is formed. The decrease in  $dG'/dt$  at long times is attributed to a decrease in the number of interactions between the PU-dispersed particles as the gelation process evolves. The shift of the inflection point to longer time at a lower temperature is directly related to the longer time needed for gelation, particularly at 55 °C. Similar behavior has been reported in the literature by Zlatanovic et al. [134]; i.e.,  $dG'/dt$  was found to increase with curing time in the early stage of curing process and then decreased at the late stage in the rheological study of the copolymerization reaction of acrylate-terminated unsaturated copolyesters with styrene. The authors ascribed this behavior to not only the change of cross-linking reaction rate with time but also to the autocatalytic effect of the cross-linking process related to the microphase separation that occurs in the initial time before the inflection point for the specific system studied.

The effect of temperature on the gelation kinetics can be quantified by calculating the average rate of change of the viscoelastic material functions ( $G'$ ,  $G''$  and  $\eta^*$ ) with time from the following equation:

$$\left(\frac{df}{dt}\right)_{av} = \frac{1}{t_2 - t_1} \int_{t_1}^{t_2} \frac{df}{dt} dt \quad (15)$$



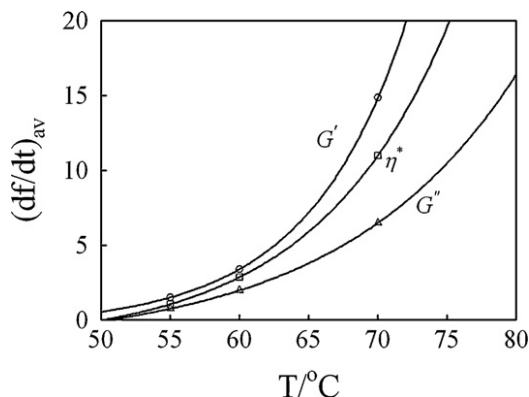


**Fig. 33.** Temperature dependence of the average rate change of  $G'$ ,  $G''$  and  $\eta^*$  as described in the text (adapted from [133]).

where  $f$  is the viscoelastic material function ( $G'$ ,  $G''$  or  $\eta^*$ ) and  $t_1$  and  $t_2$  are the times at the beginning and ending of gelation process, respectively. This equation has been used previously by Lopes da Silva et al. [135] for the rheological data of the storage modulus only to evaluate the temperature dependence of structure development of gelation for high-methoxy pectin/sucrose system [135]. Fig. 33 shows the change of  $(df/dt)_{av}$  as a function of temperature;  $(df/dt)_{av}$  increases exponentially with temperature for the three different viscoelastic material functions, indicating that the reaction rate increases with temperature as expected.

#### 4.11. Isothermal gelation kinetics

The kinetics of the thermal-induced gelation of PUDs can be evaluated rheologically by applying fundamental rate laws with traditional model-fitting methods [136]. Such kind of analysis requires a knowledge of the best model that can fit the experimental data followed by a simple evaluation of the kinetics parameters such as the activation energy ( $E_a$ ) and pre-exponential factor using Arrhenius equation [136–140]. This method is reported in the literature to give a single value of activation energy for an overall process [136–140]. The  $E_a$  value obtained in this manner is in fact an average value that does not reflect the effects of changes in the reaction mechanism and kinetics with the degree of conversion and temperature. Another approach used in the literature to evaluate  $E_a$  as a function of the degree of conversion is the isoconversional method that is based on replicated experimental data and model-free kinetics calculations, i.e., no assumptions model [141–144]. In the next two sections the isothermal gelation kinetics of PUD (40 wt% PU) will be described using the two analysis methods just mentioned above (i.e., model-fitting and isoconversional methods).

#### 4.12. Model-fitting method

The Malkin and Kulichikhin [145] model was found to be an excellent model to describe the rheological data of the gelation process based on the following phenomenological

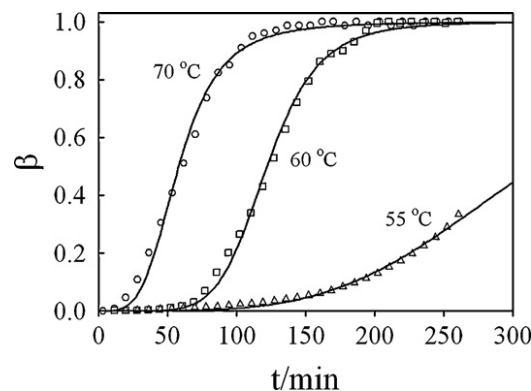


**Fig. 34.** Rheological degree of conversion,  $\beta$ , as a function of gelation time for different constant temperatures. The symbols are experimental data obtained from Eq. (17) (adapted from [133]).

equation:

$$\frac{d\beta}{dt} = (k_1 + k_2\beta^m)(1 - \beta)^n \quad (16)$$

where  $\beta$  is the rheological degree of conversion,  $n$  and  $m$  are empirical constants, the sum of which gives the order of reaction; and  $k_1$  and  $k_2$  are the temperature-dependent rate constants for the early and late stages of the gelation reaction. This model (Eq. (16)) was predicted originally for the isothermal curing kinetics of thermosetting polymers studied by differential scanning calorimetry (DSC) and was used recently to interpret the rheological kinetics data of similar systems [133,140,146]. The above equation describes the overall kinetics in both the early and late stages of a reaction. The rheological degree of conversion,  $\beta$ , can be evaluated at different constant temperatures from the time dependence of  $G'$  (Fig. 24) using the following relation:

$$\beta = \frac{(G'_t - G'_0)}{(G'_{\infty} - G'_0)} \quad (17)$$

where  $G'_t$  is the value of the storage modulus at time  $t$ ; and  $G'_0$  and  $G'_{\infty}$  are the values of storage modulus at the beginning of the experiment and at the maximum gelation time, respectively. Fig. 34 shows the rheological degree of conversion (calculated from Eq. (17)) as a function of gelation time at different constant temperatures [133]. Obviously, the degree of conversion is almost zero before the onset of gelation process and then increased strongly with gelation time. The maximum degree of conversion is almost unity at 70 and 60 °C, however it is very small or experimentally inaccessible at 55 °C due to the very slow gelation process at this temperature over the time scale of the measurements reported here (see Fig. 34) [133].

Fig. 35 shows the rate of conversion,  $d\beta/dt$ , as a function of gelation time for different constant temperatures. Again, at 70 and 60 °C, the gelation rate proceeds rapidly; however, it is very slow at 55 °C, requiring very long gelation time (outside the experimental time-scale) to reach the inflection point. Similar to Fig. 32, the inflection point shifts to longer time with decreasing temperature since the reaction at low temperature needs very long time in order to kinetically proceed to completion [133].

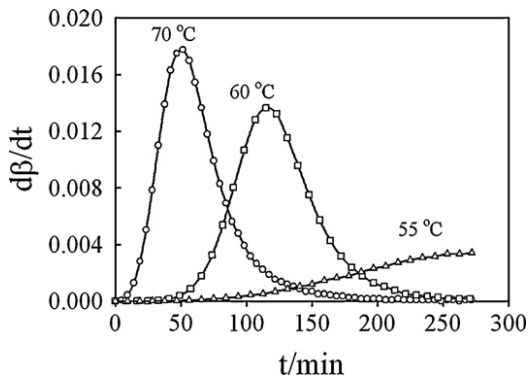


Fig. 35. Variation of  $d\beta/dt$  as a function of gelation time for different constant temperatures (adapted from [133]).

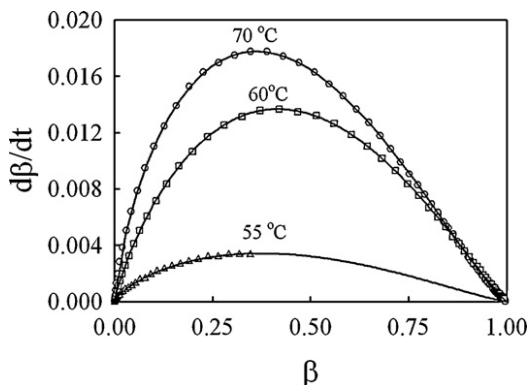


Fig. 36. Variation of  $d\beta/dt$  as a function of  $\beta$  for different constant temperatures. The symbols are experimental data while the lines are calculated from Eq. (16) (adapted from [133]).

Fig. 36 shows the rate of rheological degree of conversion ( $d\beta/dt$ ) as a function of  $\beta$  for different isothermal temperatures. One can obtain the kinetic parameters of Eq. (16) ( $m$ ,  $n$ ,  $k_1$  and  $k_2$ ) by fitting the experimental data of Fig. 36 to Eq. (16) using standard nonlinear regression analysis. Here, the symbols are experimental data while the lines are computed from the equation using  $m$ ,  $n$ ,  $k_1$  and  $k_2$  as fitting parameters. The obtained parameters are listed in Table 7 with correlation coefficient or  $R^2$  better than 99%. One can see that an excellent representation of the data was obtained using this model, giving a value of  $m+n \sim 2$  that is independent of the change in the temperature and in good agreement with reported data in the literature. As already mentioned, this kinetic model depicted in Eq. (16) was originally used for interpreting the curing kinetics in a number of investigations of thermosetting polymers monitored by DSC reported in literature; in many of these cases the curing reaction was found to be sec-

**Table 7**  
Kinetic parameters of thermal-induced gelation of PUD (40 wt% PU) given by Eq. (16).

Temperature (°C)	$k_1$ (min <sup>-1</sup> )	$k_2$ (min <sup>-1</sup> )	$m$	$n$
55	$3.35 \times 10^{-4}$	0.0183	0.75	1.25
60	$5.00 \times 10^{-4}$	0.0302	0.82	1.158
70	$1.00 \times 10^{-3}$	0.064	0.711	1.259

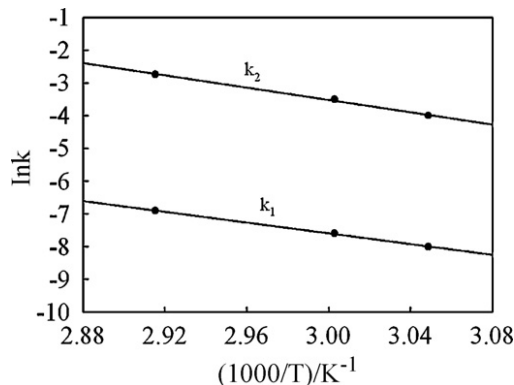


Fig. 37. Arrhenius treatment of the temperature dependence of the rate constants,  $k_1$  and  $k_2$  of Eq. (16) (adapted from [133]).

ond order ( $m+n=2$ ) [147–150]. On the basis of the above, it is apparent that the rheological kinetics of thermally activated gelation reaction of PUD can be well described by the Malkin and Kulichikhin model, in good agreement with reported studies in the literature [133,140,146].

The temperature dependence of the apparent rate constants,  $k_1$  and  $k_2$ , of Eq. (16) obtained from the above regression (Table 7) can be described by the Arrhenius relationship:

$$k = k_0 \exp\left(\frac{-E_a}{RT}\right) \quad (18)$$

where  $k_0$  is the pre-exponential factor,  $E_a$  is the apparent activation energy,  $R$  is the universal gas constant and  $T$  is the absolute isothermal cure temperature. One can determine the value of  $E_a$  from the slope of the linear relationship between  $\ln(k)$  and the inverse of absolute temperature as demonstrated in Fig. 37. It was found that  $E_a = 125$  and  $129$  kJ/mol for the temperature dependence of  $k_1$  and  $k_2$ , respectively. This value of  $E_a$  is higher than the value obtained for the gelation process of other different cross-linking systems reported in the literature [140,151,152]. For example, the values of rheological  $E_a$  determined by Fernandez et al. [151] for tetrafunctional epoxy resin and its blends with poly(methyl methacrylate) and poly(ethersulfone) were 71, 73 and 69 kJ/mol, respectively. The high value of  $E_a$  for the present system (PUDs) is due to the very strong physical interaction between the PU-dispersed particles which in turn leads to formation of a very strong elastic gel [59,60].

Similarly, the gelation activation energy can be evaluated from the following equation:

$$\ln(T_{gel}) = \text{constant} + \frac{E_a}{RT} \quad (19)$$

The values of  $t_{gel}$  at different temperatures were calculated from the plots of  $\tan \delta$  versus  $T$  as a function of shear frequency as already described in Fig. 26. From the slope of the linear relationship between  $\ln(t_{gel})$  and the inverse of absolute temperature (Fig. 38) one can obtain the apparent activation energy of the gelation process to be  $E_a = 125$  kJ/mol, a value in good agreement with the values obtained earlier.

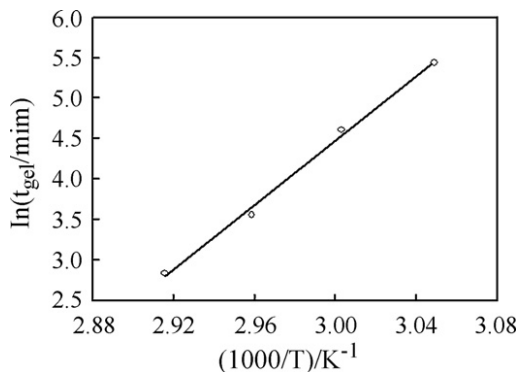


Fig. 38. Dependence of  $t_{gel}$  on the absolute inverse temperature,  $1/T$ , of the gelation process (adapted from [133]).

#### 4.13. Isoconversional method

On the basis of the isoconversional or model-free method, the gelation kinetics can be described using the following equation [141–144]:

$$g(\beta) = A \exp(-E_\beta/RT) t_\beta \quad (20)$$

where  $g(\beta)$  is the integral reaction model,  $E_\beta$  is the activation energy at constant value of conversion and  $A$  is the pre-exponential factor. Taking the natural logarithm of the above equation yields:

$$-\ln t_\beta = \ln \left( \frac{A}{g(\beta)} \right) - \frac{E_\beta}{RT} \quad (21)$$

From the slope of the linear relationship of  $-\ln t_\beta$  versus  $1/T$  one can evaluate  $E_\beta$  at different values of  $\beta$  as shown in Fig. 39. Clearly all the curves have approximately constant slope and the calculated value of activation energy is approximately constant regardless of the degree of conversion (i.e.,  $E_\beta = 120 \pm 3$  kJ/mol), indicating that the rate of gelation is controlled by a single step (homogeneous) process with no change in the aggregation mechanism at different degrees of conversions. This is an interesting result that is in good agreement with the curing kinetics of

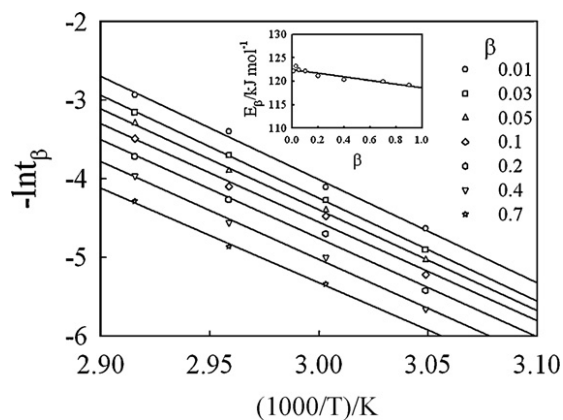


Fig. 39. Isoconversional plots for the gelation process of PUD (40 wt% PU) as functions of the degree of conversion discussed in the text. The inset plot shows the variation of the activation energy with the degree of conversion (adapted from [133]).

diglycidyl ether of bisphenol A with m-phenylenediamine with nonstoichiometric ratio studied recently using DSC by Sbirrazzuoli et al. [142]. They reported that, the variation of the activation energy with degree of conversion is mainly dependent on the stoichiometric ratio of the reactants. For nonstoichiometric system they showed that the activation energy is almost constant and independent of the extent of conversion as for the PUD system described here [142]. However, the activation energy decreased strongly with increasing the degree of conversion for stoichiometric system [142]. Recently, Khawam and Flanagan [144] reported that the variation of activation energy with degree of conversion could be real or an artifact. A true variation in activation energy is one that occurs because of the inherent complexity of the solid sample, which includes different reactivity of individual particles due to the particle size variations or crystal imperfections. Artifacts arise from the kinetics calculation methods employed. Khawam and Flanagan suggested that care should be taken when interpreting kinetic results from isoconversional methods, if the variation in activation energy is an artifact, this variation can lead to a conclusion about a reaction being complex while, in fact, it is not [144].

#### 4.14. Non-isothermal gelation kinetics

Non-isothermal reaction kinetics was described as functions of time, temperature and concentration by a model proposed by Swartzel et al. [153,154]. This model was developed to include the classical rate equation, the Arrhenius equation, and the time–temperature relationships according to the following equation [135,155]:

$$\ln \left( \frac{1}{G^n} \frac{dG}{dt} \right) = \ln k_0 - \left( \frac{E_a}{RT} \right) \quad (22)$$

The gelation process is a second-order reaction as we found in the previous section ( $n + m = 2$ ); therefore  $n$  was replaced in Eq. (22) by 2, and consequently the apparent activation energy can be obtained from the following relationship:

$$\ln \left( \frac{1}{G^2} \frac{dG}{dt} \right) \text{ vs } \frac{1}{T} \quad (23)$$

The  $E_a$  determined from the slope of this relation was found to be frequency independent and equal to 125 kJ/mol, in very good agreement with the value obtained isothermally from the temperature dependence of  $t_{gel}$ ; and also in reasonable agreement with the values obtained from the slopes of the two plots in Fig. 37 (i.e.,  $E_a = 129$  and 125 kJ/mol). Fig. 40 shows clear straight lines with identical slopes regardless of the values of shear frequency.

### 5. PU/POSS nanocomposites

Incorporation of a well-defined nanostructured inorganic cluster to a polymer matrix to form special organic/inorganic hybrids represent the first entirely new chemical feedstock advancement within the past 50 years [156]. The technology merges the properties of fillers with the versatility and precision of chemistry. Their nanoscale size affords molecular level control over polymer dynamics, surface-bulk properties, and biological function. As

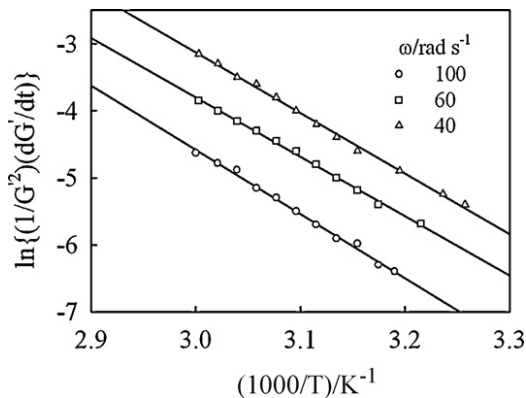


**Fig. 40.** Arrhenius-type plots for the change of  $G'$  during the nonisothermal gelation of PUD, assuming a second-order reaction kinetics (adapted from [133]).

an example of a well characterized inorganic cluster just mentioned, reactive polyhedral oligomeric silsesquioxanes (POSS) belong to a special class of functional nanoscale fillers consisting of an eight-corner,  $-(\text{SiO}_{1.5})_n$ -based cage bearing one or more functional groups [156–163]. POSS has been used as an interesting class of precursors for the synthesis of molecularly designed organic/inorganic hybrids. Nanostructured POSS chemicals bridge the gap between fillers and monomers in offering shrinkage control and reinforcement of polymer chains (see Fig. 41). When appropriately functionalized they can also bridge the gap between polymers and plasticizers, without plasticizer migration. The nanostructured POSS materials afford the modification of surfaces with well-defined inorganic/organic segments and offer an alternative to traditional chemical coupling agents such as silanes. The size of the pendant POSS cage is comparable to the dimensions of the linear polymer, enabling POSS to control the motions of the chains at the molecular level with enhanced benefits while retaining the processability and mechanical properties of the base resin.

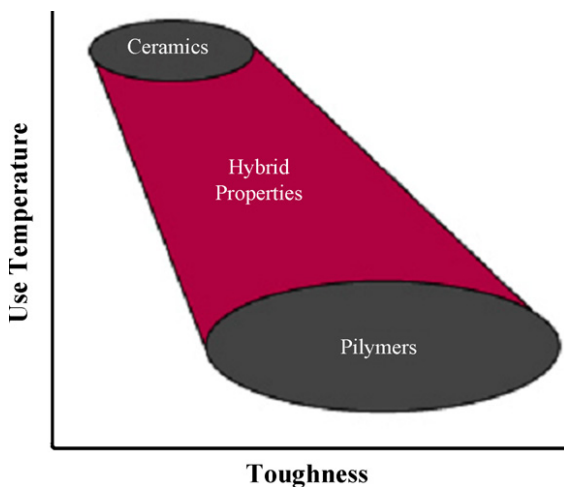


**Fig. 41.** Toughness as a function of temperature for polymers, polymer hybrids, and ceramics (adapted from [156]).

Despite the growing number of scientific and patent literature on POSS and related materials, there are few reported examples of practical and optimal exploitation of POSS [164–166]. Such nanoreinforced polymers lead to significant thermomechanical property enhancements, while simultaneously improving or retaining the material's other physical properties such as optical clarity, stiffness, strength, and processability. Other property enhancements such as gas permeability may also be realized to an extent that depends on the type and concentration of POSS used. Typically, high thermal stability, improved environmental durability in special aggressive environments (e.g., exposure to atomic oxygen and fire resistance), and, in some cases, improvement in mechanical properties (reinforcement) have been reported for POSS-modified polymers [167–169]. In general POSS can be incorporated into a polymer matrix by two different methods (i.e., mechanical melt blending or chemical functionalization of one or more functional groups into the corner of the POSS chemical structure). When the functionalized POSS is chemically reacted (via covalent bonds) with the polymer matrix, the resulting POSS-modified polymer is more thermally stable and reinforced at the molecular level [170]. These desirable attributes of the POSS-modified polymer are ascribed to relatively strong POSS–POSS and POSS–polymer interactions in nanocomposites [170–173].

#### 5.1. Typical synthesis of PU/POSS hybrids (10 wt% POSS)

Two different kinds of POSS are used in this review article to illustrate synthesis of typical PU/POSS hybrids from homogenous aqueous solution [174,175]. The first one is 3-(2-aminoethylamino) propyl-heptaisobutyl-POSS (diamino-POSS) and the second one is 2,3-propanediol propoxy-heptaisobutyl-POSS (diol-POSS) as shown in Fig. 42. The so-called acetone process has been used to synthesize the PU/POSS hybrid dispersion because acetone is a common solvent for POSS. The chemical structure of group R in Fig. 42 is isobutyl. In a 500 mL round bottom flask, 10.0 g diamino-POSS (0.021 amine equiv.) was added to 125 g of acetone, followed by the dropwise addition of 23.0 g of isophorone diisocyanate (IPDI) (0.207 isocyanate equiv.) while stirring using a magnetic stirrer at 20 °C. After 20 min three drops of dibutyltin dilaurate (DBTDL) were added [174]. After 10 min the flask was fitted with a mechanical stirrer, a thermocouple controlled heating mantle, a condenser with nitrogen bubbler and a pipette outlet. The polyester polyol (61.1 g, 0.06 hydroxyl equiv.) and dimethylolpropionic acid (DMPA) (3.1 g, 0.046 hydroxyl equiv., and 0.023 acid equiv.) were charged into the flask and stirring was continued while the temperature was raised to 60 °C. The isocyanate (NCO) content was monitored during the reaction using the standard dibutylamine back titration method [58]. Upon reaching the theoretical NCO value, the prepolymer was chain extended with 1,4-butanediol (BD) (2.6 g, 0.057 hydroxyl equiv.) and the reaction continued for 2 h to complete polymerization, yielding the desired polyurethane-urea/POSS copolymer. In the last step, the polymer was neutralized by the addition of 2.3 g of triethyl amine (0.023 equiv.) and stirred for 30 min while maintaining the temperature at 55 °C.

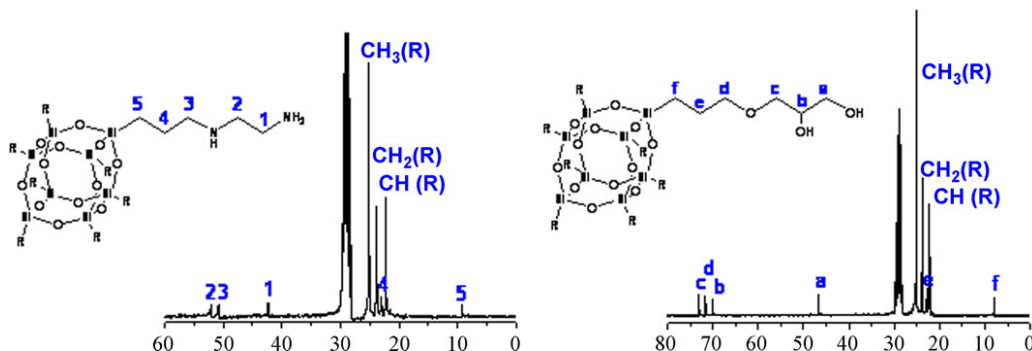
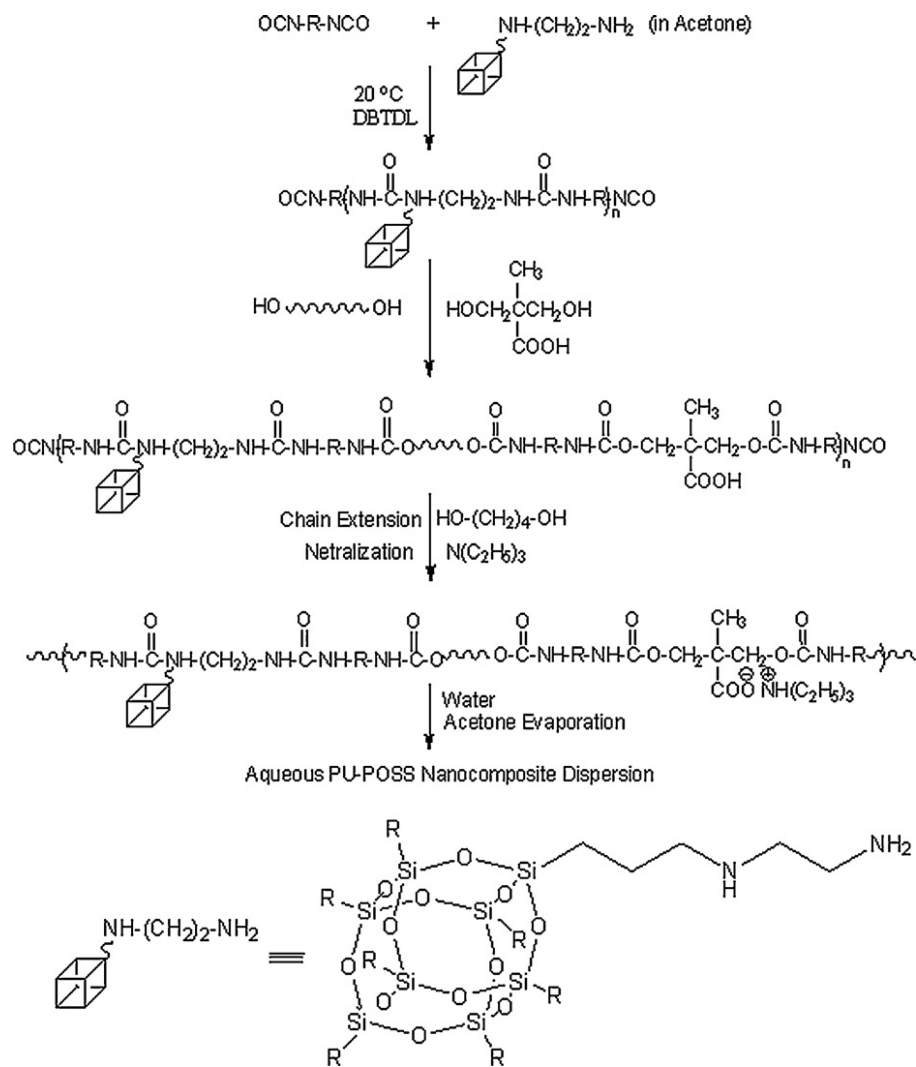


Fig. 42. Structures of diamino-POSS and diol-POSS, R= isobutyl (modified from [174]).

Formation of the dispersion was accomplished by slowly adding water to the neutralized acetone solution of the polyurethane-urea polymers at 45–50°C over 30 min with agitation speed of 600 rpm. After stirring for 30 min the reaction mixture was transferred to a rotary evap-

orator and the acetone removed at 35°C and a partial vacuum of 70 mm Hg to afford organic solvent free dispersions with 32 wt% solids. The reaction in Scheme 5 shows the elementary steps for the synthesis of hybrid PU/POSS nanocomposite dispersion [174,175]. The so-called ace-



Scheme 5.

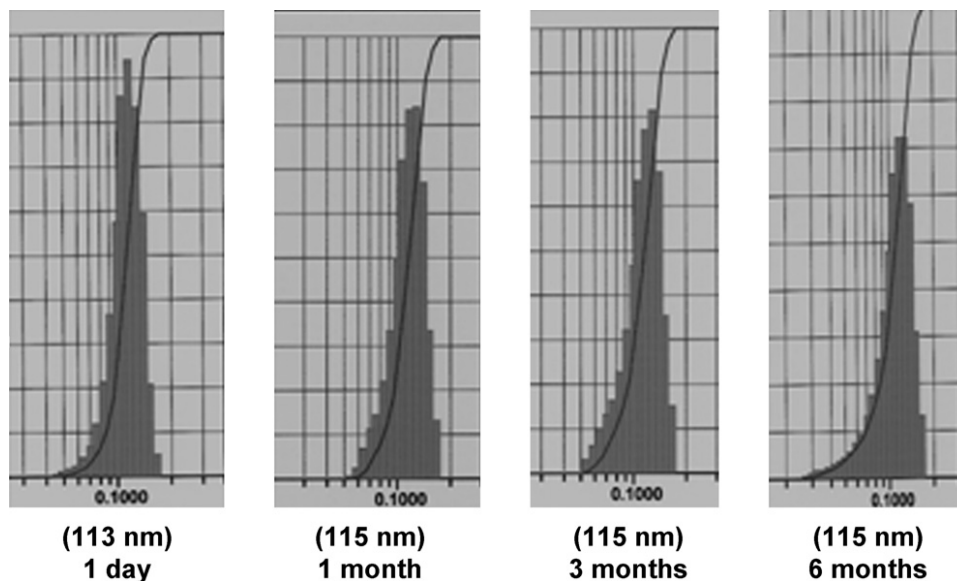


Fig. 43. Particle sizes of **PU10** during storage as described in the text (adapted from [174]).

tone process used in the preparation of PU dispersions was evaluated for the formation of PU/POSS hybrids with POSS contents on total polymer solids of 4, 6 and 10 wt% (**PU4**, **PU6** and **PU10** respectively). The following variables were held constant for all of the samples: [DMPA] at 3 wt% based on total concentration of polymer (i.e., [polymer] = 32 wt%), and chain extension at 90%. To compensate for the inclusion of the POSS monomers, the polyester diol content was reduced from 73 to 62 wt% of the total polymer solids as the [POSS] was varied from 0 to 10 wt%. In the process reported here (Scheme 5), the diamino-POSS was first dissolved in acetone, before reaction with IPDI. Subsequent steps of prepolymer formation, chain extension and neutralization were maintained as for the method used for non-POSS containing control dispersion (**PU0**). Carrying out the first step of the synthesis in acetone was essential to obtain a homogeneous reaction mixture, as the urea formed precipitated in the absence of acetone.

The inclusion of the POSS monomers did not have a major impact on the solution properties of the dispersions relative to that of the control (**PU0**). The minor differences in particle size and viscosity with increasing POSS content are within the limits of reproducibility, indicating that the POSS monomers do not affect the dispersion step. The dispersion particle sizes for all the samples were found to be unimodal and remained constant over six months of storage at room temperature (Fig. 43).

The inclusion of the POSS monomers did not have a major impact on the solution properties of the dispersions relative to that of the control (**PU0**). The minor differences in particle size and viscosity with increasing POSS content are within the limits of reproducibility, indicating that the POSS monomers do not affect the dispersion step. The dispersion particle sizes for all the samples were found to be unimodal and remained constant over six months of storage at room temperature (Fig. 43).

The reaction mixtures were analyzed at each step of the sequence to verify that the comonomer was incorporated [174]. Fig. 44 shows the GPC traces of the diamino-POSS monomer and the three steps of polymerization prior to neutralization. The molecular weights determined by GPC, though not absolute, are useful to qualitatively follow the increase in molecular weight at different stages of the polymerization. It is clearly evident in Fig. 44 that the vast majority of the diamino-POSS is incorporated in the first step; and that the final polymer is virtually free of residual POSS comonomer ( $M_n \sim 700$  g/mol).

A series of linear ionomeric polyurethanes were synthesized and obtained as stable aqueous dispersions using various amounts (ca. 6–20%) of a diol functionalized polyhedral oligomeric silsesquioxane (POSS) comonomer using NMP process by Turri and Levi [176]. All the aqueous dis-

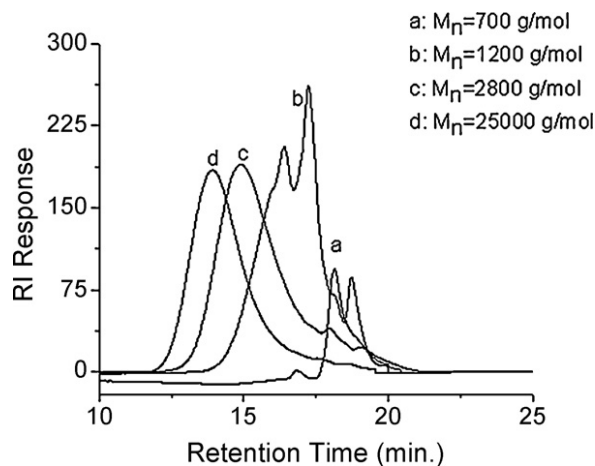


Fig. 44. GPC chromatograms of: (a) diamino-POSS, (b) diamino-POSS + IPDI, (c) prepolymer and (d) final polymer of **PU10** (adapted from [174]).

persions obtained were stable (i.e., no settling) for at least 6 months at ambient temperature, except for one sample containing the highest level of POSS macromer (18.8 wt% POSS) incorporated in the prepolymer. That sample also showed very poor film-forming properties and was little characterized.

## 5.2. Characterization of PU/POSS nanocomposites films

### 5.2.1. Wide angle X-ray analysis

Determining the phase segregation behavior of the POSS moieties in films prepared from the dispersions already discussed is critical to the understanding of the relationship between POSS content and the resulting physical properties. In general, films prepared from aqueous polyurethane dispersions do not exhibit the clear formation of crystalline hard segment domains that are found in many polyurethane elastomers or plastics. The chemistry of the film products and the need to coalesce into a continuous film precludes the high level of crystallinity that is found in typical melt or solvent processed polyurethanes. The presence of the hard-segment domains is inferred from the high-temperature change in physical properties (i.e., softening point) that is not accompanied by a detectable thermal transition in DSC measurements.

Depending on which phase the POSS moieties partition to, inclusion of the POSS monomers could affect visual properties of the film (clarity, etc.), morphology and physical properties. As a first indicator of film heterogeneity, film clarity normally imply the absence of macro phase separation and the clarity should decrease if large POSS rich domains are formed in the solid state. All the films prepared from the dispersions discussed in this review article were found to be optically clear and defect free, but additional analysis is required to identify structural changes on the microscopic scale [174].

Further evidence of the homogeneity can be gleaned from wide angle X-ray analysis of the films (Fig. 45a). The X-ray pattern for the control sample (**PU0**) shows a small sharp reflection at  $2\theta = 20.9^\circ$  superimposed on a broad amorphous halo centered at  $2\theta = 19.5^\circ$  from the polyurethane hard segment. With the inclusion of 4 wt% POSS (**PU4**), the sharp peak and broad reflection of PU is still present with an additional broad peak at  $2\theta = 8.6^\circ$ . For samples containing 6 and 10 wt% POSS (i.e., **PU6** and **PU10**, respectively) the sharp reflection found in **PU0** completely disappears, leaving the two amorphous halos centered at  $2\theta = 8.6^\circ$  and  $19.5^\circ$  as the only features seen in the X-ray pattern [174]. The X-ray pattern obtained for the unreacted

diamino-POSS monomer showed well defined reflections found at  $2\theta = 8.1^\circ, 10.8^\circ, 12.1^\circ$  and  $18.8^\circ$  (see Fig. 45a) [176]. These sharp reflections corresponding to the crystalline monomeric POSS were not detected in any of the films prepared from samples ranging from **PU4** to **PU10** as depicted in this figure. The amorphous halo centered at  $8.6^\circ$  indicates that the presence of POSS moieties is either causing some type of additional order or is more likely increasing the volume of the hard segment phase into which it partitions.

X-ray data for the PU/POSS nanocomposite films obtained from the NMP process is presented in Fig. 45b [176]. All the samples show two broad peaks centered at about  $18^\circ$  and  $6^\circ$ , which could be attributed to the amorphous polyether phase and to hard-soft interactions in analogy to other conventional PU systems. It is clear that all the POSS-modified samples showed some residual crystallinity in the form of 101 reflection at about  $8^\circ$ ; the intensity of the peak just mentioned is very small in the case of A6 polymer (5.8 wt% POSS). This experimental fact would mean that POSS cages maintain a relevant self-assembling ability with formation of nanocrystal phases even when copolymerized by a predominantly statistical process.

### 5.2.2. Tensile and DMA tests

The materials prepared from acetone process have a very soft base formulation; therefore, any partitioning of the POSS moieties into the soft segment phase would result in a large increase of the soft segment  $T_g$ . Partitioning of POSS into the hard segment phase could lead to an increase in softening temperature based on either increased integrity or through an increase in the volume fraction of the hard segment. An increase in the volume fraction of the hard segment would also have a predictable impact on modulus above the glass temperature of the soft segment. Partitioning to form its own phase, separate from those already present in the polyurethane, would be readily observable as a new thermal transition in DMA or DSC [174].

Preliminary tensile tests on films prepared from the PU/POSS samples (acetone process) revealed major changes based on the inclusion of POSS as Table 8 shows. The physical properties changed systematically with POSS content as evidenced by tensile strength at break increasing by a factor of 10, from  $60 \text{ N/cm}^2$  for the control (**PU0**) up to more than  $600 \text{ N/cm}^2$  for the samples containing 10% of the POSS monomers (**PU10** and **PU10A**). Where **PU10** and **PU10A** are the nanocomposites with 10 wt% diamino-POSS and diol-POSS, respectively. As expected, there is a drop in

**Table 8**  
Physical properties of the hybrid PU/POSS nanocomposite films discussed in the text.

Sample	Contact angle ( $^\circ$ )	$T_g$ ( $^\circ\text{C}$ ) (hard segment)	At break	
			Tensile strength ( $\text{N/cm}^2$ )	Elongation (%)
<b>PU0</b>	$64.1 \pm 2$	53	60	2000
<b>PU4</b>	$82.0 \pm 2$	56	102	1200
<b>PU6</b>	$85.0 \pm 2$	66	210	1100
<b>PU10</b>	$89.0 \pm 2$	90	625	900
<b>PU10A</b>	$88.4 \pm 2$	91	620	900

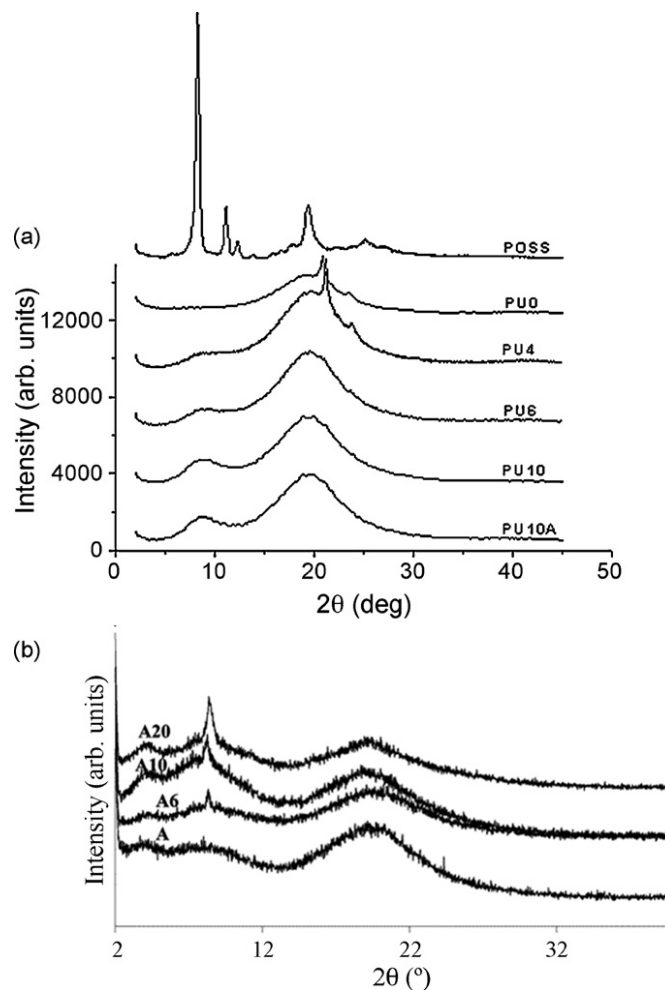


**Fig. 45.** (a) WAXD patterns of the PU/POSS hybrids containing diamino-POSS and **PU0** (control) (adapted from [174]). (b) WAXD patterns of the PU/POSS of different POSS contents, Pure PU (A), 5.8 wt% POSS (A6), 9.4 wt% (A10), and 18.8 wt% POSS (A20) (adapted from [176]).

elongation at break, although the stiffest films with 10 wt% POSS exhibited a 900% elongation before breaking [174]. This is a remarkable result that could be exploited in applications where both stiffness and ductility are important performance requirements.

The differences in physical properties caused by the inclusion of POSS are also apparent from the results obtained from DMA testing (Fig. 46). At low temperatures,  $E'$  increases moderately with POSS content, and becomes significant at elevated temperatures (Fig. 46a). Fig. 46b shows  $\tan \delta$  versus temperature for the PU/POSS samples. Obviously, no significant variation in the lower temperature maximum between  $-15$  and  $-20^\circ\text{C}$  arising from the soft segment  $T_g$  as the amount of POSS is increased. By contrast, at the high temperature range where the hard segments softening point is normally located, there is a large change with the temperature corresponding to the  $\tan \delta$  maximum rising incrementally from  $53$  to  $90^\circ\text{C}$  as the amount of POSS is increased [174].

These results suggest that the POSS moieties are incorporated in the hard segments rather than the soft segments.

The noted changes in physical properties are consistent with that expected with increasing hard segment content of a polyurethane, and are also consistent with first order estimates of hard segment content as the amount of POSS is increased. The latter estimates for the present PU/POSS samples in Table 9, were made assuming that the “hard segment” content of the control polyurethane (**PU0**) is comprised of the 1,4-butane diol, DMPA, and the reacted molar equivalents of isocyanate. If the functionalized POSS

**Table 9**

Calculated weight percent of the “hard segments” content for POSS partitioned into soft segment or hard segment phases of the PU.

	POSS wt% in the soft segment	POSS wt% in the hard segment
<b>PU0</b>	17	17
<b>PU4</b>	17	22
<b>PU6</b>	17	24
<b>PU10</b>	17	30
<b>PU10A</b>	17	30



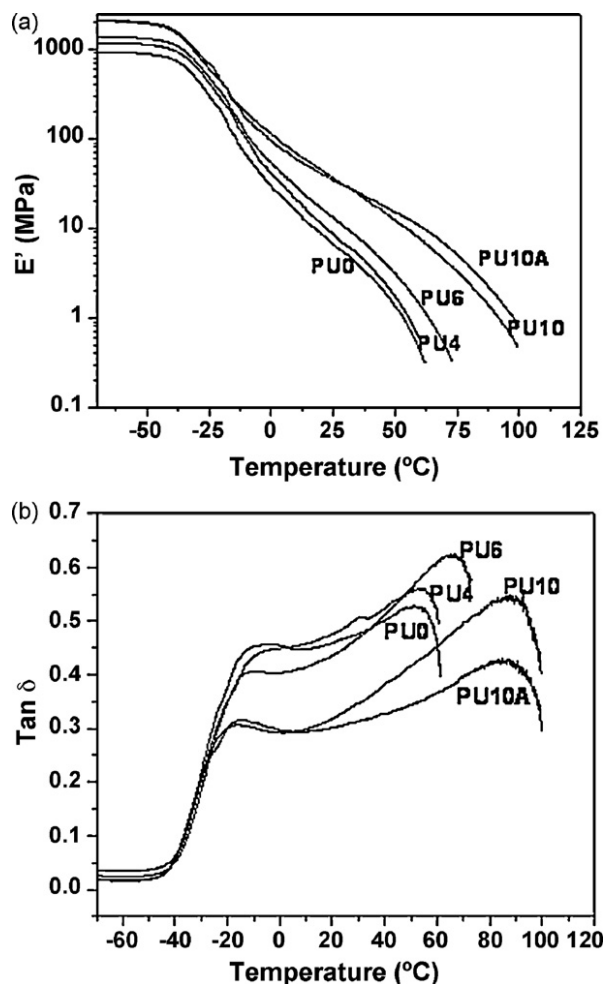


Fig. 46. (a) Elastic modulus versus temperature of the PU/POSS hybrid films discussed in the text (adapted from [174]). (b)  $\tan \delta$  versus temperature of the PU/POSS hybrid films discussed in the text (adapted from [174]).

reaction products partition into the soft segment domains there would be no change in hard segment domain content. On the other hand, if the POSS partitions into the polyurethane rich hard segment phase there would be an overall increase in hard segment content from 17 to 30 wt% (Table 9) as the POSS level is increased to 10% of total composition.

Similar DMA measurements for PU/POSS samples obtained from NMP process are shown in Fig. 47a and b [176]. One can see that both  $G'$  and  $\tan \delta$  are not affected by addition of POSS. This experimental fact suggests that POSS has no reinforcement effect on the PU matrix. One reason may be due to the relatively poor solubility of pure POSS in NMP, and, therefore, the polymerization reaction might not have proceeded to completion as expected. In contrast, the improved reinforcement of the mechanical properties of PU/POSS obtained from the acetone process can be attributed to the excellent solubility of POSS in acetone.

### 5.3. Rheological behavior of pure PU and PU/POSS nanocomposites films

This section begins by first investigating the linear viscoelastic behavior of pure PU and subsequently followed by considering the effects of incorporation of small amounts (up to 10 wt%) of POSS nanoscale grafted filler on the rheology, morphology, and thermal stability of the PU matrix.

#### 5.3.1. Pure PU film (PU0)

The master curves of the dynamic shear moduli,  $G'$  and  $G''$  can be constructed based on the concept of thermorheological simplicity. For example, the storage modulus can be superimposed by horizontal shifts along the  $x$ -axis (frequency axis), according to the following equation:

$$G'(\omega a_T, T_0) = G'(\omega, T) \quad (24)$$

where  $\omega$  is the magnitude of the shear frequency,  $a_T$  is the horizontal shift factor and  $T_0$  is the reference temperature. The time–temperature superposition or Williams–Landel–Ferry (WLF) equation increases the accessible frequency window of the linear viscoelastic experiments. This principle applies to stable materials without thermal-induced physical or chemical reactions or transitions during the dynamic measurements, and only the effect of temperature on the relaxation process is considered. Therefore, the principle works well when the stress-sustaining structure in the system does not change with temperature, and when the relaxation times of all modes of this structure change with temperature by the same factor. Fig. 48 shows the master curves of the dynamic shear moduli,  $G'$  and  $G''$  for pure PU sample (PU0) at  $T_0 = 120^\circ\text{C}$ . Clearly there is strong deviation in the terminal zone of the master curve of  $G'$  starting at about  $140^\circ\text{C}$ . This deviation means that the WLF Eq. (26) is no longer valid at high temperature range. This behavior is attributed to the fact that the PU chemical structure is a multiblock copolymer comprised of alternating soft polyester and hard polyurethane–urea segments. These two segments undergo microphase separation into hard and soft phases, respectively, below and above their glass transition temperatures. This microphase separation is responsible for the excellent elastomeric properties of PU. The  $G''$  does not show any deviation in the terminal zone of the master curve indicating that the stress induced in the system by the concentration fluctuations accompanying the microphase separation transition is mostly elastic in origin. It is apparent from this figure that the WLF principle is only valid for temperatures lower than  $140^\circ\text{C}$ ; the WLF principle failed for  $T \geq 149^\circ\text{C}$ . The existence of microphase separation transition in PU elastomers has been clearly demonstrated beyond doubt in the literature using different techniques [177–180]. Similar breakdown in the WLF principle has been observed in several diblock and triblock copolymers, and polymer blends with lower and upper critical solution temperatures phase diagram (LCST and UCST, respectively). For a number of diblock and triblock copolymer reported in the literature this breakdown of WLF principle has been shown to be related to a microphase separation transition. The microphase separation of PU based on soft segments of polycaprolactone

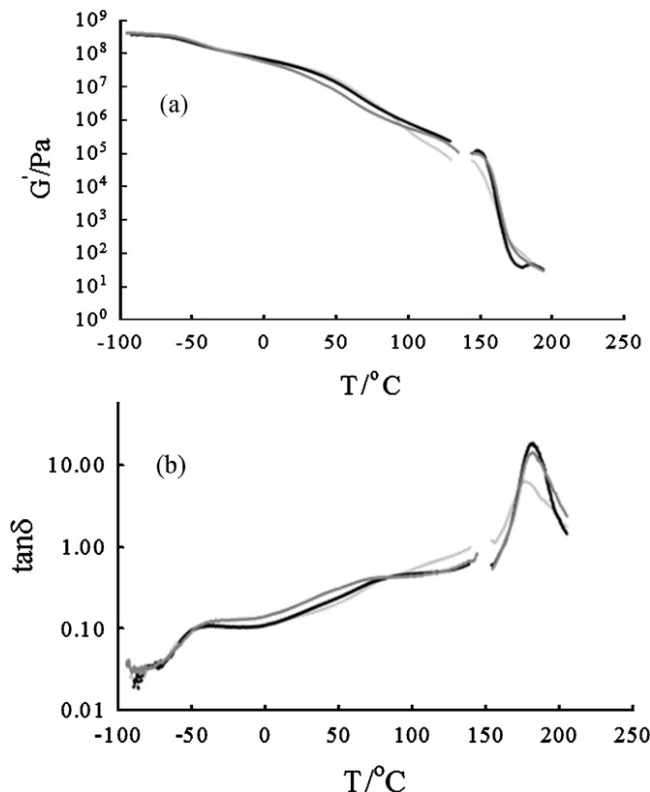


**Fig. 47.** (a) Elastic share modulus versus temperature of the PU/POSS hybrid films of different POSS contents (0–18.8 wt% POSS) (adapted from [176]). (b)  $\tan \delta$  versus temperature of the PU/POSS hybrid films of different POSS contents (0–18.8 wt% POSS) (adapted from [176]).

as a function of block length has been investigated rheologically and by using small angle X-ray scattering (SAXS) measurements by Velankar and Cooper [180]. They showed for the systems studied that the WLF principle failed at high temperatures to an extent that depends on the multiblock lengths.

Fig. 49 depicts schematically the structure of PU elastomer as multiblock hard segments (urethane) and soft segments (polyester diol). The TEM shows how these two segments can phase separate into nanoscale morphology. The very small dark particles in the micrograph are the hard segments and the bright matrix is the soft segments of the Yang et al. [181] confirmed the occurrence of microphase separation in pure PU using a tapping mode atomic force microscopy (AFM). Their results of phase lag spectra are shown in Fig. 50, in which one can clearly see that samples without annealing (room temperature) and annealed at 55 °C (i.e., temperatures well below  $T_{MPS}$ ), exhibited a heterogeneous morphology with soft domains of irregular shapes (dark area) randomly dispersed in a hard matrix (gray area). For sample quenched from an annealing temperature of 88 °C, which is above the  $T_{MPS}$ , a homogeneous morphology was observed. For the sample quenched from a higher annealing temperature of 98 °C a more homogeneous picture was obtained. The morphological changes just mentioned confirm the destruction of domain morphology and the complete mixing of the soft and hard segments. The value of  $T_{MPS}$  for pure PU was reported by Yang et al. to be about 70 °C as measured by rheology [181].

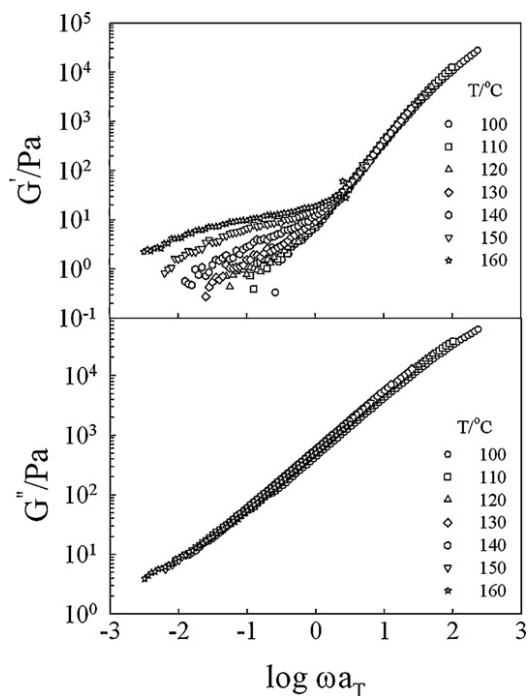


**Fig. 48.** Master curves of the dynamic shear moduli,  $G'$  and  $G''$  for PU0 at reference temperature,  $T_0 = 120$  °C (adapted from [175]).

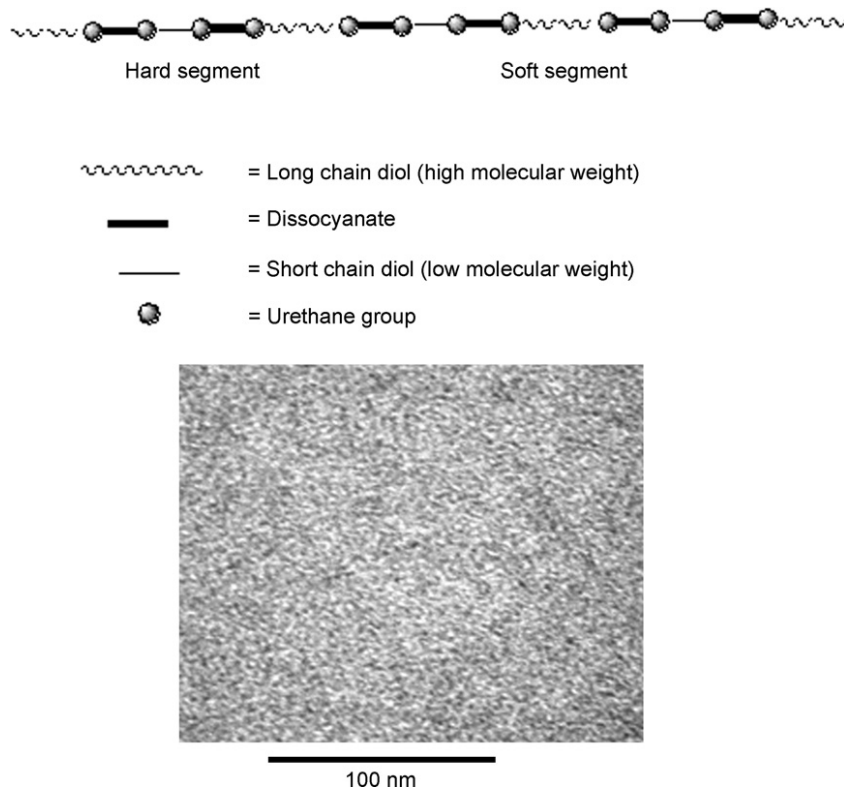


**Fig. 49.** Schematic diagram of the hard and soft segments of PU structure. The TEM shows microphase separation morphology for the hard segments (dark particles) and polyester soft segments (bright matrix) (adapted from [175]).

The temperature dependence of the shift factor ( $a_T$ ) can be studied using the Arrhenius (Eq. (25)) and the WLF (Williams–Landel–Ferry) (Eq. (26)) expressions [182]:

$$\log a_T = \frac{E_A}{2.303R} \left( \frac{1}{T} - \frac{1}{T_0} \right) \quad (25)$$

$$\log a_T = \frac{-c_1(T - T_0)}{c_2 + (T - T_0)} \quad (26)$$

where  $R$  is the universal gas constant,  $E_A$  is the activation energy of flow, and  $c_1$  and  $c_2$  are the WLF parameters. Fig. 51 shows the temperature dependence of the shift factor  $a_T$  for the data of Fig. 48. The experimental points are fitted by the WLF equation using  $c_1$  and  $c_2$  as fitting parameters. Although, there is a considerable deviation from the master curve of  $G'$  at high temperatures in the terminal zone, the temperature dependence of the shift factor is well described by the WLF and Arrhenius equations over the entire temperature range. This experimental fact suggests that the contribution of concentration fluctuations to the viscoelastic material functions caused by microphase separation of the hard and soft segments of PU is not big enough to lead to a considerable deviation from the two equations (25) and (26). However, these parameters should be taken with extreme caution giving the lack of thermorheological simplicity of the nanocomposite system discussed in this review article [175]. The inset plot of Fig. 51 shows the Arrhenius plot for the same experimental data. The value of the  $E_A$  obtained from the slope of this straight line is 88 kJ/mol.

The microphase separation of the hard and soft segments of PU can be easily detected from rheological data by using the Cole–Cole plot (or Han plot) as shown in Fig. 52. In the low temperature range, all curves coincide; however, the curves deviate at high temperatures due to microphase separation. Clearly, the curves start to deviate at 140 °C, indicating that 140 °C is the microphase separation temperature of the hard and soft segments of PU, in good agreement with the value obtained from the deviation in the master curve of  $G'$  as shown in Fig. 48. The deviation in the curve at the microphase separation temperature is very sharp due to the big difference in  $T_g$  of the hard and soft segments (i.e., 50 and –50 °C, respectively) [175].

The complex viscosity of **PUO** as a function of angular frequency for different temperatures is shown in Fig. 53. Clearly, the viscosity of **PUO** slightly depends on shear frequency and decreases with increasing temperature at low temperatures ( $T < 140$  °C). At  $T = 140$  °C, the viscosity increases slightly in the low shear frequency range and becomes non-Newtonian over a wide frequency range at  $T \geq 160$  °C. Note that in Fig. 53 the lines are computed from Cross model (Eq. (1)), while the symbols are experimental data. The value of zero shear viscosity calculated from this fitting as a function of temperature is considered with other PU/POSS composites in the next section.

### 5.3.2. PU/POSS nanocomposites

The master curves of the dynamic shear moduli,  $G'$  and  $G''$  for PU/POSS nanocomposite with 10 wt% diamino-POSS

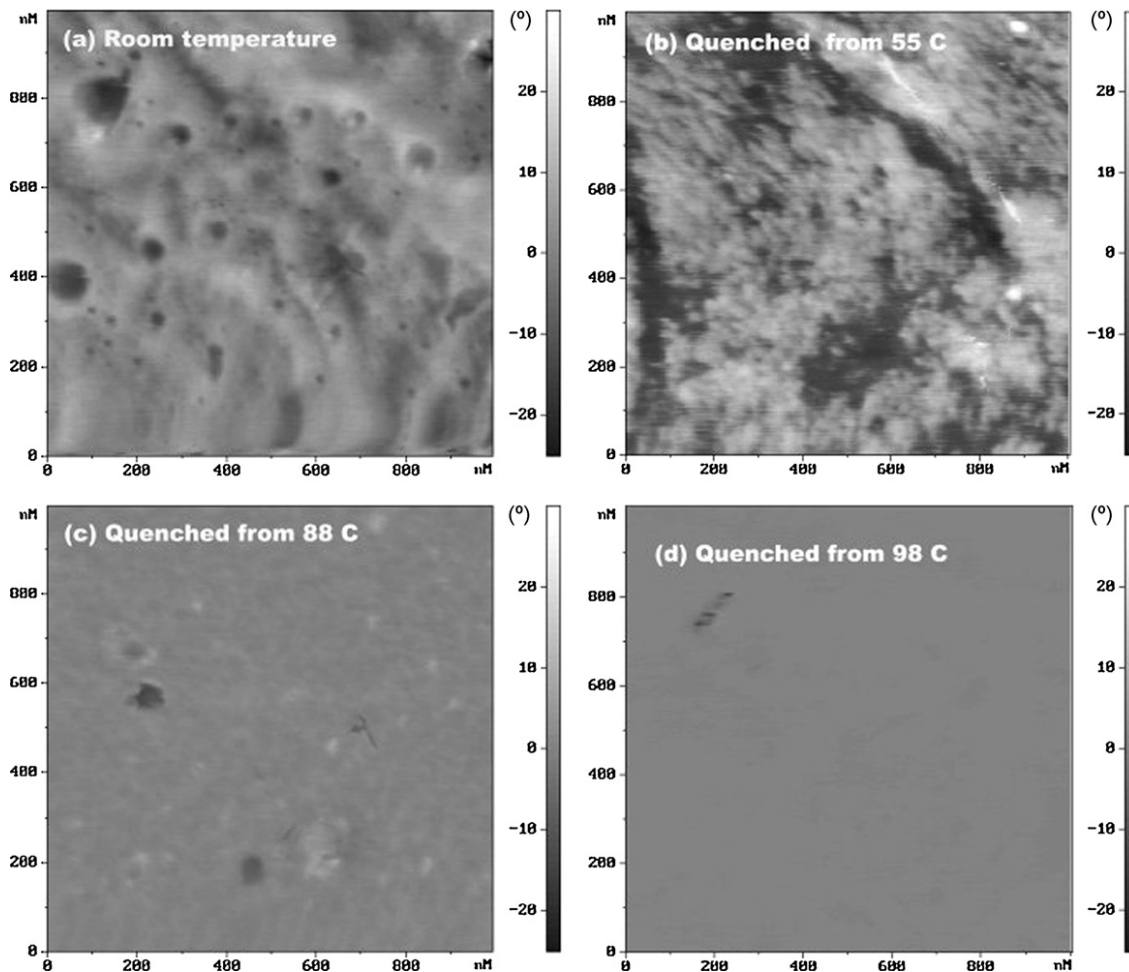


Fig. 50. Atomic force microscopy of PU sample quenched from different annealing temperatures indicated (adapted from [181]).

(PU10) are shown in Fig. 54. Similar to Fig. 48, there is a considerable deviation in the terminal zone of the master curve of  $G'$  only in the high-temperature range. As before, this deviation indicates failure of the WLF equation to describe the viscoelastic behavior of both PU and

PU/POSS at high temperatures due to the microphase separation of the hard and soft segments. It is also clear from this figure that the incorporation of reactive POSS in the PU chains can significantly affect the microphase separation temperature as evidenced by the reduced deviation in the terminal zone compared to that of pure PU already

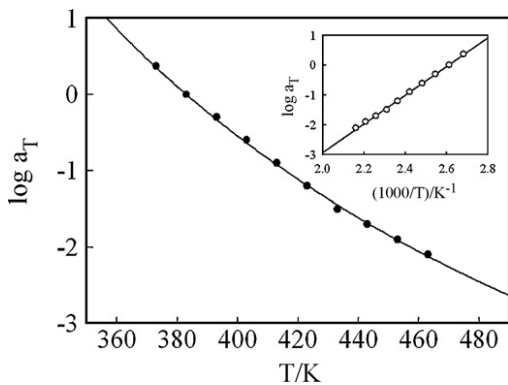


Fig. 51. Shift factor  $a_T$  as a function of temperature for PU0. The inset plot shows the Arrhenius-type plot for the temperature dependence of  $a_T$  (adapted from [175]).

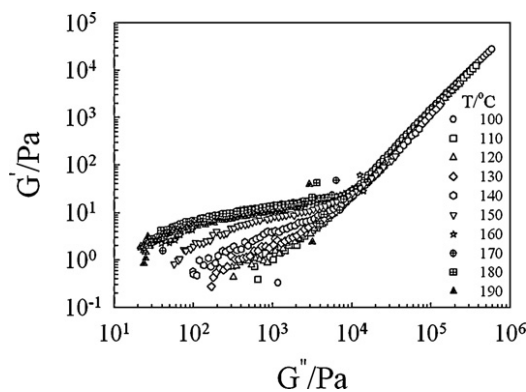


Fig. 52. Cole-Cole plot for PU0 at different temperatures (adapted from [175]).

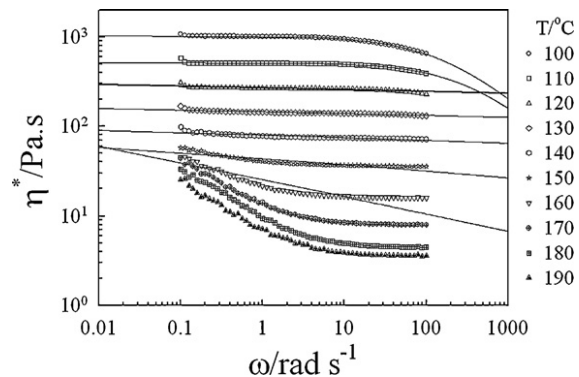


Fig. 53. Frequency dependence of dynamic viscosity for **PUO** at different temperatures. Solid lines are fits of Eq. (1) to the experimental data (adapted from [175]).

described. In addition, the  $G'$  starts to deviate from the master curve at 160 °C, which is 20 °C higher than that of pure PU (i.e., **PUO**) as shown in Fig. 54. This experimental fact suggests that the incorporation of small amounts of nanoscale POSS to the hard segments of PU enhances the miscibility between the hard and soft segments, producing relatively more homogenous composite at elevated temperatures. This enhancement in the miscibility and phase homogeneity is confirmed by TEM investigation as will be discussed later.

The shift factor as a function of temperature was also found to be consistent with the Arrhenius equation (25) as depicted in Fig. 55. The activation energy of flow for

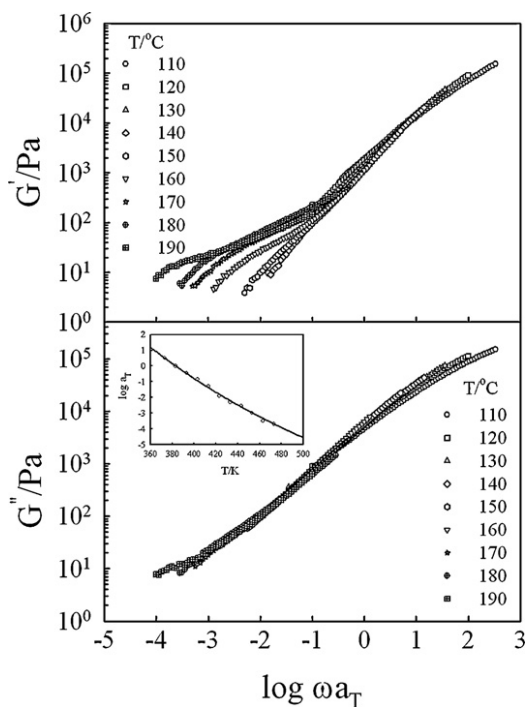


Fig. 54. Master curves of the dynamic shear moduli,  $G'$  and  $G''$  for **PU10** at reference temperature,  $T_0 = 120$  °C. The inset plot represents the shift factor  $a_T$  as a function of temperature (the solid line is calculated from Eq. (26) (adapted from [175])).

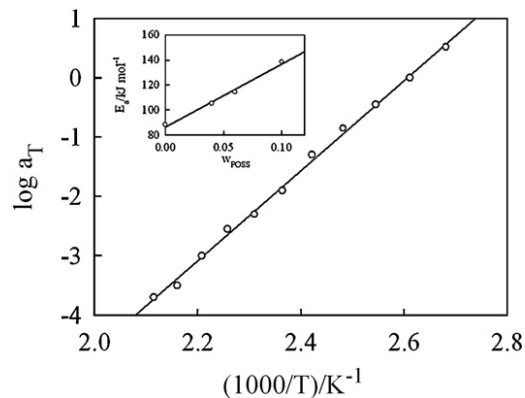


Fig. 55. Arrhenius-type plot for the temperature dependence of  $a_T$  for **PU10**. The inset-plot shows POSS concentration dependence of the activation energy of flow for PU/POSS nanocomposites (adapted from [175]).

the PU/POSS with 10 wt% POSS (**PU10**) obtained from the slope of the straight line of Fig. 55 is about 138 kJ/mol, a value much higher than that calculated for the pure PU (88 kJ/mol). The inset plot of Fig. 55 demonstrates the composition dependence of POSS on the activation energy of flow for PU/POSS nanocomposite. Clearly, the activation energy increases linearly with increasing POSS concentration. Based on this experimental fact one can say that the incorporation of POSS nanofiller to the polymer chains of PU can increase the phase homogeneity of the hard and soft segments, producing more homogeneous materials with high temperature dependent viscosities.

The complex viscosity of **PU10** as a function of shear frequency at different constant temperatures is shown in Fig. 56. The absolute value of  $\eta^*$  is about 1.5 orders of magnitude higher than that of pure PU at identical temperature and shear frequency (Fig. 56). The lines in Fig. 56 are computed from Cross model (Eq. (1)) and the symbols are experimental data. Similar to the behavior of pure PU, the viscosity increases at high temperatures ( $T \geq 160$  °C), especially at low shear frequency due to the microphase separation of the hard and soft segments [175]. The composition and temperature dependencies of zero shear viscosity and its relationship to the microphase separation transition will be considered later.

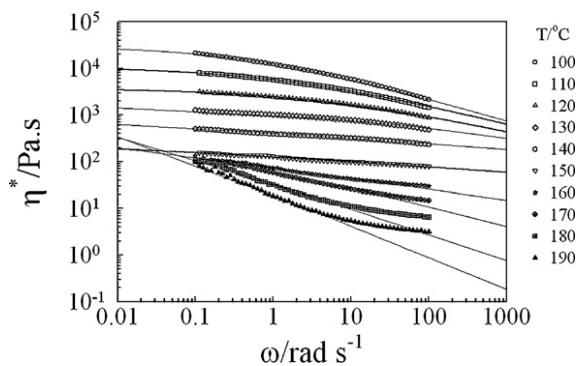
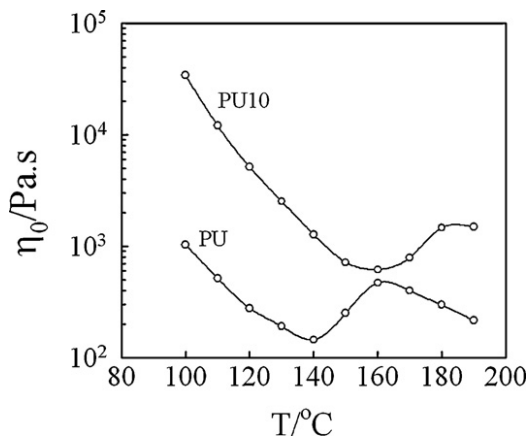
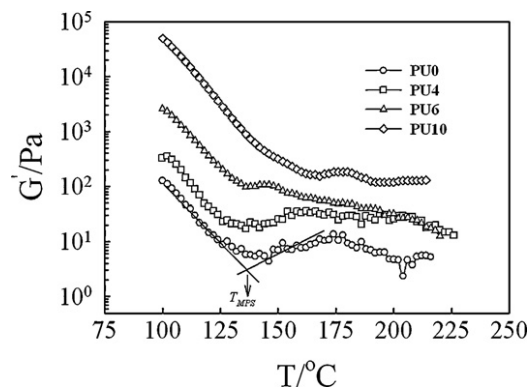


Fig. 56. Frequency dependence of dynamic shear viscosity for **PU10** at different temperatures. Solid lines are fits of Eq. (1) to the experimental data (adapted from [175]).



**Fig. 57.** Temperature dependence of the zero shear viscosity for **PU0** and **PU10** (adapted from [175]).

The calculated values of  $\eta_0$  at different temperatures based on Cross model for **PU0** and **PU10** (Figs. 53 and 56, respectively) is shown in Fig. 57. Clearly, this figure shows that  $\eta_0$  decreases with increasing temperature in the low temperature range due to the increase in mobility of the polymer chains caused by Brownian motion. At the microphase separation temperature, a considerable change in the slope of  $\eta_0$  was observed. The value of the microphase separation temperature ( $T_{MPS}$ ) can be obtained from the onset temperature at which the slope of  $\eta_0$  versus  $T$  starts to deviate. Based on this method the  $T_{MPS}$  for **PU0** and **PU10** are 140 and 160 °C, respectively. This observation supports our suggestion that POSS can enhance the miscibility of the hard and soft segments of PU to produce a relatively more homogenous nanoscale morphology, as will be confirmed by TEM investigations described later. A similar behavior was also seen in the dynamic heating ramps (2 °C/min heating rate at  $\omega = 1$  rad/s) of the viscoelastic material functions such as  $G'$  as shown in Fig. 58 for pure PU and PU/POSS composites of different POSS concentrations. The value of  $G'$  is observed to be very sensitive to the phase separation temperatures. Both the temperature dependencies of  $\eta_0$  (Fig. 57) and  $G'$  (Fig. 58) give the same values of the microphase separation temperatures  $T_{MPS}$ . It



**Fig. 58.** Temperature dependence of the storage modulus of PU/POSS nanocomposites for different POSS concentrations at 1 rad s<sup>-1</sup> shear frequency and 2 °C/min heating rate. The arrow shows the value of  $T_{MPS}$  (adapted from [175]).

is also very clear from Fig. 58 that the value of  $T_{MPS}$  is relatively unaffected by POSS concentrations up to 6 wt% POSS. At 10 wt% POSS (**PU10**) the  $T_{MPS}$  increased by about 20 °C, as shown in Fig. 58. Therefore, the morphology of **PU10** is considered below to get deeper understanding of the structure/property relationships in this important class of material [175].

Fig. 59 shows a comparison between the TEM photograph of **PU0** and **PU10**. The other concentrations (POSS ≤ 6 wt%) have almost similar morphologies to that of pure PU (not shown). It is clearly evident from this figure that the morphology of **PU10** does not show any segregation or aggregation of POSS particles, but exhibits a finer structure compared to that of pure PU. This experimental evidence indicates that the diamino-POSS is completely chemically reacted with the hard segments and that the incorporation of POSS in the molecular chains of PU enhances the miscibility between these incompatible hard and soft segments to produce a more homogenous structure.

The large surface area of the POSS nanoparticles that creates a large interaction zone with the PU segments is thought to be the major reason for the high miscibility of the PU hard and soft segments. It is well established in the

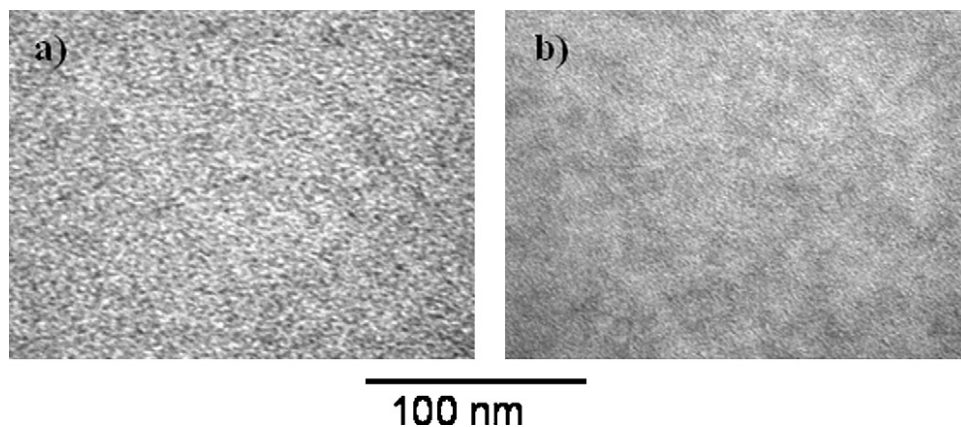


**Fig. 59.** TEM photographs for **PU0** and **PU10**. The dark particles represent the hard segments and the bright matrix represents the polyester soft segments. The **PU10** sample shows finer morphology than that of pure PU (adapted from [175]).

literature that the high surface area of nanoparticles leads to a large volume fraction of the polymer matrix, which in turn leads to different bulk properties of the polymer nanocomposite that is enhanced by the interaction zone. Depending on the degree of the interaction between the polymer and nanoparticles, this interaction region can have a higher or lower mobility than that of the bulk material [183,184]. The large surface area can lead to changes in the morphology of the polymers, as reported in the literature [183,184].

In the current PU/POSS system, the total free energy should include the interaction parameters of POSS with the PU hard and soft segments. The PU/POSS mixture can form a thermodynamically stable system when the Gibbs free energy of mixing is negative (i.e.,  $\Delta G_{\text{mix}} < 0$ ) as a consequence of the interactions of the POSS with both of the hard and soft segments of the PU backbone. In this context, two possible distinct situations can be envisaged. First, the POSS nanoparticles may have favorable interactions with the PU hard and soft segments, leading to a negative value of  $\Delta G_{\text{mix}}$ . In this case, the mixture should be miscible without any phase separation. Second, the POSS may have strong interactions with one segment and weak interactions with the other segment of the PU. In this case, the system may show either an increase in viscosity or a shift in the critical point to an extent that depends on the specific composition of the system and the relative degree of the interaction parameters. On the basis of the TEM morphologies presented in Fig. 59, it is apparent that the incorporation of POSS can induce a more miscible structure between the hard and soft segments of PU. While this experimental fact is attributed to the interactions of POSS with the PU hard and soft segments, it is noteworthy that the degree of interactions is not sufficient to produce a completely miscible system like other researchers have reported for other polymer nanocomposites. For example, a number of researchers have reported that organoclays can effectively reduce the domain size of immiscible polymer blends [185–188]. This is attributed to the clay acting as a physical barrier that slows the coalescence of the dispersed phases through pinning or increasing viscosity of the system. Si et al. [188] reported the morphology of blends of PS/PMMA, PC/SAN24, and PMMA/EVA with modified organoclays (Cloisite 20A and Cloisite 6A). The authors just mentioned found a large reduction in domain sizes and the localization of the clay platelets along the interfaces of the two components. It is noteworthy that our results and that of prior work reported by others on somewhat similar polymer nanocomposites are consistent with the expectation of POSS-induced enhancement in the miscibility of the PU hard and soft segments and with the observed consequent improvement in the phase homogeneity. As already discussed, these experimental facts can be ascribed to the large surface area of the nanoparticle producing relatively large interaction zones with the PU hard and soft segments.

### 5.3.3. Effect of POSS concentration on zero shear viscosity and thermal stability

The complex viscosity of pure PU and PU/POSS as a function of angular frequency for different concentrations of

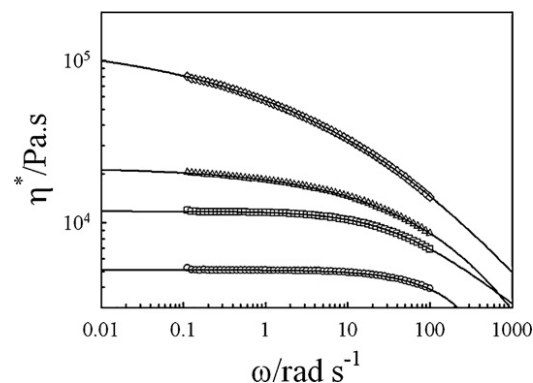


**Fig. 60.** Angular frequency dependence of complex viscosity for PU/POSS nanocomposites with different POSS concentrations at 110 °C. The solid lines are calculated from Eq. (1) using non-linear regression technique (adapted from [175]).

POSS at 110 °C is shown in Fig. 60. The  $T = 110$  °C is selected for this comparison because it is lower than the  $T_{\text{MPs}}$  of all samples. The viscosity of PU changed greatly with increasing concentration of POSS (i.e., the higher the concentration of POSS the larger the increase in the complex viscosity). The viscosity increased by more than 1.5 orders of magnitude for **PU10** and exhibits more non-Newtonian behavior over the entire range of shear frequency compared to that of **PU0** at the same temperature (see Fig. 60). The lines passing through the experimental data were calculated using Cross model (Eq. (1)), as described above.

Fig. 61a illustrates the volume fraction ( $\phi$ ) dependence of the dimensionless viscosity of the PU/POSS composites,  $\eta_r$  (reduced by the viscosity of **PU0**). The critical volume fraction of POSS ( $\phi_c$ ) at which the viscosity of the composite increased strongly was determined using Krieger–Dougherty equation (2). The value of  $\phi_c$  obtained from this regression analysis was found to be 0.14. The Krieger–Dougherty equation works well for hard sphere dispersions with volume fraction less than 0.55. It is well known that the value of  $\phi_c$  strongly depends on the specific system under consideration. For example small, mono-dispersed samples show smaller  $\phi_c$  than do large ones, and  $\phi_c$  increases with polydispersity [91]. Clearly, Fig. 61a shows an excellent description of the experimental data using Eq. (2). The Einstein or the modified Einstein–Batchelor equation (Eq. (27)) [189] for hard-sphere suspensions shown by the dotted line in Fig. 61a clearly deviates from the experimental data. Normally, the Einstein–Batchelor equation predicts a slight increase in the zero shear viscosity for suspensions of hard-sphere particles in a polymer matrix [191].

$$\eta_0(\phi) = \eta_0(0) \{ 1 + 2.5\phi + 6.2\phi^2 + \dots \} \quad (27)$$

The value of reduced viscosity as a function of volume fraction calculated from the Einstein–Batchelor equation is shown in the inset plot of Fig. 61a. Clearly, the magnitude of the elevation in the reduced zero shear viscosity caused by the hard-sphere particles is very small compared to the actual increase in viscosity in the present system (PU/POSS).

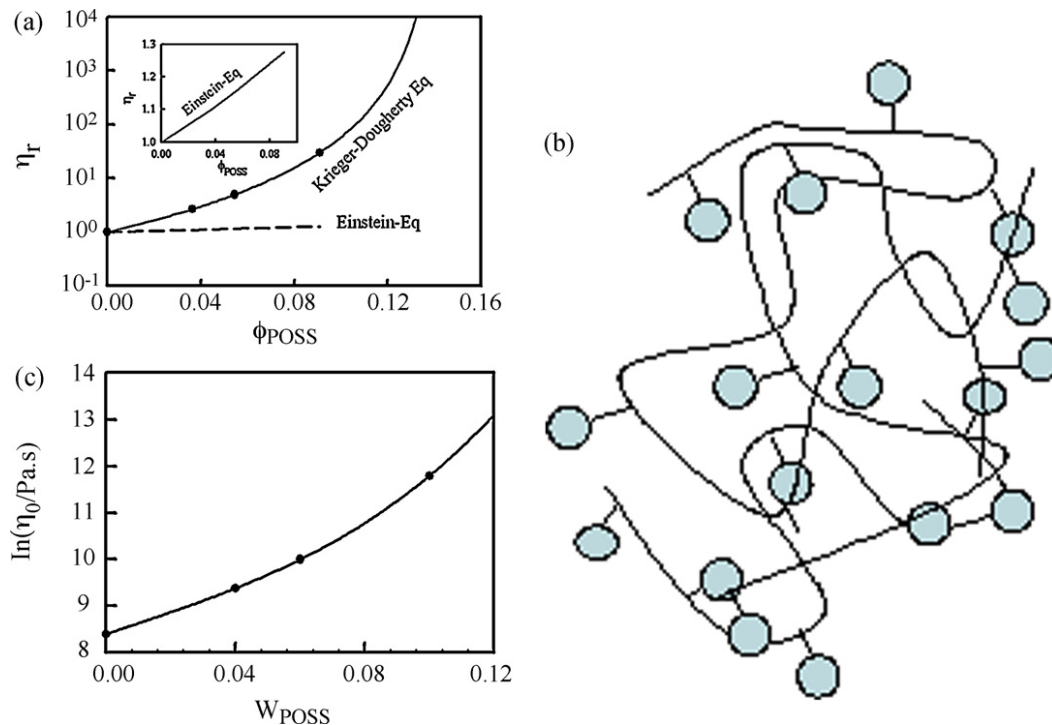


**Fig. 61.** (a) Reduced zero shear viscosity ( $\eta_r$ ) as a function of volume fraction of POSS ( $\phi_{\text{POSS}}$ ) at 110 °C for PU/POSS nanocomposites. The solid and broken lines are given by Krieger–Dougherty and Einstein–Batchelor equations, respectively. The inset plot shows the elevation of reduced zero shear viscosity by adding POSS nanofiller to the PU polymer matrix using Einstein–Batchelor equation (Eq. (27)) (adapted from [175]). (b) Schematic diagram of PU/POSS nanocomposite discussed in the text (adapted from [175]). (c) Zero shear viscosity as a function of weight fraction of POSS at 110 °C for PU/POSS nanocomposites. The solid line is calculated from the Lecyar model (Eq. (28)) (adapted from [175]).

Although the empirical Krieger–Dougherty equation works well for this system, it is well established that this equation is traditionally applied to hard spheres dispersions. Here, the Krieger–Dougherty equation is used for the current PU/POSS system since the POSS molecules can be thought of as the smallest particles of silica possible. The chemical structure of POSS is an inorganic/organic hybrid that is intermediate ( $\text{RSiO}_{1.5}$ ) between that of silica ( $\text{SiO}_2$ ) and silicone ( $\text{R}_2\text{SiO}$ ). However, unlike silica or modified clays, each POSS molecule contains covalently bonded reactive functionalities suitable for polymerization or grafting POSS monomers to polymer chains. In fact, POSS is reported in the literature to form spherical particles with 1.5 nm diameter, and its inorganic/organic hybrid nature makes it reasonable to conceptually think of them as hard spheres, in contrast to the relatively soft PU chains. Therefore, by copolymerizing or grafting POSS with PU, the POSS can be conjectured to preserve its spherical shape, as schematically depicted in Fig. 61b.

However, in the current PU/POSS system, the POSS is completely reacted with the hard segments of PU and there is no unreacted dispersed phase in this nanocomposite as confirmed by the TEM. Therefore, the current system is a homogeneous nanocomposite containing POSS that is completely reacted with the hard segments (urethane segments) to form part of the PU main chain. Therefore, it is reasonable to examine the composition dependence of zero shear viscosity of this composite using another model for miscible polymer mixtures, such as, the Lecyar model

described by the following equation [190]:

$$\ln \eta_b = Aw_1^3 + Bw_2^3 + Cw_1^2w_2 + Dw_1w_2^2 \quad (28)$$

where  $w_1$  and  $w_2$  are the weight fractions of PU and POSS, respectively. The constants  $A$ ,  $B$ ,  $C$  and  $D$  are material parameters that are both functions of shear frequency and temperature. A slightly negative deviation from the linear mixing rule ( $\ln \eta_b = w_1 \ln \eta_1 + w_2 \ln \eta_2$ , where  $\eta_1$  and  $\eta_2$  are the zero shear viscosity of PU and POSS, respectively) was detected for this composite, as clearly seen in Fig. 61c. The line is computed from Eq. (28) using a nonlinear regression method, while the symbols are experimental data; a good description of the data was obtained using this model. This equation is normally used to describe the composition dependence of shear viscosity of miscible polymer blends. Recently, we reported a negative deviation from the additivity rule in miscible polymer blend of poly(methyl methacrylate)/poly(methyl styrene-co-acrylonitrile), and the data was well described by Lecyar model [191]. It is noteworthy that this is not a general behavior for all miscible polymer mixtures. To our knowledge, there is no generally acceptable and universal valid mixing rule for the viscosity of polymer mixtures [192].

Fig. 62a shows the TGA measurements for pure PU and PU/POSS composites of different POSS concentrations. This figure shows the percent mass loss as a function of temperature at 10 °C/min heating rate under nitrogen atmosphere. Obviously, the PU and composites undergo thermal degradation beginning at 270 °C, regardless of the concentration



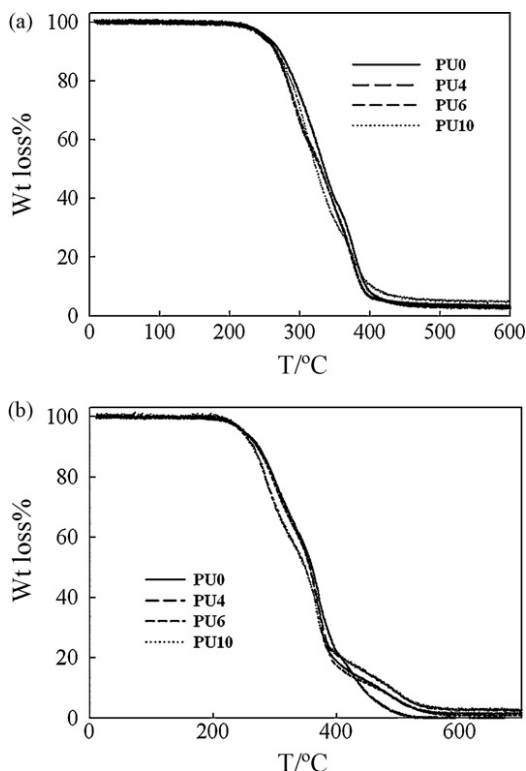


**Fig. 62.** (a) TGA data for PU/POSS nanocomposites with different POSS concentrations indicated at 10 °C/min heating rate under nitrogen atmosphere (adapted from [175]). (b) TGA data for PU/POSS nanocomposites with different POSS concentrations indicated at 10 °C/min heating rate under oxygen atmosphere (adapted from [175]).

of POSS. It is also clear from this figure that the soft segments of PU start to degrade first at 270 °C and the hard segments degrades later on at 350 °C. This figure suggests that the incorporation of POSS to the hard segments of PU does not significantly enhance the thermal stability of PU under a nitrogen atmosphere. Fig. 62b shows the same measurements carried out under an oxygen atmosphere. Clearly, the **PU10** nanocomposite becomes more thermally stable at high temperature than PU. For example, at 510 °C PU completely degrades without any inert residue. In contrast, more than 15% of **PU10** remains at this temperature. At temperatures higher than 550 °C, about 5 wt% inert residue remains for **PU10** nanocomposite.

## 6. PU/POSS nanocomposites obtained from non-dispersion methods

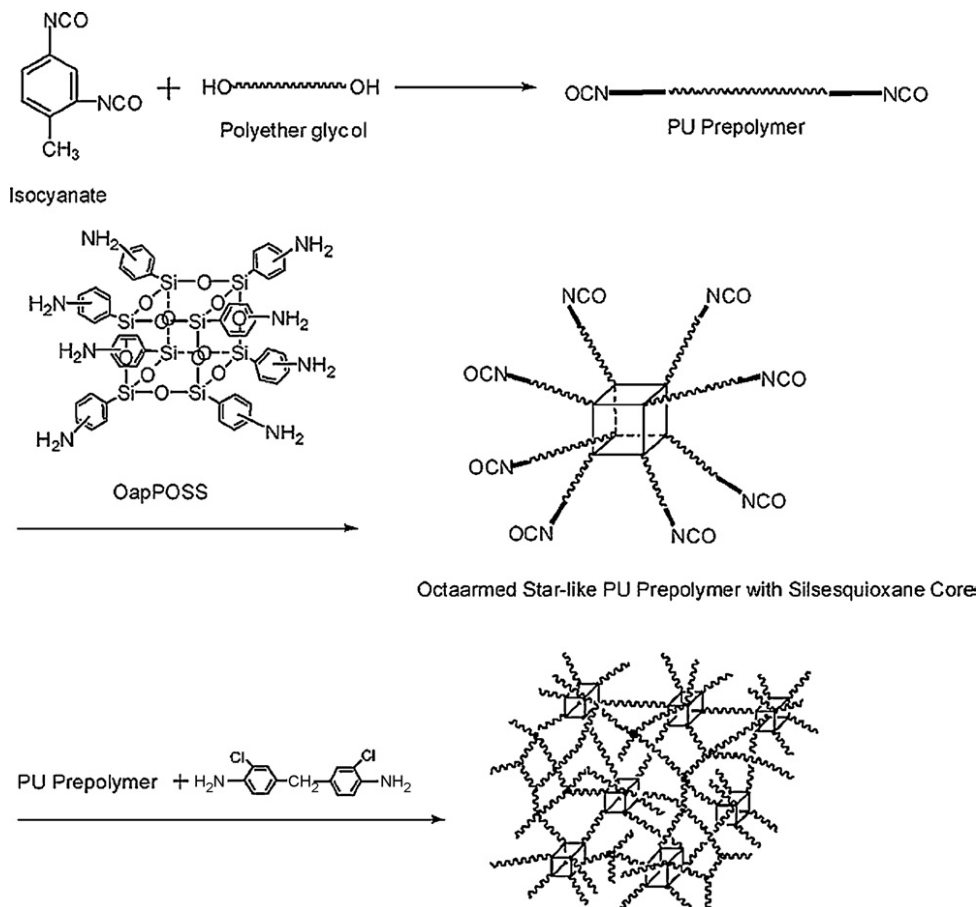
It is worth noting that there are very few reported studies on PU/POSS nanocomposites obtained from waterborne dispersions. In contrast, the number of publications on PU/POSS nanocomposites obtained from non-dispersion methods is relatively high [193–201]. In this section, a brief summary of recent publications of PU/POSS nanocomposites synthesized via nondispersion methods is presented.

Liu and Zheng [193] used octaaminophenyl polyhedral oligomeric silsesquioxane as a cross-linking agent to prepare polyurethane hybrid networks. The PU/POSS

nanocomposites were synthesized from polyether glycol and toluene-2,4-diisocyanate (TDI). The reaction was performed under a nitrogen atmosphere at 80 °C for 2 h to afford the polyurethane prepolymer. Solution of POSS in *N,N*-dimethylformamide (DMF) was added to the above PU prepolymer at 80 °C with vigorous stirring for 2 h. The POSS-containing octa-armed star-like polyurethane prepolymer was obtained. An equal molar amount of 4,4'-methylenebis-(2-chloroaniline) (MOCA) cross-linking agent with respect to the remnant number of –NCO groups in the POSS-containing polyurethane prepolymers was added to the system. The resulting mixtures were then cast into a pre-heated stainless steel mold. The samples were sealed in the molds and cured at 100 °C for 2 h and at 120 °C for 3 h. The preparation procedure for the PU/POSS is depicted in Scheme 6.

The mechanical damping ( $\tan \delta$ ) as a function of temperature for the PU/POSS nanocomposites with different POSS contents prepared using the method just described is shown in Fig. 63. Clearly, this figure shows that POSS has strong influence on the molecular dynamics of the glass relaxation process of pure PU. The control PU network structure exhibits a well-defined relaxation peak at –7 °C ascribed to the glass transition of the cross-linked polyurethane. The PU/POSS nanocomposites containing 5 and 10 mol% of POSS also displayed single  $\alpha$ -relaxations that correspond to the glass-transition of the composites. It can be seen that the temperatures corresponding to the  $\tan \delta$  peaks increase with increasing POSS concentration. For the nanocomposites containing 15 mol% of POSS, a peak appeared at approximately 50 °C, suggesting the formation of an inhomogeneous structure with a relatively higher glass-transition temperature. This observation is ascribed to the nano-reinforcement effect of the POSS cages on polyurethane networks. The relatively massive and bulky POSS cages could restrict the motion of the macromolecular chains, implying that higher temperatures are required to provide the requisite thermal energy for the occurrence of a glass transition in hybrid materials. In addition, the  $\tan \delta$  peaks were significantly broadened when the content of POSS cages was increased. The width of the  $\tan \delta$  peaks reflects the structural homogeneity of the cross-linked networks. TGA measurements of the pure PU and its nanocomposites with POSS displayed similar degradation profiles, suggesting that the existence of the POSS did not significantly alter the degradation mechanism of the matrix polymers.

Oaten and Choudhary [194] reported the synthesis of transparent PU/POSS nanocomposite for thin film applications that was carried out by the reaction of HDI and trisilanol isobutyl POSS with a stoichiometric molar ratio of 2:1 using dibutyl tin dilaurate (DBTL) as catalyst. The resulting material was characterized using various spectroscopic, microscopic, thermal, and scattering techniques. Silicon solid-state nuclear magnetic resonance spectroscopy results proved the formation of the hybrid POSS/polyurethane nanocomposite. The evolution of the hybrid structure during the reaction was investigated using small-angle neutron scattering (SANS). The PU/POSS coating, when applied to clean steel substrates via dip coating, revealed a uniform, dense, and essentially defect-free mor-



Scheme 6.

phology. Angle-resolved X-ray photoelectron spectroscopy (XPS) analysis allowed the interface between the substrate and the coating to be probed. It was found that the POSS-urethane coating formed a lamellar structure instead of a random 3D structure. This nanocomposite system just mentioned was designed for fabricating a hard, abrasion- and corrosion-resistant, barrier thin film coating for metals.

Synthesis and characterization of a novel POSS possessing eight isocyanate groups via the hydrosilylation of octakis(hydridodimethylsiloxy)octasilsesquioxane ( $Q_8M_8^H$ ) and *m*-isopropenyl- $\alpha,\alpha'$ -dimethylbenzyl isocyanate (*m*-TMI) has been reported by Neumann et al. [195] (see Scheme 7). The suitability of this new macromer to the synthesis of organic-inorganic hybrids has been explored by forming a new type of highly cross-linked polyurethane elastomer via reaction of the macromer with poly(ethylene glycol) using dibutyl tin dilaurate catalyst (Scheme 7). Analysis by FT-IR and near-IR spectroscopy analysis confirmed the complete reaction of isocyanate groups ( $\nu_{NCO} = 2262\text{ cm}^{-1}$ ) with the hydroxyl groups of the PEG-600 forming urethane linkages ( $\nu_{NHCO} = 3330, 1728\text{ cm}^{-1}$ ). Thermogravimetric analysis of the hybrid displayed a broad weight loss beginning at  $190^\circ\text{C}$  due to the cleavage of urethane linkages, followed by decomposition of the core itself.

Polyurethane elastomer containing POSS as molecular reinforcement in the hard segment was investigated by means of wide-angle X-ray diffraction (WAXD) and small-angle X-ray scattering (SAXS) techniques [196]. The WAXD

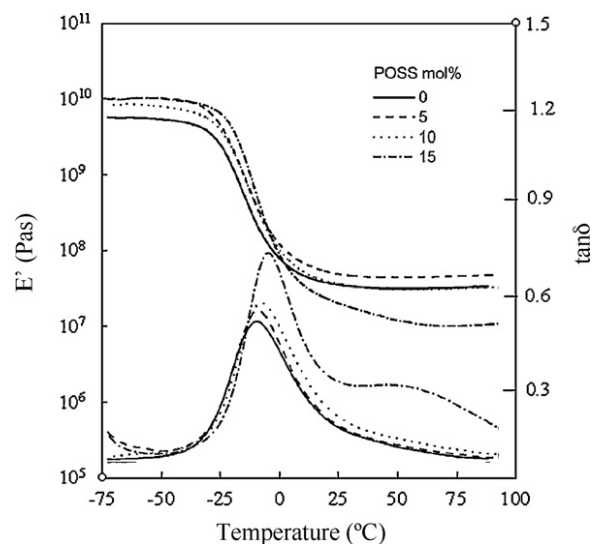
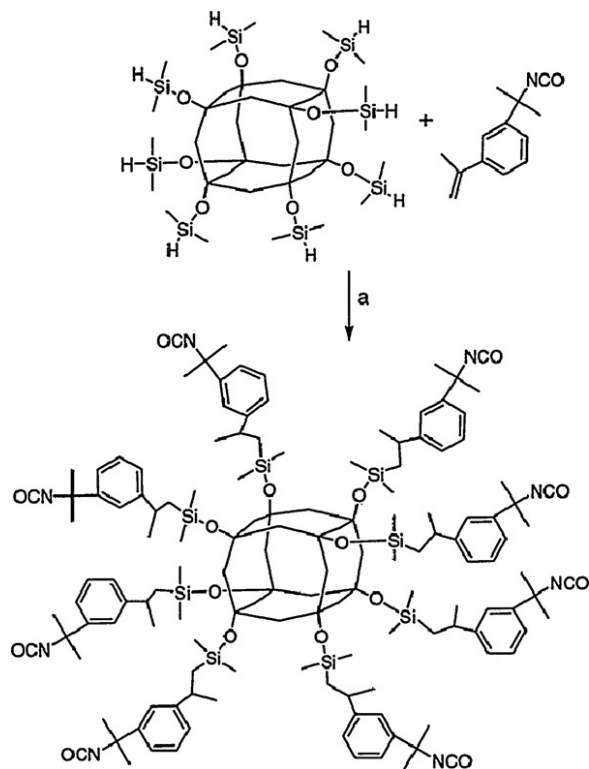


Fig. 63. DMA measurements for pure PU and PU/POSS nanocomposite of different POSS content (adapted from [193]).



Scheme 7.

results indicated that POSS molecules form nanoscale crystals showing distinct reflection peaks. The formation of POSS crystals is probably prompted by the microphase separation between solid-like hard segments and rubbery soft segments in PU. The microphase separation of hard and soft segments was observed by SAXS, which showed a long period of 111 Å for 34 wt% POSS/PU and 162 Å for 21 wt% POSS/PU; and hard segment domains with sizes of about 34 Å for both of them. WAXD data from a series of POSS compounds with a corner substituted by a functional group of varying length were compared with that of POSS/PU and the results confirmed the presence of nanoscale POSS crystals in the polymer matrix.

PU/POSS nanocomposites based on diphenylmethane-4,4'-diisocyanate and polytetra-methylene glycol were synthesized using a mixture of POSS-diol and 1,4-butanediol as chain extenders [197]. The polymers were characterized by DSC, WAXD, SAXS, and tensile property tests. Microphase separation between the hard and soft segment domains was observed in all the samples by SAXS. An increase of the POSS concentration was found to reduce the microphase separation between the domains and increase the  $T_g$  of the soft segments. The WAXD results showed that when the POSS concentration was greater than 10 wt%, the 1 0 1 diffraction peak from the POSS crystals could be observed, suggesting the formation of POSS nanocrystals in the hard domain. The tensile property tests showed that polyurethanes containing the nanostructured POSS molecules had higher moduli, but lower maximum elongation ratios than that of the pure polyurethane.

Fu et al. [198] prepared PU/POSS nanocomposites from polytetramethylene glycol (PTMG) soft segments and 4,4'-methylenebis (phenylisocyanate) (MDI) hard segments. The MDI hard segment was chain-extended by octasiloxane-POSS. The nanocomposites were investigated using WAXD, SAXS, and transmission electron microscopy (TEM) techniques. The mechanical properties of POSS modified polyurethane (POSS/PU) were also compared to that of polyurethane without POSS. WAXD data was collected during tensile deformation in order to determine the crystal structural changes in POSS and strain-induced crystallization of soft segment chains. Fig. 64a shows a series of WAXD patterns from the PU/POSS nanocomposite with 34 wt% POSS recorded with imaging plates during deformation. The equatorial profiles extracted from the patterns are shown in Fig. 64b. Before stretching, the profile shows a broad amorphous polyurethane peak at about 15°, which is overlapped with 0 3 0, 1 1 3 and 1 2 2 reflection peaks from the POSS crystal. At strains >100%, two reflection peaks resulting from the strain-induced crystallization of the soft segment (marked by an asterisk in Fig. 64b) are observed. These two peaks can be indexed as 1 0 0 and 1 0 1 reflections from the soft segment PTMG crystals. When the strain was increased to above 200%, the strain-induced crystallization peak (PTMG crystals with good orientation) became dominant over the amorphous peak at 15°. The SAXS results showed microphase structure typical of segmented polyurethanes, with an initial long spacing of 110 Å between the domains. At high strains, the average length of strain-induced microfibrillar soft-segment crystals was estimated to be about 60 Å by SAXS. The TEM analysis of highly stretched samples showed a preferred orientation of deformed hard domains perpendicular to the stretching direction, indicating the destruction of hard segment domains by strain.

PU nanocomposites containing polyester resins and POSS were prepared using reactive POSS as a partial substitution for diol monomer. The PU/POSS nanocomposites were investigated by FT-IR, rheometry, dynamic mechanical analysis, WAXD, contact-angle measurement, AFM, and TGA. Fig. 65 shows shear rate dependence of apparent viscosity for PU/POSS nanocomposites containing 0, 1.0, 2.8, 5.6, and 8.5 wt% POSS. It was found that the pure polyester resin displayed Newtonian flow behavior while the PU/POSS nanocomposites showed higher viscosity and evidence of shear thinning that increased with increasing POSS concentration. This behavior was attributed to the physical and chemical interactions between the rigid and dimensionally large POSS cage with polyester chains. The dynamic loss curves of the PU/POSS hybrids as a function of temperature are illustrated in Fig. 66. The  $\alpha$ -relaxation process is attributed to micro-Brownian segmental motion of amorphous polyester molecular chains and was designated as the glass-transition temperature ( $T_g$ ). In comparison with pure PU, the  $T_g$  increased with increasing POSS content. There are two competitive factors which affect the  $T_g$ s. On the one hand, the dispersion of POSS cages at the molecular level could restrict the motion of macromolecular chains, which would enhance  $T_g$ . On the other hand, the inclusion of the bulky POSS group may increase the free volume of the system, resulting in the depression of  $T_g$ . In this

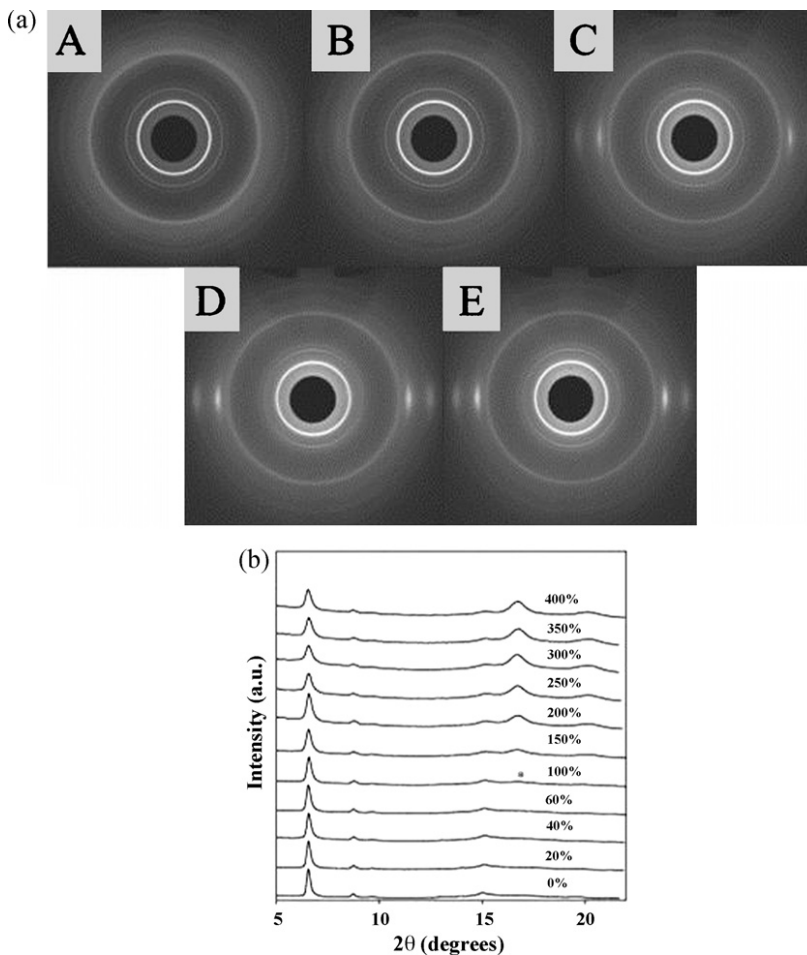


**Fig. 64.** (a) Two-dimensional WAXD patterns of PU/POSS nanocomposite with 34 wt% POSS at stretching ratio of: (A) 0; (B) 100; (C) 200; (D) 300; and (E) 400%. The exposure time of each pattern was 1 min. (b) WAXD profiles of POSS-PU-34 along the equatorial direction at different strains. The symbol asterisk indicates the strain-induced crystallization of the soft segment (adapted from [198]).

case, POSS cages had a dominating impact on the segmental motion in PUs as the large and rigid POSS cages chemically bonded onto the soft polyester segments as pendants significantly restricts the motion of the polyester segments.

In addition, similar results have been observed for all the PU/POSS nanocomposites regardless of the concentration of POSS, suggesting that the incorporation of POSS did not significantly alter the degradation mechanism of PU.

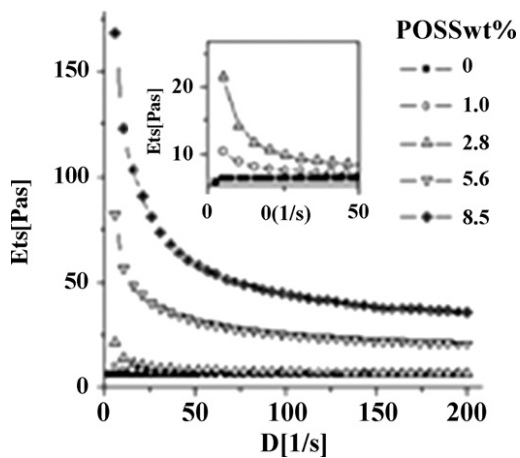


**Fig. 65.** The apparent viscosity of polyester-POSS resins as a function of shear rate at different POSS contents (adapted from [199]).

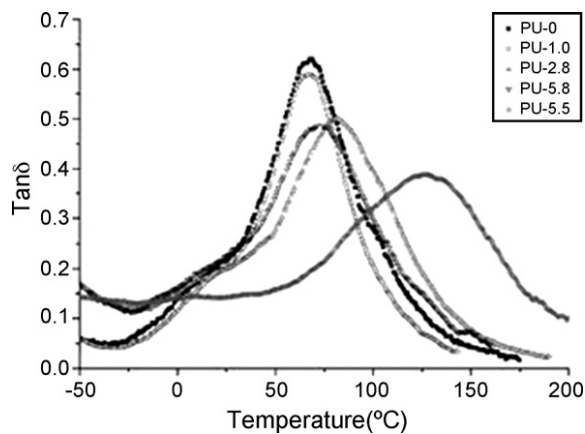


**Fig. 66.** Loss-tangent curves versus temperature for PU/POSS nanocomposites (adapted from [199]).

Janowski and Pielichowski [200] investigated the thermo(oxidative) stability of some novel PU/POSS nanohybrids using TGA. The PU/POSS nanocomposites were synthesized from diphenylmethane-4,4'-diisocyanate (MDI), polytetramethylene glycol (Terathane 1000, 1400 and 2000), 1,4-butanediol and octasiloxane-POSS. The TGA data showed that the highest thermal stability, in inert and oxidative atmospheres, was obtained from the samples containing 4 and 6 wt% POSS. These results were explained in terms of restricted molecular mobility of PU macrochains in the presence of POSS and by reduction of rate of emission of volatile products.

Recently, Bliznyuk et al. [201] synthesized structural organization of two different series of PU/POSS copolymers (branched and cross-linked) based on a mixture of variable size oligomeric silsesquioxanes (POSS-M). The chemical structure of the synthesized POSS-M-containing PUs has been confirmed by GPC and IR spectroscopic studies. Complex several-level hierarchy of their physical structural organization was revealed by SAXS and AFM. The SAXS experiments showed that microphase segregation and formation of nano-sized domains enriched with the inorganic phase (i.e., POSS fragments) take place during synthesis of the organic-inorganic hybrid systems. These nano-heterogeneity regions contain up to 66 vol% of  $\text{SiO}_{1.5}$  and form a paracrystalline lattice with hexagonal symmetry and characteristic interplanar periodicity of around 15 nm. The average size of the inorganic phase nano-inclusions was estimated as 2–3 nm, a value which corresponds to the size of several POSS moieties. A topologically more complex system (i.e., cross-linked POSS-M-containing PUs) showed evidence of diffusion-limited microphase segregation features. In the complex system just mentioned, the regions of nano-heterogeneity were relatively smaller in size, had smaller content of the inorganic phase (ca. 54 vol%), and formed a less perfect para-crystalline order with a periodicity of 9.7 nm. In general, the replacement of regular POSS moieties with the POSS-M mixtures could lead to nanocomposite systems with an ordered supramolecular structural organization and simultaneous reduction of their production cost due to relative simplicity of their synthesis.

## 7. Conclusions and outlook

Recent advances in synthesis, characterization, phase structure evolution and kinetics, rheological properties, and modeling of PUDs and novel hybrid PU/POSS nanocomposites dispersions and films were reviewed in this article. Well-characterized model systems of PUDs and hybrid PU/POSS nanocomposites have been synthesized via homogenous solution polymerization in aqueous dispersions using the so-called acetone and prepolymer emulsification processes. The viscoelastic properties of the PUDs changed dramatically by varying the degree of post-neutralization and solid content. The steep viscosity increase with increasing solid content and degree of post-neutralization is attributed to the increase in the PUD particle sizes and the associated decrease in the free volume. The degree of chain extension was found to have a negligible effect on the rheological behavior of the PUDs. The viscoelastic material functions of the PUDs are well

described by simple power-law equations, WLF principle, and a Maxwellian (Hookean) model with up to three relaxation times at certain PU concentrations and degrees of post-neutralization at 30 °C. The viscoelastic properties of PUDs have also been investigated over a wide range of temperature and frequency for different PU concentrations. Thermal-induced gelation has been observed for PUDs with high PU concentration (i.e., PU wt%  $\geq 36$ ) as evidenced by an abrupt increase in the temperature dependencies of some of the viscoelastic material functions ( $G'$ ,  $G''$  and  $\eta^*$ ) at the onset of gelation at different angular frequencies. In contrast, the low concentration samples i.e., PU wt%  $\leq 34$  did not show any tendency for thermal-induced gelation. This observation is thought to be related to differences in the particle sizes of the dispersions; with increasing concentrations, the PU particle size increases which in turn leads to increasing hydrodynamic interactions that can be increased by thermal energy and consequently leading to thermal-induced gelation. The morphology of the dispersions for some different PU concentrations showed a network structure with a unique periodicity and phase connectivity. On the basis of the observed morphology just mentioned, an LCST-type phase diagram was constructed for these dispersions and found to be consistent with the simultaneous occurrence of liquid-liquid and liquid-solid transitions at the same temperature range, like others have reported for other complex fluids such as biopolymer solutions.

The thermal-induced formation of an elastic fractal gel in PUDs of 40 wt% PU has been extensively investigated rheologically using time evolution measurements of viscoelastic material functions, such as, ( $G'$ ,  $G''$ ,  $\eta^*$  and  $\tan \delta$ ) over a wide range of frequencies under selected isothermal conditions. The  $G'$  and  $G''$  data were found to follow a power law behavior as a function of frequency ( $G'' \sim G' \sim \omega^n$ ) with exponents,  $n'$  and  $n''$  equal to 0.53 and 0.51, respectively. The exponent values are very close to that obtained for different systems and in good agreement with that predicted theoretically based on the percolation theory ( $n \sim 2/3$ ). In addition, the zero-shear viscosity,  $\eta_0$ , and the equilibrium shear modulus,  $G_{eq}$ , have also been expressed in power law scaling functions with the relative distance from the gel point,  $\varepsilon$ , i.e.,  $\eta_0 \sim \varepsilon^{-k}$  and  $G_{eq} \sim \varepsilon^z$  with  $k=0.95$  and  $z=0.85$  in close agreement with the predicted values based on the well-known percolation theory reported in the literature.

The model of Malkin and Kulichikhin, which was predicted originally for the isothermal curing kinetics of thermosetting polymers measured by differential scanning calorimetry (DSC), worked very well in describing the isothermal rheological kinetics of the present polyurethane dispersion system. Extensive isothermal kinetics analysis of the PUD gelation process using the *model-free* isoconversional method showed that the activation energy was constant regardless of the extent of the degree of conversion, indicating that the gelation process is controlled by a single step (homogenous) process with no change in the fractal gel formation or aggregation mechanism. The non-isothermal kinetics reaction rate was found to be well described by a model proposed by Swartzel et al. that was originally developed to include the classical rate equation, the Arrhenius equation, and the time-temperature equiva-

lence relationships. Under non-isothermal conditions, the apparent activation energy was found to be frequency independent and equal to 125 kJ/mol, in excellent agreement with the value obtained isothermally from the temperature dependence of  $T_{gel}$ .

It has been shown that waterborne hybrid polyurethane/POSS nanocomposite dispersions have been successfully synthesized by incorporating amino- and hydroxy-functionalized POSS macromers into polyurethane ionomeric backbones using the so-called acetone process. The resulting PU/POSS dispersions are stable for more than six months, and their low level of VOC (<1%) shows the advantages of the acetone process over the prepolymer method. The POSS macromers appear to be incorporated in the PU hard segments as evidenced by the absence of crystalline domains and the steady increase in hard segment  $T_g$  with increasing POSS content. Storage modulus, tensile strength, complex viscosity, and  $T_g$  of the hard segments of PU films increased as the level of POSS was increased. It is worthy to note that the PU/POSS films are transparent with incorporation of up to 10 wt% POSS monomers. The viscoelastic data in the melt state confirmed the existence of microphase separation transition,  $T_{MPS}$ , of the hard and soft segments at about 140 °C for pure PU. For samples containing POSS  $\leq$  6 wt%, the value of  $T_{MPS}$  was found to be concentration independent, i.e., the  $T_{MPS}$  remains constant at 140 °C regardless of the different concentrations of POSS used. The  $T_{MPS}$  shifted to higher temperature ( $T_{MPS} = 160$  °C) for the 10 wt% POSS/PU nanocomposite. This experimental fact suggests that the incorporation of diamino-POSS to the hard segments of PU enhances their miscibility; producing a more homogenous structure as confirmed by the TEM (i.e., finer nano-scale morphology was observed for 10 wt% POSS/PU nanocomposite compared to that of pure PU). In addition, the incorporation of POSS produces nanocomposites with viscosities showing strong temperature dependence as confirmed by the linear increase in the activation energy of flow with increasing concentration of POSS. Furthermore, a summary of PU/POSS nanocomposites synthesized from non-dispersion methods with improved properties is also presented in this review article.

The research studies reviewed in this article demonstrate that PUDs and hybrid PU/POSS nanocomposites possess a rich rheological behavior within experimentally accessible shear frequencies and can, therefore, serve as excellent model systems for exploring details of rheology and macromolecular structure dynamics of this class of industrially useful aqueous polymer dispersions and films with enhanced benefits in a number of new and existing applications. Further, the results of the research studies reviewed here confirm that homogeneous dispersion of POSS in polyurethane-ureas can be reliably probed by rheological and TEM methods and that the sequencing of the reaction steps previously reported in details elsewhere [174] dictate the quality of POSS dispersion, making it possible to prepare nanostructured PU/POSS films with prescribed morphology and physical properties, and invent new applications. It is hoped that this review article may stimulate a better understanding of the rational incorporation of nanostructured chemical feedstocks such as POSS

into already existing polymer systems to generate new nanostructured hybrid polymer nanocomposites systems with improved properties, and facilitate progress in this emerging area.

In some aspects, a number of the foregoing experimental results are similar to those obtained from other cross-linking polymer networks and gels in the literature, yet in very important ways the present aqueous PUD system is quite unique and little studied. Therefore, this review article may stimulate development of a new theory that explicitly takes into account direct coupling of the rate of gel structure formation with fundamental gelation concepts for aqueous PUDs and other related water soluble polymers undergoing high deformation flows under both isothermal and non-isothermal conditions.

### Acknowledgements

We thank the U.S. National Science Foundation Division of Chemical, Bioengineering, Environmental, and Transport Systems (contract grant number NSF-CBET 07-52150) and the Division of Materials Research (contract grant number NSF-DMR 02-13883) for funding. Hybrid Plastics is acknowledged for their donation of the POSS samples. We thank Anton Paar USA for providing us with direct access to their new MCR 501 rheometer. We are indebted to our collaborators – Drs. Douglas Wicks and Ajaya Nanda – with whom we had the privilege to work on projects cited in this review article. The research work of J.U.O.'s former graduate students and postdocs is gratefully acknowledged.

### References

- [1] Tirpak RE, Markusch PH. Aqueous dispersions of crosslinked polyurethanes. *J Coat Tech* 1986;58:49–54.
- [2] Seneker SD, Rosthauser JW, Markusch PH. Polyurethane elastomers based on aliphatic diisocyanates. In: *Polyurethanes 92: proceedings of the 34th SPI annual tech/mark conference*. 1992. p. 588–97.
- [3] Kim BK, Kim TK, Jeong HM. Aqueous dispersion of polyurethane anionomers from H12MDI/IPDI, PCL, BD, and DMPA. *J Appl Polym Sci* 1994;53:371–8.
- [4] Dieterich D, Keberle W, Witt H. Polyurethane ionomers, a new class of block polymers. *Angew Chem* 1970;9:40–50.
- [5] Eisenberg A. Clustering of ions in organic polymers. A theoretical approach. *Macromolecules* 1970;3:147–54.
- [6] Visser SA, Cooper SL. Comparison of the physical properties of carboxylated and sulfonated model polyurethane ionomers. *Macromolecules* 1991;24:2576–83.
- [7] Kim CK, Kim BK. IPDI[isophorone diisocyanate]-based polyurethane ionomer dispersions: effects of ionic, nonionic hydrophilic segments, and extender on particle size and physical properties of emulsion cast film. *J Appl Polym Sci* 1991;43:2295–301.
- [8] Kim BK. Aqueous polyurethane dispersions. *Colloid Polym Sci* 1996;274:599–611.
- [9] Coutinho FMB, Delpech MC. Some properties of films cast from polyurethane aqueous dispersions of polyether-based anionomer extended with hydrazine. *Polym Test* 1996;15:103–13.
- [10] Chen GN, Chen KN. Self-curing behaviors of single pack aqueous-based polyurethane system. *J Appl Polym Sci* 1997;63:1609–23.
- [11] Jhon YK, Cheong IW, Kim JH. Chain extension study of aqueous polyurethane dispersions. *Colloid Surf A* 2001;179:71–8.
- [12] Narayan R, Chattopadhyay DK, Sreedhar B, Raju KVS, Mallikarjuna NN, Aminabhavi TM. Synthesis and characterization of crosslinked polyurethane dispersions based on hydroxylated polyesters. *J Appl Polym Sci* 2006;99:368–80.
- [13] Dieterich D, Keberle W, Wuest R. Aqueous dispersions of polyurethane ionomers. *J Oil Colloid Chem Assoc* 1970;53:363–79.

- [14] Dieterich D. Aqueous emulsions, dispersions and solutions of polyurethanes; synthesis and properties. *Prog Org Coat* 1981;9:281–340.
- [15] Lorenz O, August HJ, Hick H, Triebs F. Anionic polyurethane ionomers with 1,2,4-benzenetricarboxylic acid anhydride. *Angew Makromol Chem* 1977;63:11–22.
- [16] Seefried CG, Koleske JV, Critchfield FE. Thermoplastic urethane elastomers. I. Effects of soft-segment variations. *J Appl Polym Sci* 1975;19:2493–502.
- [17] Wicks DA, Wicks ZW. Blocked isocyanates III: Part A. Mechanisms and chemistry. *Prog Org Coat* 1999;36:148–72.
- [18] Wicks ZW. Research challenges in coatings science. *Polym Mater Sci Eng* 1988;59:269–72.
- [19] Wicks DA, Yeske PE. Amine chemistries for isocyanate-based coatings. *Prog Org Coat* 1997;30:265–70.
- [20] Wicks DA, Shaffer MW. Two-component waterborne polyurethanes. In: Book of abstracts, 214th ACS national meeting. 1997. p. 7–11. PMSE-024.
- [21] Best K, Wicks D. Film properties of polyisocyanate based coatings with mixed amine coreactants. *Polym Mater Sci Eng* 1998;79:398.
- [22] Wicks DA, Wicks ZW. Multistep chemistry in thin films; the challenges of blocked isocyanates. *Prog Org Coat* 2001;43:131–40.
- [23] Yang Z, Wicks DA, Hoyle CE, Pu H, Yuan J, Wan D, et al. Newly UV-curable polyurethane coatings prepared by multifunctional thiol- and ene-terminated polyurethane aqueous dispersions mixtures: preparation and characterization. *Polymer* 2009;50:1717–22.
- [24] Asif A, Shi W, Shen X, Nie K. Physical and thermal properties of UV curable waterborne polyurethane dispersions incorporating hyperbranched aliphatic polyester of varying generation number. *Polymer* 2005;46:11066–78.
- [25] Durrieu V, Gandini A. Preparation of aqueous anionic poly(urethane-urea) dispersions. Influence of the incorporation of acrylic, polycarbonate and perfluoro-oligoether diols on the dispersion and polymer properties. *Polym Adv Tech* 2005;16:840–5.
- [26] Parmar R, Patel K, Parmar J. High-performance waterborne coatings based on epoxy-acrylic-graft-copolymer-modified polyurethane dispersions. *Polym Inter* 2005;54:488–94.
- [27] Tanaka H, Suzuki Y, Yoshino F. Synthesis and coating application of waterborne fluoroacrylic-polyurethane composite dispersions. *Colloid Surf A* 1999;153:597–601.
- [28] Vijayendran BR, Derby R, Gruber BA. Aqueous polyurethane-vinyl polymer dispersions for coating applications. US Patent 5,173,526; 1992.
- [29] De Gennes PG. Polymers at an interface; a simplified view. *Adv Colloid Interface Sci* 1987;27(3–4):189–209.
- [30] Ilett SM, Orrock A, Poon WCK, Pusey PN. Phase behavior of a model colloid-polymer mixture. *Phys Rev E* 1995;51:344–52.
- [31] Napper DH. Polymeric stabilization of colloidal dispersions. New York: Academic; 1983.
- [32] Wei X, Yu X. Synthesis and properties of sulfonated polyurethane ionomers with anions in the polyether soft segments. *J Polym Sci Part B: Polym Phys* 1997;35:225–32.
- [33] Wei X, He Q, Yu X. Synthesis and properties of polyoxyethylated amine polyurethane ionomers. *J Appl Polym Sci* 1998;67:2179–85.
- [34] Petrovic ZS, Ferguson J. Polyurethane elastomers. *Prog Polym Sci* 1991;16:695–836.
- [35] Miller JA, Hwang KKS, Cooper SL. Properties of polyether-polyurethane anionomers. *J Macromol Sci Phys* 1983;B22:321–41.
- [36] Visser SA, Cooper SL. Analysis of small-angle X-ray scattering data for model polyurethane ionomers: evaluation of hard-sphere models. *Macromolecules* 1991;24:2584–93.
- [37] Hwang KS, Yang GH, Cooper SL. Properties of polyether-polyurethane zwitterionomers. *Polym Eng Sci* 1981;21:1027–36.
- [38] Huang YS, Dong SL, Yang KH, Chwang GP, Chao DY. Study of anionic polyurethane ionomer dispersant. *J Coat Tech* 1997;69:69–74.
- [39] Frisch KC. Recent advances in the chemistry of polyurethanes. *Rub Chem Tech* 1972;45:1442–66.
- [40] Szycher M, Poirier VL, Dempsey DJ. Development of an aliphatic biomedical-grade polyurethane elastomer. *J Elast Plast* 1983;15:81–95.
- [41] Schollenberger CS, Stewart FD. Thermoplastic urethane structure and ultraviolet stability. *J Elastoplast* 1972;4:294–331.
- [42] Brauman SK, Mayorga GD, Heller J. Light stability and discoloration of segmented polyether urethanes. *Annal Biomed Eng* 1981;9:45–58.
- [43] Schollenberger CS, Scott H, Moore GR. Polyurethane VC, a virtually cross-linked elastomer. *Rubber World* 1958;137:549–55.
- [44] Adams R, Anderson JL. Quinone imines. II. p-Quinone diacyl- and diarylimines. *J Am Chem Soc* 1950;72:5154–7.
- [45] Hepburn C. Polyurethane elastomer. 2nd ed. New York: Elsevier Applied Science; 1992.
- [46] Kim BS, Kim BK. Enhancement of hydrolytic stability and adhesion of waterborne polyurethanes. *J Appl Polym Sci* 2005;97:1961–9.
- [47] Frisch KC, Dieter JA. Overview of urethane elastomers. *Polym-Plast Tech Eng* 1975;4(1):1–21.
- [48] Dieterich D, Grigat E, Hahn W, Hesse, Schmelzer H. Principles of polyurethane chemistry and special applications. In: Oertel G, editor. *Polyurethane handbook*. 2nd ed. Munich: Hanser Publishers; 1993. p. 11–53.
- [49] Anderle GA, Lenhard SL, Lubnin AV, Snow GE, Tamareselvy K. Plasticized waterborne polyurethane dispersions and manufacturing process. US Patent 6576702; 2003.
- [50] Rajan H, Rajalingam P, Radhakrishnan G. Synthesis and solution properties of polyurethane anionomers. *Polym Commun* 1991;32:93–6.
- [51] Kim BK, Lee YM. Structure-property relationship of polyurethane ionomer. *Colloid Polym Sci* 1992;270:956–61.
- [52] Visser SA, Cooper SL. Morphology and properties of mixed anion ionomers. *Polymer* 1992;33:3790–6.
- [53] Kim BK, Lee JC. Waterborne polyurethanes and their properties. *J Polym Sci Part A: Polym Chem* 1996;34:1095–104.
- [54] Tharanikkarasu K, Kim BK. Modification of aqueous polyurethane dispersions via tetraphenylethane iniferterers. *J Appl Polym Sci* 1999;73:2993–3000.
- [55] Hourston DJ, Williams GD, Satguru R, Padgett JC, Pears D. The influence of the degree of neutralization, the ionic moiety, and the counterion on water-dispersible polyurethanes. *J Appl Polym Sci* 1999;74:556–66.
- [56] Kwak YS, Kim, Yoo BH, Kim HD. Preparation and properties of waterborne poly(urethane urea)s for adhesives: the effects of the 2,2-bis(hydroxymethyl)propionic acid content on the properties. *J Appl Polym Sci* 2004;94:1743–51.
- [57] Zhang S, Cheng L, Hu J. NMR Studies of water-borne polyurethanes. *J Appl Polym Sci* 2003;90:257–60.
- [58] Nanda AK, Wicks DA, Madbouly SA, Otaigbe JU. Effect of ionic content, solid content, degree of neutralization, and chain extension on aqueous polyurethane dispersions prepared by prepolymer method. *J Appl Polym Sci* 2005;98:2514–20.
- [59] Madbouly SA, Otaigbe JU, Nanda AK, Wicks DA. Rheological behavior of aqueous polyurethane dispersions: effects of solid content, degree of neutralization, chain extension, and temperature. *Macromolecules* 2005;38:4014–23.
- [60] Madbouly SA, Otaigbe JU, Nanda AK, Wicks DA. Thermal-induced simultaneous liquid-liquid phase separation and liquid-solid transition in aqueous polyurethane dispersions. *Polymer* 2005;46:10897–907.
- [61] Reichl A, Dieterich D, Witt H. Process for the production of microporous polyurethane(urea)sheets structures permeable to water vapor. US Patent 3,763,054; 1973.
- [62] Li Q-A, Sun D-C. Synthesis and characterization of high solid content aqueous polyurethane dispersion. *J Appl Polym Sci* 2007;105:2516–24.
- [63] (a) Flickinger GL, Dairanieh IS, Zukoski CF. The rheology of aqueous polyurethane dispersions. *Non-Newtonian Fluid Mech* 1999;87:283–305; (b) Buscall R, Goodwin JW, Hawkins MW, Ottewill RH. Viscoelastic properties of concentrated latices: I Methods of examination; II Theoretical analysis. *J Chem Soc Faraday Trans* 1982;78, 2873–2887, 2889–2899.
- [64] Haberle K, Claassen P, Seher A, Schumacher KH, Seyffer H. Sterile nonwovens bonded using polyurethane dispersions. United States Patent 6063498; 2000.
- [65] Cheng KL, Chen WT. Method of the preparation of water-borne polyurethane adhesive. US Patent 6,191,214; 2001.
- [66] Woods G. *The ICI polyurethane book*. New York: John Wiley & Sons; 1987.
- [67] Lewandowski K, Krepski LR, Mickus DE, Roberts RR, Heilmann SM, Larson WK, et al. Synthesis and properties of waterborne self-crosslinkable sulfo-urethane silanol. *J Polym Sci Part A: Polym Chem* 2002;40:3037–45.
- [68] Oertel G, editor. *Polyurethane handbook*. Munich: Carl Hanser Publishers; 1985.

- [69] Yang CH, Lin SM, Wen TC. Application of statistical experimental strategies to the process optimization of waterborne polyurethane. *Polym Eng Sci* 1995;35:722–30.
- [70] Wen TC, Wu MS, Yang CH. Spectroscopic investigations of poly(oxypropylene) glycol-based waterborne polyurethane doped with lithium perchlorate. *Macromolecules* 1999;32:2712–20.
- [71] Wen TC, Wang YJ, Cheng TT, Yang CH. The effect of DMPA units on ionic conductivity of PEG-DMPA-IPDI waterborne polyurethane as single-ionelectrolytes. *Polymer* 1999;40:3979–88.
- [72] Yang CH, Yang HJ, Wen TC, Wu MS, Chang JS. Mixture design approaches to IPDI-H6XDI-XDI ternary diisocyanate-based waterborne polyurethanes. *Polymer* 1999;40:871–85.
- [73] Barni A, Levi M. Aqueous polyurethane dispersions: a comparative study of polymerization processes. *J Appl Polym Sci* 2003;88:716–23.
- [74] Chinwanitcharoen C, Kanoh S, Yamada T, Hayashi S, Sugano S. Preparation of aqueous dispersible polyurethane: effect of acetone on the particle size and storage stability of polyurethane emulsion. *J Appl Polym Sci* 2004;91:3455–61.
- [75] Nanda AK, Wicks DA. The influence of the ionic concentration, concentration of the polymer, degree of neutralization and chain extension on aqueous polyurethane dispersions prepared by the acetone process. *Polymer* 2006;47:1805–11.
- [76] Aruna P, Kumar DBR. Anionomeric waterborne poly(urethane semicarbazide) dispersions and their adhesive properties. *J Appl Polym Sci* 2008;110:2833–40.
- [77] Barikani M, Ebrahimi MV, Mohaghegh SMS. Preparation and characterization of aqueous polyurethane dispersions containing ionic centers. *J Appl Polym Sci* 2007;104:3931–7.
- [78] Rahman MM, Kim HD. Synthesis and characterization of waterborne polyurethane adhesives containing different amount of ionic groups. *J Appl Polym Sci* 2006;102:5684–91.
- [79] Wei Y, Xin H. Effect of diisocyanates on the structure and properties of UV-curable polyurethane dispersions with nano-scale particles. *e-Polymers* 2008;169:1–11.
- [80] Park SH, Lee SK, Choi HY, Lee EM, Kim EY, Lim CH, et al. Mechanical and surface properties and hydrolytic stability of cycloaliphatic polyester-based waterborne polyurethanes modified with fluoro oligomer. *J Appl Polym Sci* 2009;111:1828–34.
- [81] Lu Y, Larock RC. Soybean-oil-based waterborne polyurethane dispersions: effects of polyol functionality and hard segment content on properties. *Biomacromolecules* 2008;9:3332–40.
- [82] Bao LH, Lan YJ, Zhang SF. Effect of NCO/OH molar ratio on the structure and properties of aqueous polyurethane from modified castor oil. *Iran Polym J* 2006;15:737–46.
- [83] Lee DK, Tsai HB, Tsai RS. Effect of composition on aqueous polyurethane dispersions derived from polycarbonatediols. *J Appl Polym Sci* 2006;102:4419–24.
- [84] Chen RS, Cheng YL, Chang KW. Synthesis and properties of novel poly(urethane-imide) dispersions based on 2,2-bis[*N*-(3-hydroxyphenyl)phthalimidy]hexafluoropropane. *J Appl Polym Sci* 2009;111:517–24.
- [85] Bao LH, Lan YJ, Zhang SF. Synthesis and properties of waterborne polyurethane dispersions with ions in the soft segments. *J Polym Res* 2006;13:507–14.
- [86] Gao C, Xu X, Ni J, Lin W, Zheng Q. Effect of castor oil, glycol semi-ester, and polymer concentration on the properties of waterborne polyurethane dispersions. *Polym Eng Sci* 2009;49:162–7.
- [87] Nasrullah MJ, Bahr JA, Gallagher-Lein C, Webster DC, Roesler RR, Schmitt P. Automated parallel polyurethane dispersion synthesis and characterization. *J Coat Technol Res* 2009;6:1–10.
- [88] Segre PN, Prasad V, Schofield AB, Weitz DA. Glasslike kinetic arrest at the colloidal-gelation transition. *Phys Rev Lett* 2001;86:6042–5.
- [89] Cross MM. Rheology of non-Newtonian fluids: a new flow equation for pseudoplastic systems. *J Colloid Sci* 1965;20:417–37.
- [90] Krieger IM, Dougherty TJ. A mechanism for non-Newtonian flow in suspensions of rigid spheres. *Trans Soc Rheol* 1959;3:137–52.
- [91] (a) Farris RJ. Influence of vacuole formation on the response and failure of filled elastomers. *Trans Soc Rheol* 1968;12:315–34; (b) Farris RJ. Prediction of the viscosity of multimodal suspensions from unimodal viscosity data. *Trans Soc Rheol* 1968;12:281–301.
- [92] Brady JF. The rheological behavior of concentrated colloidal dispersions. *J Chem Phys* 1993;99:567–81.
- [93] Bender JW, Wagner NJ. Optical measurement of the contributions of colloidal forces to the rheology of concentrated suspensions. *J Colloid Interface Sci* 1995;172:171–84.
- [94] Jones AR, Leary B, Boger DV. The rheology of a sterically stabilized suspension at high concentration. *J Colloid Interface Sci* 1992;150:84–96.
- [95] Lattuada M, Sandkuehler P, Wu H, Sefcik J, Morbidelli M. Kinetic modeling of aggregation and gel formation in quiescent dispersions of polymer colloids. *Macromol Symp* 2004;206:307–20.
- [96] Winter HH, Chambon F. Analysis of linear viscoelasticity of a crosslinking polymer at the gel point. *J Rheol* 1986;30:367–82.
- [97] Chambon F, Winter HH. Linear viscoelasticity at the gel point of a crosslinking PDMS with imbalanced stoichiometry. *J Rheol* 1987;31:683–97.
- [98] Shikata T, Niwa H, Morishima Y. Viscoelastic behavior of bimodal suspensions. *J Rheol* 1998;42:765–80.
- [99] Macosko CW. *Rheological principles, measurements and applications*. New York: Wiley-VCH; 1994.
- [100] Madbouly SA, Otaigbe JU, Nanda AK, Wicks DA. Effect of preparation method on the rheological behavior of waterborne polyurethane dispersion. *Ann Tech Conf Soc Plast Eng* 2006;64:2366–70.
- [101] Madbouly SA, Uogizawa T. Thermal crosslinking of poly(vinyl methyl ether): I. Effect of crosslinking process on the viscoelastic properties. *J Macro Sci-Phys* 2004;B43:471–87.
- [102] Zhao Y, Cao Y, Yang Y, Wu C. Rheological study of the sol-gel transition of hybrid gels. *Macromolecules* 2003;36:855–9.
- [103] Winter HH, Morganelli P, Chambon F. Stoichiometry effects on rheology of model polyurethanes at the gel point. *Macromolecules* 1988;21:532–5.
- [104] San Biagio PL, Bulone D, Emanuele A, Palma-Vittorelli MB, Palma MU. Spontaneous symmetry-breaking pathways: time-resolved study of agarose gelation. *Food Hydrocolloid* 1996;10:91–7.
- [105] Tanaka T, Swislow G, Ohmine I. Phase separation and gelation in gelatin gels. *Phys Rev Lett* 1979;42:1556–9.
- [106] Kaya M, Toyama Y, Yamada A, Sakanishi A, Kubota K. Temperature induced gelation of fibrinogen. *Trans MRS—Japan* 2002;27:597–600.
- [107] Takahashi M, Shimazaki M. Formation of junction zones in thermoreversible methylcellulose gels. *J Polym Sci Part B: Phys* 2001;39:943–6.
- [108] Kita R, Kaku T, Ohashi H, Kurosu T, Iida M, Yagihara S, et al. Thermally induced coupling of phase separation and gelation in an aqueous solution of hydroxypropylmethylcellulose (HPMC). *Physica A* 2003;319:56–64.
- [109] Scanlan JC, Winter HH. Composition dependence of the viscoelasticity of end-linked poly(dimethylsiloxane) at the gel point. *Macromolecules* 1991;24:47–54.
- [110] Izuka A, Winter HH, Hashimoto T. Molecular weight dependence of viscoelasticity of polycaprolactone critical gels. *Macromolecules* 1992;25:2422–8.
- [111] Adolf D, Martin JE, Wilcoxon JP. Evolution of structure and viscoelasticity in an epoxy near the sol-gel transition. *Macromolecules* 1990;23:527–31.
- [112] Hodgson DF, Amis EJ. Dynamic viscoelastic characterization of sol-gel reactions. *Macromolecules* 1990;23:2512–9.
- [113] Muller R, Gerard E, Dugand P, Rempp P, Gnanou Y. Rheological characterization of the gel point: a new interpretation. *Macromolecules* 1991;24:1321–6.
- [114] Takahashi M, Yokoyama J, Masuda T, Takigawa T. Dynamic viscoelasticity and critical exponents in sol-gel transition of an end-linking polymer. *J Chem Phys* 1994;101:798–804.
- [115] Martin JE, Adolf D, Wilcoxon JP. Viscoelasticity near the sol-gel transition. *Phys Rev A* 1989;39:1325–32.
- [116] Muthukumar M. Dynamics of polymeric fractals. *J Chem Phys* 1985;83:3161–8.
- [117] Takigawa T, Takahashi M, Urayama K, Masuda T. Comparison of model prediction with experiment for concentration-dependent modulus of poly(vinyl alcohol) (PVA) gels near the gelation point. *Chem Phys Lett* 1992;195:509–12.
- [118] Hess W, Vilgis TA, Winter HH. Dynamical critical behavior during chemical gelation and vulcanization. *Macromolecules* 1988;21:2536–42.
- [119] Muthukumar M. Screening effect on viscoelasticity near the gel point. *Macromolecules* 1989;22:4656–8.
- [120] Lairez D, Adam M, Emery JR, Durand D. Rheological behavior of an epoxy/amine system near the gel point. *Macromolecules* 1992;25:286–9.
- [121] Adolf D, Martin JE. Ultraslow relaxations in networks: evidence for remnant fractal structures. *Macromolecules* 1991;24:6721–4.
- [122] Grisel M, Muller G. Rheological properties of the schizophyllan-borax system. *Macromolecules* 1998;31:4277–81.
- [123] Hone JHE, Howe AM, Cosgrove T. A rheological and small-angle neutron scattering study of the structure of gelatin/polyelectrolyte complexes under shear. *Macromolecules* 2000;33:1199–205.



- [124] Balan C, Voelger KW, Kroke E, Riedel R. Viscoelastic properties of novel silicon carbodiimide gels. *Macromolecules* 2000;33:3404–8.
- [125] Daoud M. Viscoelasticity near the sol–gel transition. *Macromolecules* 2000;33:3019–22.
- [126] Yoon PJ, Han CD. Effect of thermal history on the rheological behavior of thermoplastic polyurethanes. *Macromolecules* 2000;33:2171–83.
- [127] Tanaka F. Polymer–surfactant interaction in thermoreversible gels. *Macromolecules* 1998;31:384–93.
- [128] Matricardi P, Dentini M, Crescenzi V. Rheological gel-point determination for a polysaccharide system undergoing chemical cross-linking. *Macromolecules* 1993;26:4386–7.
- [129] Stauffer D. Introduction to percolation theory. London: Taylor and Francis; 1985.
- [130] Madbouly SA, Otaigbe JU. Rheokinetics of thermal-induced gelation of waterborne polyurethane dispersions. *Macromolecules* 2005;38:10178–84.
- [131] Schiessel H, Blumen A. Mesoscopic pictures of the sol–gel transition: ladder models and fractal networks. *Macromolecules* 1995;28:4013–9.
- [132] Winter HH. Gel point. In: Mark HF, editor. *Encyclopedia of polymer science and engineering*, Suppl. Vol., 3rd ed. New York: John Wiley & Sons; 1989. pp. 343–51.
- [133] Madbouly SA, Otaigbe JU. Kinetic analysis of fractal gel formation in waterborne polyurethane dispersions undergoing high deformation flows. *Macromolecules* 2006;39:4144–51.
- [134] Zlatanovic A, Dunjic B, Djonlagic J. Rheological study of the copolymerization reaction of acrylate-terminated unsaturated copolyesters with styrene. *Macromol Chem Phys* 1999;200:2048–58.
- [135] Lopes da Silva JA, Goncalves MP, Rao MA. Kinetics and thermal behavior of the structure formation process in HMP/sucrose gelation. *Int J Biol Macromol* 1995;17:25–32.
- [136] Guo ZS, Du SY, Zhang BM, Wu ZJ. Modeling the curing kinetics for a modified bismaleimide resin using isothermal DSC. *J Appl Polym Sci* 2004;92:3338–42.
- [137] Esteves CLC, Lucey JA, Hyslop DB, Pires EMV. Effect of gelation temperature on the properties of skim milk gels made from plant coagulants and chymosin. *Int Dairy J* 2003;13:877–85.
- [138] Baeza R, Gugliotta LM, Pilosof AMR. Gelation of  $\beta$ -lactoglobulin in the presence of propylene glycol alginate: kinetics and gel properties. *Colloid Surf B: Bioint* 2003;31:81–93.
- [139] Johnson SB, Dunstan DE, Franks GV. A novel thermally-activated crosslinking agent for chitosan in aqueous solution: a rheological investigation. *Colloid Polym Sci* 2004;282:602–12.
- [140] Ponton A, Warlus S, Griesmar P. Rheological study of the sol–gel transition in silica alkoxides. *J Colloid Interface Sci* 2002;249:209–16.
- [141] Vyazovkin S, Sbirrazzuoli N. Kinetic methods to study isothermal and nonisothermal epoxy-anhydride cure. *Macromol Chem Phys* 1999;200:2294–303.
- [142] Sbirrazzuoli N, Vyazovkin S, Mititelu A, Sladic C, Vincent L. A study of epoxy-amine cure kinetics by combining isoconversional analysis with temperature modulated DSC and dynamic rheometry. *Macromol Chem Phys* 2003;204:1815–21.
- [143] Vyazovkin S, Wight CA. Model-free and model-fitting approaches to kinetic analysis of isothermal and nonisothermal data. *Thermochem Acta* 1999;340–341:53–68.
- [144] Khawam A, Flanagan DR. Role of isoconversional methods in varying activation energies of solid-state kinetics. *Thermochem Acta* 2005;429:93–102.
- [145] Malkin AY, Kulichikhin SG. Rheokinetics rheological transformation in synthesis and reaction of oligomers and polymers. Heidelberg: Huthing&Wepf Verlag; 1996.
- [146] Dunjic B, Djonlagic J, Vukasinovic S, Sepulchre M, Sepulchre MO, Spassky N. Rheokinetic study of crosslinking of  $\alpha,\omega$ -dihydroxy oligo(alkylene maleate)s with a trisisocyanate. *J Serbian Chem Soc* 2003;68:147–62.
- [147] Lem KW, Han CD. Chemorheology of thermosetting resins. II. Effect of particulates on the chemorheology and curing kinetics of unsaturated polyester resin. *J Appl Polym Sci* 1983;28:3185–206.
- [148] Cuadrado TR, Borraro J, Williams RJJ, Clara FM. On the curing kinetics of unsaturated polyesters with styrene. *J Appl Polym Sci* 1983;28:485–99.
- [149] Pusatcioglu SY, Fricke AL, Hassler JC. Variation of thermal conductivity and specific heat during cure of thermoset polyesters. *J Appl Polym Sci* 1979;24:947–52.
- [150] Ryan ME, Dutta A. Kinetics of epoxy cure. A rapid technique for kinetic parameter estimation. *Polymer* 1979;20:203–6.
- [151] Fernandez B, Corchero MA, Marieta C, Mondragón I. Rheokinetic variations during curing of a tetrafunctional epoxy resin modified with two thermoplastics. *Eur Polym J* 2001;37:1863–9.
- [152] Rodríguez R, Alvarez-Lorenzo C, Concheiro A. Cationic cellulose hydrogels: kinetics of the cross-linking process and characterization as pH-/ion-sensitive drug delivery systems. *J Cont Rel* 2003;86:253–65.
- [153] Swartzel KR. Non-isothermal kinetics data generation for food constituents. In: Singh RP, Medina AG, editors. *Food properties and computer-aided engineering of food processing systems*. NATO science series E: applied sciences. New York: Springer-Verlag; 1989. p. 99–103.
- [154] Rhim JW, Nunes RV, Jones VA, Swartzel KR. Determination of kinetic parameters using linearly increasing temperature. *J Food Sci* 1989;54:446–50.
- [155] Fu JT, Rao MA. Rheology and structure development during gelation of low-methoxyl pectin gels: the effect of sucrose. *Food Hydrocolloid* 2001;15:93–100.
- [156] POSS is a Trademark of Hybrid Plastics, [www.hybridplastics.com](http://www.hybridplastics.com).
- [157] Lichtenhan JD. Polyhedral oligomeric silsesquioxanes: building blocks for silsesquioxane-based polymers and hybrid materials. *Comm Inorg Chem* 1995;7:115–30.
- [158] Schwab JJ, Lichtenhan JD. Polyhedral oligomeric silsesquioxane (POSS)-based polymers. *Appl Organo Chem* 1998;12:707–13.
- [159] Laine RM, Zhang C, Sellinger A, Viculis L. Polyfunctional cubic silsesquioxanes as building blocks for organic/inorganic hybrids. *Appl Organo Chem* 1998;12:715–23.
- [160] Lucke S, Stopperk-Langner K. Polyhedral oligosilsesquioxanes (POSS)-building blocks for the development of nano-structured materials. *Appl Surf Sci* 1999;145:713–5.
- [161] Shockey EG, Bolf AG, Jones F, Schwab JJ, Chaffee KP, Haddad TS, et al. Functionalized polyhedral oligosilsesquioxane (POSS) macromers: new graftable POSS hydride, POSS  $\alpha$ -olefin, POSS epoxy, and POSS chlorosilane macromers and POSS-siloxane triblocks. *Appl Organo Chem* 1999;13:311–27.
- [162] Li G, Wang L, Ni H, Pittman CU. Polyhedral oligomeric silsesquioxane (POSS) polymers and copolymers: a review. *J Inorg Organomet Polym* 2002;11:123–54.
- [163] Schmidt D, Shah D, Giannelis EP. New advances in polymer/layered silicate nanocomposites. *Cur Opin Solid State Mater Sci* 2002;6:205–12.
- [164] Gilman JW, Schlitzer DS, Lichtenhan JD. Low earth orbit resistant siloxane copolymers. *J Appl Polym Sci* 1996;60:591–6.
- [165] Phillips S, Haddad TS, Tomczak S. Developments in nanoscience: polyhedral oligomeric silsesquioxane (POSS)-polymers. *J Curr Opin Solids State Mater Sci* 2004;8:21–9.
- [166] Gonzalez RI, Phillips S, Hoflund GB. In situ oxygen-atom erosion study of polyhedral oligomeric silsesquioxane-siloxane copolymer. *J Spacecraft Rockets* 2000;37:463–7.
- [167] Gao F, Tong Y, Schrickler SR, Culbertson BM. Evaluation of neat resins based on methacrylates modified with methacryl-POSS, as potential organic–inorganic hybrids for formulating dental restoratives. *Polym Adv Technol* 2001;12:355–60.
- [168] Tegou E, Bellas V, Gogolides E, Argitis P. Polyhedral oligomeric silsesquioxane (POSS) acrylate copolymers for microfabrication: properties and formulation of resist materials. *Microelectr Eng* 2004;73–74:238–43.
- [169] Kickelbick G. Concepts for the incorporation of inorganic building blocks into organic polymers on a nanoscale. *Prog Polym Sci* 2002;28:83–114.
- [170] Lichtenhan JD, Vu NQ, Carter JA, Gilman JW, Feher FJ. Silsesquioxane-siloxane copolymers from polyhedral silsesquioxanes. *Macromolecules* 1993;26:2141–2.
- [171] Lichtenhan JD, Otonari YA. Linear hybrid polymer building blocks: methacrylate-functionalized polyhedral oligomeric silsesquioxane monomers and polymer. *Macromolecules* 1995;28:8435–7.
- [172] Tsuchida A, Bolln C, Sernetz FG, Frey H, Muelhaupt R. Ethene and propene copolymers containing silsesquioxane side groups. *Macromolecules* 1997;30:2818–24.
- [173] Mather PT, Jeon HA, Romo-Uribe A, Haddad TS, Lichtenhan DJ. Mechanical relaxation and microstructure of poly(norbornyl-POSS) copolymers. *Macromolecules* 1999;32:1194–203.
- [174] Nanda AK, Wicks DA, Madbouly SA, Otaigbe JU. Nanostructured polyurethane/POSS hybrid aqueous dispersions prepared by homogeneous solution polymerization. *Macromolecules* 2006;39:7037–43.
- [175] Madbouly SA, Otaigbe JU, Nanda AK, Wicks DA. Rheological behavior of POSS/polyurethane-urea nanocomposite films prepared by

- homogeneous solution polymerization in aqueous dispersions. *Macromolecules* 2007;40:4982–91.
- [176] Turri S, Levi M. Structure, dynamic properties, and surface behavior of nanostructured ionomeric polyurethanes from reactive polyhedral oligomeric silsesquioxanes. *Macromolecules* 2005;38:5569–74.
- [177] Koberstein JT, Russell TP. Simultaneous SAXS–DSC study of multiple endothermic behavior in polyether-based polyurethane block copolymers. *Macromolecules* 1986;19:714–20.
- [178] Ryan AJ, Macosko CW, Bras W. Order–disorder transition in a block copolyurethane. *Macromolecules* 1992;25:6277–83.
- [179] Wilkes GL, Emerson JA. Time dependence of small-angle X-ray measurements on segmented polyurethanes following thermal treatment. *J Appl Phys* 1976;47:4261–4.
- [180] Velankar S, Cooper SL. Microphase separation and rheological properties of polyurethane melts. 1. Effect of block length. *Macromolecules* 1998;31:9181–92.
- [181] Yang IK, Wang PJ, Tsai PH. Rheological investigation of microphase separation transition of polyurethane elastomer. *J Appl Polym Sci* 2007;103:2107–12.
- [182] Eckstein A, Suhm J, Friedrich C, Maier RD, Sassmannshausen J, Bochmann M, et al. Determination of plateau moduli and entanglement molecular weights of isotactic, syndiotactic, and atactic polypropylenes synthesized with metallocene catalysts. *Macromolecules* 1998;31:1335–40.
- [183] Ash BJ, Siegel RW, Schadler LS. Glass-transition temperature behavior of alumina/PMMA nanocomposites. *J Polym Sci Part B: Phys* 2004;42:4371–83.
- [184] Ma D, Schadler LS, Siegel RW, Hong J. Preparation and structure investigation of nanoparticle-assembled titanium dioxide microtubes. *Appl Phys Lett* 2003;83:1839–41.
- [185] Khatua BB, Lee DJ, Kim HY, Kim JK. Effect of organoclay platelets on morphology of nylon-6 and poly(ethylene-ran-propylene) rubber blends. *Macromolecules* 2004;37:2454–9.
- [186] Li Y, Shimizu H. Novel morphologies of poly(phenylene oxide) (PPO)/polyamide 6 (PA6) blend nanocomposites. *Polymer* 2004;45:7381–8.
- [187] Li Y, Shimizu H. Co-continuous polyamide 6 (PA6)/acrylonitrile-butadiene-styrene (ABS) nanocomposites. *Macromol Rapid Commun* 2005;26:710–5.
- [188] Si M, Araki T, Ade H, Kilcoyne ALD, Fisher R, Sokolov JC, et al. Compatibilizing bulk polymer blends by using organoclays. *Macromolecules* 2006;39:4793–801.
- [189] Batchelor GK. Mass transfer from a particle suspended in fluid with a steady linear ambient velocity distribution. *J Fluid Mech* 1979;95:369–400.
- [190] Carley JF. A simple, accurate model for viscosities of polymer blends. *Polym Eng Sci* 1985;25:1017–25.
- [191] Madbouly SA. Binary miscible blends of poly(methyl methacrylate)/poly( $\alpha$ -methyl styrene-co-acrylonitrile). IV. Relationship between shear flow and viscoelastic properties. *J Macromol Sci Phys* 2003;B42:1209–23.
- [192] Utracki LA, Kamal MR. Melt rheology of polymer blends. *Polym Eng Sci* 1982;22:63–78.
- [193] Liu H, Zheng S. Polyurethane networks nanoreinforced by polyhedral oligomeric silsesquioxane. *Macromol Rapid Commun* 2005;26:196–200.
- [194] Oaten M, Choudhury NR. Silsesquioxane–urethane hybrid for thin film applications. *Macromolecules* 2005;38:6392–401.
- [195] Neumann D, Fisher M, Tran L, Matison JG. Synthesis and characterization of an isocyanate functionalized polyhedral oligomeric silsesquioxane and the subsequent formation of an organic–inorganic hybrid polyurethane. *J Am Chem Soc* 2002;31:13998–9.
- [196] Fu BX, Hsiao BS, White H, Rafailovich M, Mather PT, Jeon HG, et al. Nanoscale reinforcement of polyhedral oligomeric silsesquioxane (POSS) in polyurethane elastomer. *Polym Int* 2000;49:437–40.
- [197] Fu BX, Zhang W, Hsiao BS, Rafailovich M, Sokolov J, Johansson G, et al. Synthesis and characterization of segmented polyurethanes containing polyhedral oligomeric silsesquioxanes nanostructured molecules. *High Perform Polym* 2000;12:565–71.
- [198] Fu BX, Hsiao BS, Pagola S, Stephens P, White H, Rafailovich M, et al. Structural development during deformation of polyurethane containing polyhedral oligomeric silsesquioxanes (POSS) molecules. *Polymer* 2001;42:599–611.
- [199] Zhang S, Zou Q, Wu L. Preparation and characterization of polyurethane hybrids from reactive polyhedral oligomeric silsesquioxanes. *Macromol Mater Eng* 2006;14:895–901.
- [200] Janowski B, Pielichowski K. Thermo(oxidative) stability of novel polyurethane/POSS nanohybrid elastomers. *Thermochem Acta* 2008;478:51–3.
- [201] Bliznyuk VN, Tereshchenko TA, Gumenna MA, Gomza YP, Shevchuk AV, Klimentenko NS, et al. Structure of segmented poly(ether urethane)s containing amino and hydroxyl functionalized polyhedral oligomeric silsesquioxanes (POSS). *Polymer* 2008;49:2298–305.